Damage assessment of coastal structures in climate change adaptation

CoMEM Master Thesis

Ermano de Almeida Sousa

TU Delft Delft University of Technology

CoMEM

Deltares Enabling Delta Life

Erasmus+

UNIVERSITAT POLITÈCNICA DE CATALUNYA BARCELONATECH

NTNU Norwegian University of Science and Technology

University of Southampton

City University of London EST 1894

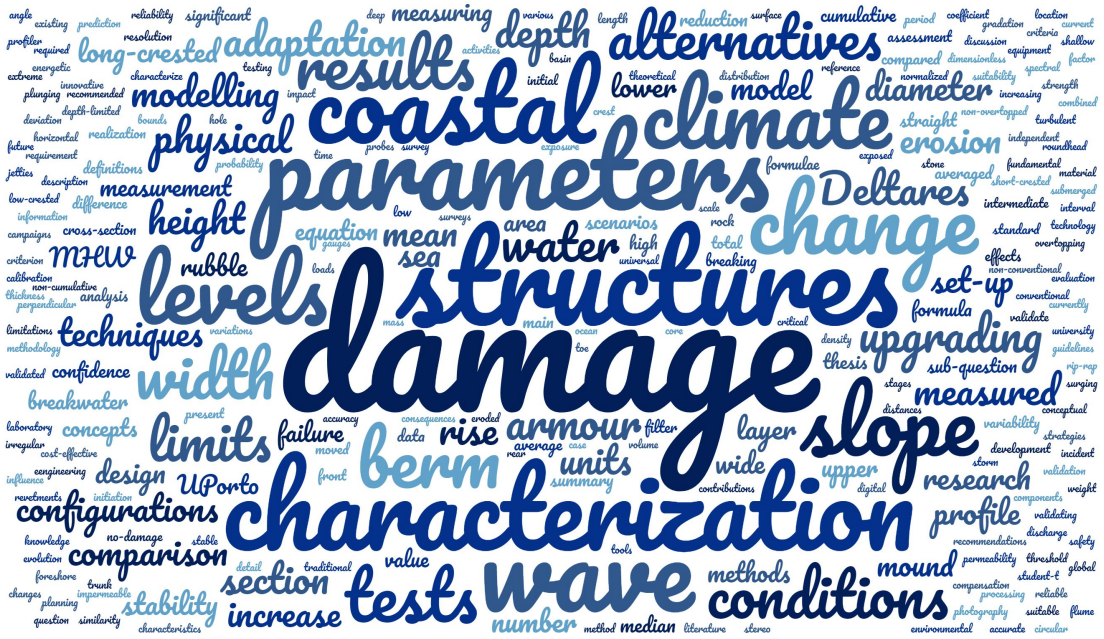

Cover photo: Ligura (Italy) licensed by iStock
Word cloud source: wordclouds.com

Damage assessment of coastal structures in climate change adaptation

CoMEM Master Thesis

by

Ermano de Almeida Sousa

As a requirement to attend the degree of

Erasmus+: Erasmus Mundus Master in Coastal and Marine Engineering and Management (CoMEM)

Erasmus+: Erasmus Mundus Mobility Programme

Taught at the following educational institutions:

Norges Teknisk- Naturvitenskapelige Universitet (NTNU)
Trondheim, Norway

Technische Universiteit Delft (TU Delft)
Delft, The Netherlands

University of Southampton
Southampton, United Kingdom

At which the student has studied from August 2015 to July 2017

to be defended publicly on Tuesday July 11, 2017 at 08:30 AM
at the Delft University of Technology

Under supervision of:	Prof. dr. ir. W. S. J. Uijttewaal,	TU Delft
	Dr. ir. B. Hofland (daily supervisor),	TU Delft/Deltares
	Dr. ir. M. R. A. van Gent,	Deltares
	Ir. J. P. van den Bos,	TU Delft

The Erasmus+: Erasmus Mundus MSc in Coastal and Marine Engineering and Management is an integrated programme including mobility organized by five European partner institutions, coordinated by Norwegian University of Science and Technology (NTNU).

The joint study programme of 120 ECTS credits (two years full-time) has been obtained at two or three of the five CoMEM partner institutions:

- Norges Teknisk- Naturvitenskapelige Universitet (NTNU) Trondheim, Norway
- Technische Universiteit (TU) Delft, The Netherlands
- Universitat Politècnica de Catalunya (UPC). BarcelonaTech. Barcelona, Spain
- University of Southampton, Southampton, Great Britain
- City, University London, London, Great Britain

During the first three semesters of the programme, students study at two or three different universities depending on their track of study. In the fourth and final semester an MSc project and thesis has to be completed. The two-year CoMEM programme leads to a multiple set of officially recognized MSc diploma certificates. These will be issued by the universities that have been attended by the student. The transcripts issued with the MSc Diploma Certificate of each university include grades/marks and credits for each subject.

Information regarding the CoMEM programme can be obtained from the programme coordinator:

Øivind A. Arntsen, Dr.ing.
Associate professor in Marine Civil Engineering
Department of Civil and Transport Engineering
NTNU Norway
Telephone: +4773594625 Cell: +4792650455 Fax: + 4773597021
Email: oivind.arntsen@ntnu.no

CoMEM URL: https://www.ntnu.edu/studies/mscomem

Preface

This master thesis is submitted as part of the requirement for obtaining the Master of Science in Coastal and Marine Engineering and Management (CoMEM), in the track of Coastal Engineering, at the Technical University of Delft. The work has been conducted in collaboration between the Technical University of Delft and Deltares, under the supervision of Bas Hofland. This thesis was sponsored by Deltares via Hydralab+ and includes physical modelling experiments carried out at Deltares and UPorto laboratory facilities.

This work was only possible with the guidance and support I could count on, to which I would like to express my gratitude. First of all, I would like to thank Bas Hofland for making this thesis possible. Thanks for giving me the opportunity of joining this amazing project and the continuous discussions, guidance and support throughout all the steps and aspects of this thesis.

Thanks to Wim Uijttewaal, Marcel van Gent and Jeroen van den Bos for being part of my Committee and for steering my progress during the thesis. Furthermore, I would like to thank Marcel van Gent for the constant guidance on the planning and execution of physical modelling tests and the analysis of the results.

I would like to acknowledge Deltares for sponsoring this thesis and the physical modelling tests via Hydralab+, making it possible to carry out the two measurement campaigns that support the conclusions of this thesis. It should also be highlighted the valuable advice from experts in different fields, in special Guido Wolters, Ivo van der Werf, Paul Meys and Wim Taal. In addition I would also like to acknowledge UPorto for having allowed and sponsored the tests carried out in their laboratory.

I would also like to express my gratitude towards Øivind Arntsen and Raed Lubbad from NTNU for providing me the opportunity of carrying out my first experiments in a wave flume, in the first semester of this master. That chance of working during one month in a wave flume allowed me not only to learn about physical modelling, but also to enjoy this research technique.

In addition, the work for long hours in a a wave flume or wave basin is much easier with the support of our laboratory technicians with so much experience and determination to make our experiments possible. Thanks to Gustav Jakobsen, Job Waaijerink, Peter Alberts and Pieter Pasterkamp for making all the tests possible. In addition, a very special thanks to Miguel Guerra for 3 months of working together in the laboratory and thus a significant contribution to this thesis.

In conclusion, thanks to everybody that contributed to this thesis, to all my previous projects and the new challenges still to come. The long list of people that makes everything possible includes professors, supervisors and colleagues from UPM, IST, Wasser, UPC, RWTH, Hilti, NTNU, UPorto, TUDelft, Deltares together with friends, family and the person with whom I enjoy the adventure of living.

Ermano de Almeida Sousa
Delft, July 2017

Summary

Coastal areas around the world have attracted settlements and human activities since the early stages of the history until nowadays. This has introduced continuous modifications to the natural characteristics of these coastal regions by means of coastal structures and engineering interventions. The design of such coastal structures has evolved significantly since the first quarter of the XXth Century, when more scientific design methods and formulae were developed. Nevertheless, further research is required given the stochastic nature of the environmental loads involved, the remaining uncertainties regarding the response of these structures to the applied loads and the growing impacts of climate change and sea level rise.

Four knowledge gaps are identified regarding the *Damage assessment of coastal structures in climate change adaptation*. Based on these, the objectives of this thesis are summarized as follows:

- **Climate change adaptation:** demand for validated upgrading alternatives.
- **Damage characterization:**

  Concepts: demand for unified damage characterization concepts.

  Parameters: demand for universal and more accurate damage characterization parameters.

  Measuring techniques: demand for validating the suitability of innovative survey methods.

These knowledge gaps are addressed using physical modelling results from two test campaigns. First, the UPorto deep water tests were done in a wave basin without a foreshore (non depth-limited waves), a 1:2 slope and permeable core. Second, the Deltares shallow water tests were carried out in a wave flume with a foreshore (depth-limited waves), a 1:3 slope, impermeable core and included both straight slope and four different berm configurations.

Damage characterization concepts

This first knowledge gap was addressed in two parts. First, defining a standard characterization width for physical modelling tests for coastal structures: $25D_{n50}$. For damage parameters that evaluate the width-averaged profiles (S and E_{2D}), this minimum width should be considered, taking into account the effects that wider test sections will have in the measured damage. For damage parameters that consider the maximum eroded depth within a characterization width ($E_{3D,1}$ and $E_{3D,5}$), this standard width should also be considered, in combination with an extreme value distribution in order to account for the increase in the probability of observing a maximum erosion in wider structures (length effect). Second, the calibrated damage limits and damage parameters for rock armoured slopes with a thickness of $2D_{n50}$ are the following:

- **Damage initiation:** defined as the condition where a circular hole of $1D_{n50}$ diameter and a depth of $1D_{n50}$ is observed in the armour layer:

  $E_{3D,1}$ = 1; $E_{3D,5}$ = 0.3; E_{2D} = 0.2; S = 1.

- **Intermediate damage:** defined as the condition where a circular hole of $1D_{n50}$ diameter and a depth of $1.5D_{n50}$ is observed in the armour layer:

  $E_{3D,1}$ = 1.5; $E_{3D,5}$ = 0.8; E_{2D} = 0.6; S = 5.

- **Failure limit:** defined as the condition where a circular hole of $1D_{n50}$ diameter and a depth of $2D_{n50}$ is observed in the armour layer:

  $E_{3D,1}$ = 2.0; $E_{3D,5}$ = 1.3; E_{2D} 1.0; S = 12.

Damage characterization parameters

This second knowledge gap was addressed by evaluating the suitability of the different damage parameters to be used as an universal damage parameter. It was defined that $E_{3D,5}$ is the parameter that can better describe the damage and remaining strength of conventional and non-conventional structures. The key reasons for defining this parameter as the reference damage characterization parameter are the following:

- **Low bias error:** the damage to the structure is clearly captured, without including hidden erosion present in the parameters that consider width-averaged profiles.
- **Low random error:** this parameter describes the damage to the structure with very low variability, what increases the confidence in the measured and expected damage.
- **Distinguish damage range:** the different states of damage to the structure can be recognized according to the limits established.
- **Constant value for different structures:** for all structure configurations this parameter can be used without any modification.

In addition, the length effect of rock armoured coastal structures, defined as the increase in the probability of observing larger damage in increasingly wider structures, was also addressed. According to the results from the physical modelling tests, it was observed that the measured damage for a coastal structure of $25D_{n50}$ can increase 150% for a similar structure 10 times wider. Thus, it is demonstrated that the damage characterization of coastal structures should include an extreme distribution in order to account for this length effect.

Damage characterization measuring techniques

This third knowledge gap was addressed by remarking the importance of innovative and high resolution measuring techniques for delivering accurate damage characterization of coastal structures. Such techniques allow the use of the most precise damage parameters ($E_{3D,5}$), the reduction of bias errors related with hidden erosion and the reduction of random errors related with the position of the measured profiles.

Climate change adaptation

This fourth knowledge gap was addressed by validating the suitability of berms as an adaptation alternative. It was observed that a slope with a berm increases significantly the stability of the structure, reducing the damage caused by the impact of extreme waves and increasing its resilience in sea level rise scenarios. In such configuration, the effects on the porosity and hydrodynamic patterns were very positive for the stability of the structure. The most favourable location of the berm was observed at one level below the design water level. Furthermore, the wide configurations ($10D_{n50}$) were more effective than the narrow configurations ($5D_{n50}$). In summary, the presence of a wide berm one level below the design water level lead to reductions of up to 80% of the measured damage in both S and $E_{3D,5}$ parameters.

Regarding the damage evaluation, it was also described the suitability and accuracy of the parameter $E_{3D,5}$ to better describe the state of the upgrading structure, instead of the parameter S. It was shown that when evaluating the damage depth with $E_{3D,5}$ it is possible to better define the damage level of the structure and the failure hazard (defined as the exposure of the filter layer to the wave action).

Thus, berm configurations have been validated with the present measurements as an upgrading alternative to face sea level rise scenarios. For damage characterization of such non-standard coastal structures, parameter $E_{3D,5}$ is also validated as the most suitable damage parameter.

Conclusions

In conclusion, this study includes the validation of the damage criteria required for a precise assessment of a coastal structure (second knowledge gap), the validation of an universal damage parameter for rubble mound structures (third knowledge gap), the validation of the benefits of innovative measuring techniques when carrying out physical modelling tests (fourth knowledge gap) and the validation of upgrading alternatives for climate change scenarios (first knowledge gap).

Thus, it can be stated that with these definitions, parameters and measuring techniques, a complete method for damage characterization of coastal structures is presented. It was also defined how this damage characterization method can be used to precisely and accurately describe the damage to conventional and non-conventional coastal structures. Furthermore, this method was also used to describe the effects of not only current environmental forces acting on the structures but also future and more energetic scenarios. For such future scenarios, adaptation alternatives for coastal structures were evaluated and berm configurations are recommended for their upgrading.

Future research on damage characterization of coastal structures is needed in order to evaluate, adjust and generalize the conclusions made in this thesis, considering additional structure configurations and environmental loading conditions. These future configurations should combine variations in the slope and porosity with the testing of conventional and non-conventional structures and 3D features such as roundheads. In addition, the environmental loads should consider different wave conditions (including non-breaking waves and a variety of breaking wave conditions), water levels (including constant and varying water levels) and overtopping conditions (including low- and high-crested structures).

Furthermore, a summary of identified key research areas still to be addressed are presented and briefly described hereafter. First, the constant damage limits observed in this thesis for different structures (slopes 1:2 and 1:3) should be further investigated given that it contradicts current design criteria. Second, the reduced difference between cumulative and non-cumulative damage measurements should be evaluated considering both rock armoured slopes and other armour units such as concrete cubes. Third, the scaling limits for physical modelling tests should also be evaluated in order to optimize the design of model set-ups, since the scale effects predicted by the existing literature were not observed in the Deltares test results. And fourth, the random behaviour of damage should be further analyzed, in special for better describing the length effect of coastal structures in order to improve the statistical tools for probabilistic design.

Future research on adaptation alternatives for coastal structures facing climate change should include the testing of not only additional upgrading solutions, but also different environmental forcing scenarios. Such different testing conditions should also include conditions where overtopping takes place and therefore the upgrading of the structure should take into account the effects at the front slope, rear slope and the activities that take place in the area protected by the structure.

Contents

Preface iii

Summary v

1 Introduction 1
- 1.1 Motivation . . . 1
  - 1.1.1 Background . . . 2
  - 1.1.2 Problem description . . . 3
- 1.2 Objectives . . . 4
- 1.3 Methodology . . . 5
- 1.4 Structure . . . 6

2 Literature 7
- 2.1 Rubble mound coastal structures . . . 7
  - 2.1.1 General concepts . . . 7
  - 2.1.2 Stability of straight slopes . . . 9
  - 2.1.3 Stability of slopes with a berm . . . 11
- 2.2 Damage characterization methods . . . 12
  - 2.2.1 Percentage of moved units . . . 13
  - 2.2.2 Number of moved units . . . 13
  - 2.2.3 Eroded depth . . . 15
- 2.3 Physical modelling techniques . . . 16
  - 2.3.1 Guidelines . . . 17
  - 2.3.2 Measuring tools . . . 18
- 2.4 Climate change adaptation alternatives . . . 19
  - 2.4.1 Climate change impacts . . . 19
  - 2.4.2 Upgrading alternatives . . . 20

3 Theoretical development 23
- 3.1 Definitions . . . 23
  - 3.1.1 Parameters . . . 23
  - 3.1.2 Method components . . . 24
- 3.2 Establishing damage concepts . . . 28
  - 3.2.1 Characterization width . . . 28
  - 3.2.2 Damage limits . . . 28
- 3.3 Establishing damage parameters . . . 29
- 3.4 Measuring techniques . . . 29

4 Physical modelling test set-up 31
- 4.1 Test planning . . . 31
  - 4.1.1 UPorto deep water tests . . . 31
  - 4.1.2 Deltares shallow water tests . . . 31
- 4.2 UPorto deep water tests set-up . . . 32
- 4.3 Deltares shallow water tests set-up . . . 35
- 4.4 Measuring technique . . . 38

5 Physical modelling test results 39
- 5.1 Uporto deep water test results . . . 39
- 5.2 Deltares shallow water test results . . . 42
- 5.3 Test results analysis . . . 47
  - 5.3.1 Straight slope . . . 48
  - 5.3.2 Slopes with a berm . . . 49

6 Damage characterization methods **51**
6.1 Validating damage concepts . . . 51
6.1.1 Characterization width . . . 51
6.1.2 Damage limits . . . 55
6.2 Validating damage parameters . . . 58
6.2.1 Damage parameters analysis . . . 58
6.2.2 Extreme damage distribution for $E_{3D,5}$ . . . 62
6.3 Validating measuring techniques . . . 65
6.4 Discussion of sub-questions 1, 2 and 3 . . . 66

7 Climate change adaptation alternatives **69**
7.1 Low-crested structures . . . 69
7.2 Upgrading alternatives results . . . 70
7.2.1 Straight slope . . . 71
7.2.2 Wide high berm . . . 72
7.2.3 Narrow high berm . . . 72
7.2.4 Wide low berm . . . 73
7.2.5 Narrow low berm . . . 74
7.3 Evaluation of alternatives . . . 75
7.3.1 Berm configurations compared with straignt slope . . . 75
7.3.2 Berm configurations analysis . . . 77
7.4 Discussion of sub-question 4 . . . 78

8 Conclusions and recommendations **81**

Bibliography **85**

List of Figures **87**

List of Tables **89**

A UPorto test results **91**

B Deltares test results **95**

C Characterization width analysis **105**

D Comparison damage parameters **111**

E Validation 3D damage parameters **117**

F Evaluation of adaptation alternatives **121**

G Granular material analysis **127**

H All damage measurements **131**

I Tests results comparison **137**

J Damage limits prediction **139**

1

Introduction

Coastal areas around the world have presented advantageous conditions for the establishment of settlements and human activities since the early stages of history. Among other advantages such as fertile soils, the interface between land and sea allowed the development of trading and exchange between communities otherwise isolated. These favourable conditions have then justified the significant proportion of the world population which has settled down in coastal areas. As societies have developed until nowadays, the urbanization and human activities in the coastal areas have continued to increase, accompanied by significant modifications of the natural characteristics of the coastal areas. These modifications of the coastal areas have been carried with two main objectives briefly described hereafter. First, with the aim of enhancing and protecting the development of urban areas, by means of land reclamation and flood/erosion protection using dikes, groins, revetments or seawalls. Second, with the aim of enhancing the development of human activities, by means of the construction of harbours/ports and stabilization of navigation inlets and channels using monolithic breakwaters, rouble mound breakwaters or jetties. The design of such coastal structures has evolved significantly since the first quarter of the XXth Century, when more scientific design methods and formulae were developed. Nevertheless, further research is required due to the stochastic nature of the environmental loads acting on coastal structures and the remaining limitations in the knowledge on the structure response to these loads.

This thesis addresses the required research on the assessment and characterization of damage to coastal structures produced by the impact of environmental loads. The development of consistent and accurate damage characterization methods will allow to fully describe the response, as well as the remaining strength of the coastal structures after facing a given loading condition. Climate change consequences are also part of this research, since this phenomenon is steadily increasing the environmental loads acting on coastal structures. Among others, the main consequences of climate change considered are the changes in the design water level and design wave loads. Furthermore, the analysis of sea level rise impacts on various reinforcement alternatives will provide a guide for the upgrade of coastal structure facing climate change scenarios.

In the next sections the following is presented: the motivations that justify this thesis, the objectives and research questions to be addressed, the research methodology and the structure of the thesis.

1.1. Motivation

The aim of this section is to describe the demand for the research completed during this master thesis. This is addressed in the two following sub-sections: a review of the field of study (Background) and the analysis of the limitations in the current knowledge (Problem description).

1.1.1. Background

Coastal structures are designed in order to address a variety of requirements in the protection, development and management of coastal areas and human activities (see Figure 1.1). For the various possible requirements a number of different structures can be designed, such as earthen dikes, groins, revetments, seawalls, monolithic breakwaters, rubble mound breakwaters and jetties, among others. The research developed in this thesis is focussed on the damage to structures protected with a randomly placed rock armour, i.e. revetments, rubble mound breakwaters and jetties. From now on, such structures will be described as rubble mound structures.

Figure 1.1: Punta Langosteira breakwater, singular coastal structure (Source: EFE).

The design methods for rubble mound structures have developed significantly since the first studies on the stability and required weight of armourstone and concrete units in the armour layers of coastal structures (Iribarren 1938). In the following decades (Hudson 1959) contributed with a more general and simple formulae for the design or rubble mound structures with rock armour and concrete armour units based on physical modelling with regular wave action. van der Meer (1988) presented a significant step forward with the development of more sophisticated design formulae for rock armour layers based in small-scale and large-scale physical modelling tests with irregular wave action. CIRIA et al. (2007) is currently the most referred guideline for the design of rubble mound structures. In future designs the effects of climate change (IPCC 2013, Weisse et al. 2014) on the stability of coastal structures should also be considered. The increase in water depths and extreme wind/wave action will require the upgrade of coastal structures, as discussed in Burcharth et al. (2014), in order to maintain or increase currently safety levels.

In the design and assessment of coastal structures, damage can be defined as "the movement of armour units as consequence of the impact of environmental loads" (van der Meer 1988). Although damage is an essential concept in order to describe the response of coastal structures to imposed load conditions and the remaining strength, it was not incorporated in the first stages of the development of design methods and formulae (Iribarren (1938)). The first mention to damage in the design formulae for rubble mound structures is found in Hudson (1959), who developed his formula for a single "no-damage" condition when less than 1% of the total number of units in the armour layer are displaced (D). Later on, the coefficient of the Hudson formula was calibrated for conditions when a limited amount of damage is allowed and more than 1% of stones are removed. In the study of stability of rip-rap, Thompson & Shuttler (1975) incorporates a concept of damage (N_Δ) as "the number of D_{50} spherical stones eroded from a $9d_{50}$ wide section", combined with a initial definition of "no-damage" and "failure". Also focussed on rip-rap stability, Broderick (1984) defined a damage parameter obtained from the comparison between the initial and final averaged profile over the width of the test section. This damage parameter (originally named as D', but currently known as S) is obtained considering the eroded area "divided by the cube-root squared of the median stone weight divided by the unit weight of rip-rap". This author also introduces a different definition of "no-damage" and "failure" conditions.

van der Meer (1988) renamed the damage parameter from Broderick (1984), naming it as the currently known damage parameter "S" with the simplified form of eroded area (calculated as the difference between the initial and final width-averaged profiles) divided by the nominal diameter of the armour units. This expression of damage (S) is present in the Van der Meer formulae, which is nowadays the most widely used design formulae for rock armoured slopes in deep water. In this formula, "no-damage" and "failure" conditions are defined following the contributions of Broderick (1984): "start of damage" is described when S is smaller than 2 and "failure" is reached when the filter layer becomes exposed. Later on, Melby & Kobayashi (1998) introduced 3 additional damage parameters such as the normalized erosion depth (E), the normalized erosion length (L) and the normalized cover depth (C) obtained for averaged profiles over the width. Hofland et al. (2014, 2011) recently incorporates innovative and more accurate measuring techniques for the survey of damage in physical modelling tests and presents a three dimensional erosion depth parameter ($E_{3D,m}$) to be used in the damage characterization of conventional and non-conventional coastal structures.

1.1.2. Problem description

Considering the background information described in the previous sub-section, the following four areas of knowledge gaps can be identified:

First, although the research on climate change and its consequences such as the increase in water levels and wave/wind conditions is already advanced (IPCC 2013, Weisse et al. 2014), no guidelines are currently available regarding the upgrading alternatives for coastal structures facing such scenarios. Burcharth et al. (2014) provides a first contribution on upgrade alternatives based on desk tools only (see Figure 1.2). With the aim of providing more reliable recommendations for the upgrade of coastal structures facing sea level rise caused by climate change, further research is required based on physical model test results. In addition, in order to ensure a reliable evaluation of the upgrading alternatives, the limitations of the currently used damage characterization concepts, parameters and testing techniques must be overcome.

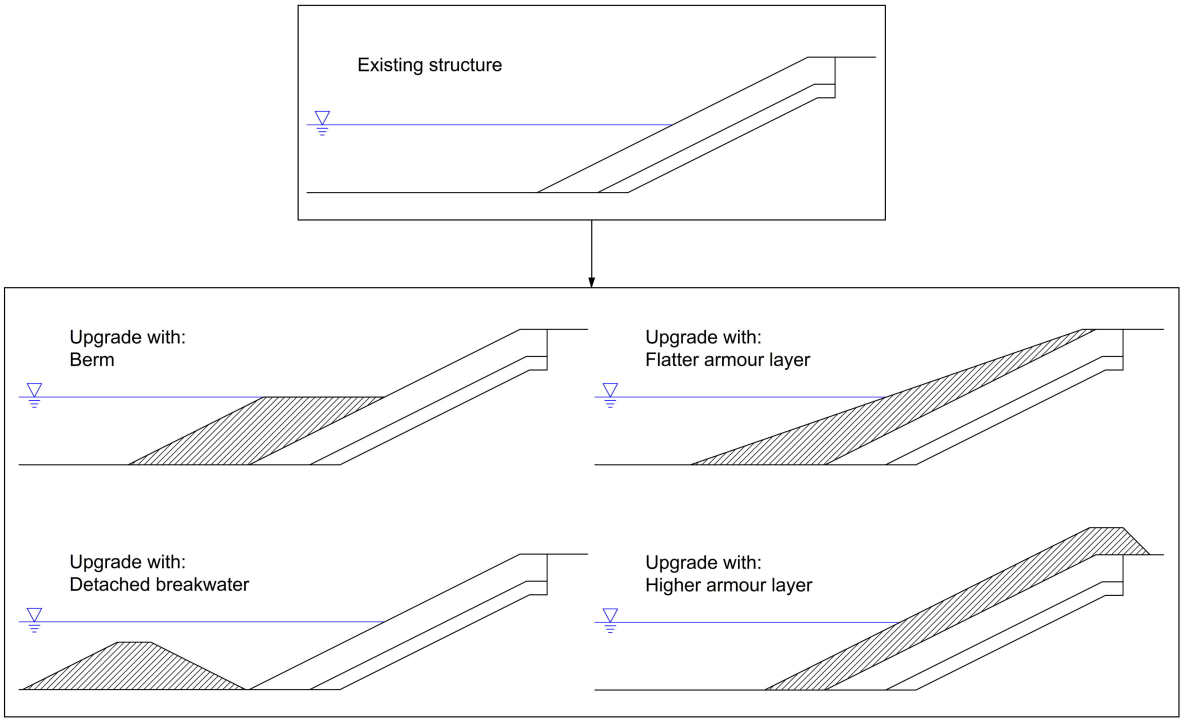

Figure 1.2: Upgrading of coastal structures (based on Burcharth et al. (2014)).

Second, the previously defined concepts of ”no-damage”, ”start of damage”, ”intermediate damage” and ”failure” are not accurately and uniformly described. Different authors established the current limits based on unconsolidated arguments, also influenced by low accuracy measurement techniques. No-damage condition was described by Thompson & Shuttler (1975) as ”the point at which the erosion of rip-rap shows sharp increase with increasing wave height” without a quantitative definition of this lower limit. Nevertheless, this author precisely defines failure ”when a hole with $D_{50}/2$ diameter is observed in the armour down to the filter layer”, measured with a hand held gauge with a hemispherical foot of $D_{50}/2$ diameter. Broderick (1984) defines the condition of no-damage as D’(or S) = 2 ”which is the lowest level of damage that can be consistently detected in the survey data” while failure is described ”when enough rip-rap is shifted to expose the filter material”. van der Meer (1988) defines these limits in a similar manner: start of damage is described as S = 2 for a 1:2 slope and failure is reached when the filter layer becomes visible, without describing an extension threshold. Taking into account the arguments described above, contributions are needed in order to develop unified descriptions of the damage limits for the assessment and design of rubble mound structures.

Third, the suitability of currently used damage parameters to accurately characterize the response and remaining strength of rubble mound structures needs to be further investigated. The damage parameter ”S” used by van der Meer (1988) provides only limited information about the structure conditions and can only be considered for conventional trunk sections. The innovative damage parameters presented by Melby & Kobayashi (1998) and Hofland et al. (2014, 2011) can provide a more accurate description of damage, providing a significant improvement in the characterization of the structure conditions. Thus, the use of a generic damage parameter which is independent of the cross-section geometry, will allow a direct characterization of conventional and non-conventional coastal structures or singular elements such as roundheads.

Fourth, damage characterization procedures for rubble mound structures can increase their accuracy and reliability due to the continuous development of testing and measuring techniques. The new measuring techniques such as Digital Stereo Photography (Hofland et al. 2014, 2011) are considered an innovative but consolidated technology that provides model surveys with millimeter resolution. In this sense it is required to elaborate a clear description of the advantages of more accurate measuring techniques and the expected improvement of the damage characterization when compared to measurements obtained by traditional equipment with lower resolution.

Following the previously identified four areas of knowledge gaps, the problem description of this thesis can be summarized as follows:

- **Climate change adaptation:** demand for validated upgrading alternatives.
- **Damage characterization:**

  Concepts: demand for unified damage characterization concepts.

  Parameters: demand for universal and more accurate damage characterization parameters.

  Measuring techniques: demand for validating the suitability of innovative survey methods.

1.2. Objectives

The four knowledge gaps identified in the previous section justify the demand for the research carried out throughout this thesis. Thus, the essential objective of this thesis is to overcome the identified knowledge gaps answering the following research question:

Research question:

How can we improve the reliability in the assessment of rubble mound structures based on physical modelling in current and future scenarios by introducing accurate and universal damage characterization methods?

This main research question is addressed based on the combined answer of the following four research sub-questions:

Research sub-questions:

1. **How can we establish and validate unified concepts of ”damage initiation”, ”intermediate damage” and ”failure” in rubble mound structures?**
2. **How can we establish and validate an universal damage parameter to accurately characterize the response as well as the remaining strength of rubble mound structures?**
3. **How can we validate the increase in reliability of physical modelling tests results based on innovative and higher accuracy testing and measuring techniques?**
4. **How can we validate the suitability of upgrading alternatives for coastal structures facing sea level rise scenarios?**

1.3. Methodology

The research questions described in the previous section are addressed into three parts. **Part I** defines the theoretical concepts, parameters and methods in order to overcome current limitations on damage characterization. **Part II** includes the validation of the theoretical damage concepts, parameters and methods based on the analysis of physical modelling tests results. **Part III** presents the contributions on suitable upgrading alternatives for coastal structures facing sea level rise scenarios. This methodology is illustrated in Figure 1.3.

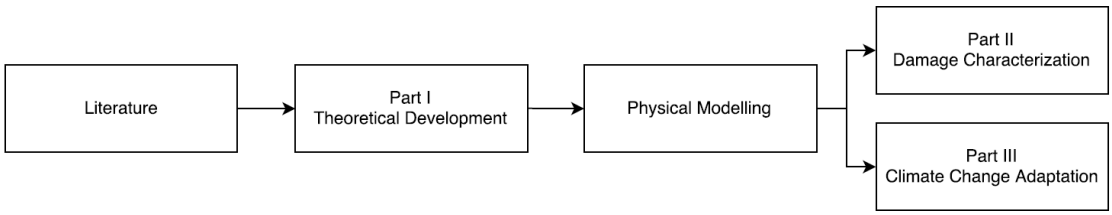

Figure 1.3: Thesis methodology and parts.

- **Part I:** initiates research sub-questions 1, 2 and 3.
- **Part II:** finalizes research sub-questions 1, 2 and 3.
- **Part II:** addresses research sub-question 4.

Two main physical modelling test campaigns are considered in this thesis, carried out within the Hydralab+ Project. The main characteristics of these tests are shown below:

- **UPorto deep water tests:** carried out in a wave basin where where damage to a rubble mound breakwater was measured on a 4 meters wide trunk section and its roundhead.
- **Deltares shallow water tests:** carried out in a wave flume where damage to a rubble mound breakwater was measured on a 1 meter wide trunk section.

The testing conditions were defined with the aim of obtaining the largest number of different conditions in order to contribute to a more reliable validation of the theoretical concepts, parameters and methods. Tests included cumulative and non-cumulative tests, constant water levels and sea level rise scenarios, long-crested and short-crested wave conditions, straight slopes and slopes with a berm, 2D trunk sections and 3D elements such as roundheads.

In order to evaluate the damage to tested structures, surveys were carried out before and after every test run with the Digital Stereo Photography technique developed by Deltares. This technique provided 3D surveys of the rubble mound structure with an resolution of 1mm.

The detailed analysis of the physical modelling results allows to complete Part II and Part III providing the required answer to the four research sub-question and, in consequence, the main research question of this thesis.

1.4. Structure

The structure of this report follows the methodology described in the previous section and is depicted in Figure 1.4. In addition, a brief summary of the chapters are presented below.

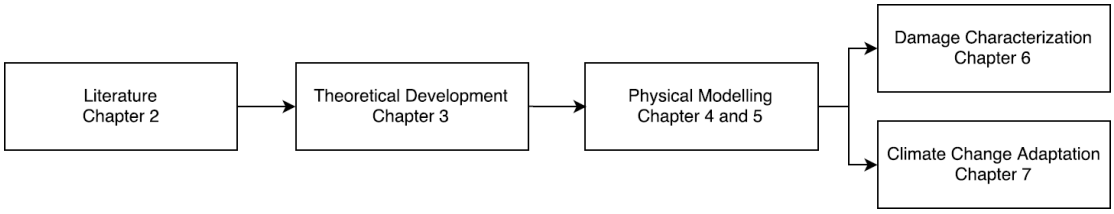

Figure 1.4: Report structure and chapters.

- **Chapter 2 - Literature:** presents the essential review of the existing knowledge and references in the fields addressed throughout this thesis.
- **Chapter 3 - Theoretical development:** establishes of the theoretical concepts, perimeters and methods to be used in the damage characterization of rubble mound structures.
- **Chapter 4 - Physical modelling test set-up:** introduces the validation tools and the conditions considered in the physical modelling tests.
- **Chapter 5 - Physical modelling test results:** analyses the validation data obtained through physical modelling tests.
- **Chapter 6 - Damage characterization methods:** validates the theoretical concepts, parameters and methods based on the physical modelling test results.
- **Chapter 7 - Climate change adaptation alternatives:** evaluates upgrade alternatives for coastal structures facing sea level rise cause by climate change.
- **Chapter 8 - Conclusions and recommendations:** provides general conclusions on the thesis study and recommendations for future research.

2

Literature

This chapter presents a summary of the existing knowledge on the topics considered in this research. It includes the most important methods and formulae for the conceptual design of rubble mound coastal structures, concepts and methods for damage characterization, physical modelling techniques and climate change adaptation alternatives.

2.1. Rubble mound coastal structures

This section describes the most important concepts, methods and formulae for the conceptual design of rubble mound coastal structures. It includes a description of basic design concepts, the development of the design methods throughout time and the currently used formulae for straight slopes and slopes with a berm.

2.1.1. General concepts

This sub-section presents general concepts to be considered in the conceptual design of coastal structures. These concepts can be divided into two groups: wave properties and slope stability.

Wave Properties

Wave action represents the main environmental load to be considered in the design of coastal structures, thus its basic properties need to be described. Figure 2.1 shows in spatial and time scales the main wave parameters.

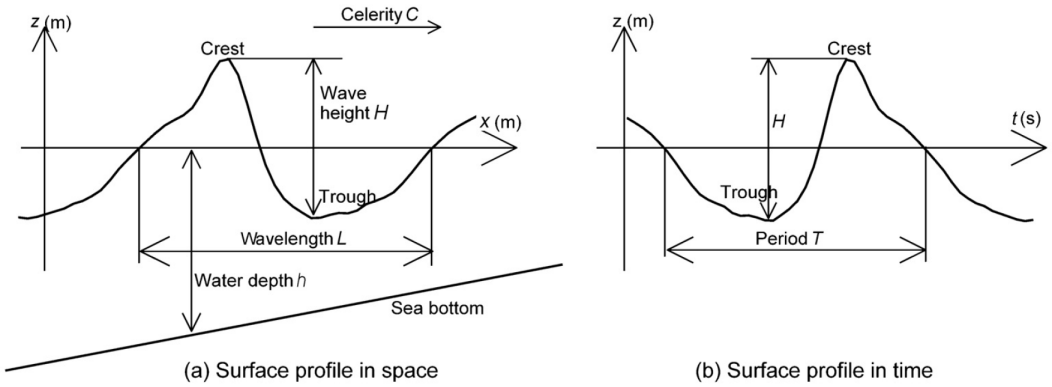

Figure 2.1: Wave parameters in space and time (CIRIA et al. 2007).

In the list below, the most important wave parameters are described. In addition, Equation 2.1 presents the dispersion relation which relates the wave parameters according to the linear wave theory.

H	=	Wave height	[m]
T	=	Wave period	[s]
L	=	Wave length	[m]
s	=	Wave steepness (H/L)	[-]
h	=	Water depth	[m]
ω	=	Angular frequency ($\omega = 2\pi/T$)	[rad/s]
k	=	Wave number ($k = 2\pi/L$)	[rad/m]
α	=	Slope angle	[°]

$$\omega^2 = gk\tanh(kh) \tag{2.1}$$

The action of waves on coastal structures is function of the wave properties in combination with the slope angle (α). The Irribaren number (ξ), also known as surf similarity parameter, can be calculated as shown in Equation 2.2 as defined in Battjes (1974). This parameter not only defines the breaking types shown in the list below, but also is present in the stability formulae described in the next sections (van der Meer 1988).

$$\xi = \frac{\tan\alpha}{\sqrt{s_0}} = \frac{\tan\alpha}{\sqrt{H/L_0}} = \frac{\tan\alpha}{\sqrt{(2\pi H)/(gT^2)}} \tag{2.2}$$

$\xi < 0.5$	$\Rightarrow$	Spilling breaking
$0.5 < \xi < 3.0$	$\Rightarrow$	Plunging breaking
$3.0 < \xi < 5.0$	$\Rightarrow$	Collapsing breaking
$\xi > 5.0$	$\Rightarrow$	Surging breaking

Slope stability

The most important parameter for the slope stability under wave attack is the stability number (N_s) defined in Equation 2.3 (CIRIA et al. 2007):

$$N_s = \frac{H}{\Delta D} \tag{2.3}$$

where:

H (m): wave height, usually described as the significant wave height (H_s), either defined as the average of the highest one third of the waves in a record ($H_{1/3}$) or by the spectral significant wave (H_{m0}) calculated as $4\sqrt{m_0}$. In deep waters, both definitions of significant wave provide equivalent results. In shallow waters, differences increase up to $H_{1/3} = 1.3H_{m0}$.

Δ (-): relative buoyant density (see Equation 2.4).

D (m): characteristic size or diameter, usually described as the median nominal diameter (D_{n50}) for rock slopes (see Equation 2.5).

$$\Delta = \frac{\rho_s - \rho_w}{\rho_w} \tag{2.4}$$

where ρ_s (kg/m^3) is the apparent mass density of the rock and ρ_w (kg/m^3) is the density of the water.

$$D_{n50} = \left(\frac{M_{50}}{\rho_s}\right)^{1/3} \tag{2.5}$$

where M_{50} (kg) is the rock mass determined by weighting and ρ_s (kg/m^3) is the apparent mass density of the rock. In addition, the nominal median diameter (D_{n50}) can be related to the diameter obtained by sieving (D) according to Equation 2.6.

$$D_n = 0.84D \tag{2.6}$$

Considering Equation 2.3 and introducing the the significant wave height (H_s) and the nominal median diameter (D_{n50}), the stability number can be be expressed as in Equation 2.7.

$$N_s = \frac{H_s}{\Delta D_{n50}} \tag{2.7}$$

2.1.2. Stability of straight slopes

This section presents the currently used design formulae for straight rock slopes. As the first developments, two contribution during the first half of the XXth Century are briefly described hereafter: Iribarren (1938) and Hudson (1959). The design formula presented by Iribarren (1938) is considered the first significant development in the conceptual design of rock slopes under wave attack. This formula is based on the equilibrium of forces, combined with a calibration coefficient to be obtained through physical modelling tests with regular wave action. Following various calibration tests for the Iribarren formula, Hudson (1959) introduced a different formula also based on physical modelling tests with regular wave action which is still in use (CERC (1977, 1984).

Following the contributions described previously, the formulae developed by van der Meer (1988, 1995) is nowadays the most widely used design reference for rock armoured slopes in deep water. These stability equations were developed based on the work of Thompson & Shuttler (1975) and additional physical modelling tests with irregular wave action including large number of different configurations. These formulae distinguishes two breaking conditions for which different equations apply (see Equations 2.11 and 2.12). For deep water conditions they are shown below:

For plunging wave breaking ($\xi_m < \xi_{cr}$) in deep water:

$$\frac{H_s}{\Delta D_{n50}} = c_{pl} P^{0.18} \left(\frac{S}{\sqrt{N}}\right)^{0.2} \xi_m^{-0.5} \tag{2.8}$$

For surging wave breaking ($\xi_m \geq \xi_{cr}$) in deep water:

$$\frac{H_s}{\Delta D_{n50}} = c_s P^{-0.13} \left(\frac{S}{\sqrt{N}}\right)^{0.2} \sqrt{\cot\alpha}\, \xi_m^P \tag{2.9}$$

where:

H_s (m): significant wave height.

Δ (-): relative buoyant density.

D_{n50} (m): median nominal diameter.

c_{pl} (-): 6.2, plunging coefficient ($\sigma = 0.4$).

c_s (-): 1.0, surging coefficient ($\sigma = 0.08$).

P (-): notional permeability (see Figure 2.2).

S (-): damage level parameter (see Equation 2.10).

ξ_m (-): surf similarity parameter using the mean wave period (T_m) (see Equation 2.11).

ξ_{cr} (-): critical value of surf similarity parameter (see Equation 2.12).

N (-): number of incident waves.

α (°): slope angle.

$$S = \frac{A_e}{D_{n50}^2} \tag{2.10}$$

where A_e (m²) is the eroded area in the averaged cross-section profile.

$$\xi_m = \frac{\tan\alpha}{\sqrt{(2\pi H_s)/(gT_m^2)}} \tag{2.11}$$

$$\xi_{cr} = \left[\frac{c_{pl}}{c_s} P^{0.31} \sqrt{\tan\alpha}\right]^{\frac{1}{P+0.5}} \tag{2.12}$$

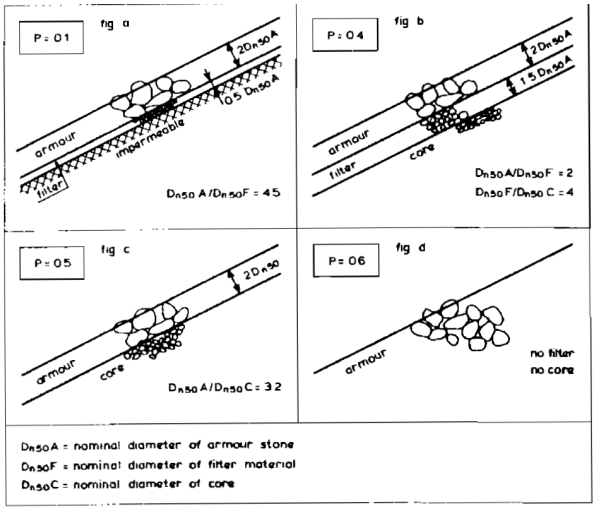

Figure 2.2: Notional permeability coefficient (van der Meer 1988).

For shallower water depths, the distribution of wave heights deviates from the Rayleigh distribution and in these conditions the 2% wave height ($H_{2\%}$) describes better the stability of the armour than the significant wave height (H_s). van der Meer (1988) proposes additional formulae for these conditions using the $H_{2\%}$, which were adapted by van Gent et al. (2003) considering the spectral wave period $T_{m-1,0}$ instead of the mean period from the time-domain T_m and recalibrating the coefficients c_{pl} and c_s:

For plunging wave breaking ($\xi_{m-1,0} < \xi_{cr}$) in shallow water:

$$\frac{H_s}{\Delta D_{n50}} = c_{pl} P^{0.18} \left(\frac{S}{\sqrt{N}}\right)^{0.2} \left(\frac{H_s}{H_{2\%}}\right) \left(\xi_{m-1,0}\right)^{-0.5} \tag{2.13}$$

For surging wave breaking ($\xi_{m-1,0} \geq \xi_{cr}$) in shallow water:

$$\frac{H_s}{\Delta D_{n50}} = c_s P^{-0.13} \left(\frac{S}{\sqrt{N}}\right)^{0.2} \left(\frac{H_s}{H_{2\%}}\right) \sqrt{\cot\alpha} \left(\xi_{m-1,0}\right)^{P} \tag{2.14}$$

where:

H_s (m): significant wave height.

Δ (-): relative buoyant density.

D_{n50} (m): median nominal diameter.

$H_{2\%}$ (m): 2% wave height.

c_{pl} (-): 8.4, plunging coefficient ($\sigma = 0.7$).

c_s (-): 1.3, surging coefficient ($\sigma = 0.15$).

$\xi_{m-1,0}$ (-): surf similarity parameter using the spectral wave period $T_{m-1,0}$ (see Equation 2.15).

$T_{m-1,0}$ (-): spectral wave period equal to m_{-1}/m_0.

$$\xi_{m-1,0} = \frac{\tan\alpha}{\sqrt{(2\pi H_s)/(gT_{m-1,0}^2)}} \tag{2.15}$$

Furthermore, van Gent et al. (2003) introduces an additional formulae for the stability of rock slopes with shallow foreshores. This formula is presented below, where the permeability of the structure is introduced as the ratio between the armour median nominal diameter (D_{n50}) and the core median nominal diameter ($D_{n50-core}$).

$$\frac{H_s}{\Delta D_{n50}} = 1.75\sqrt{\cot\alpha}\left(1 + \frac{D_{n50-core}}{D_{n50}}\right)^{2/3}\left(\frac{S}{\sqrt{N}}\right)^{0.2} \tag{2.16}$$

where:

D_{n50} (m): median nominal diameter (of the armour).

$D_{n50-core}$ (m): core median nominal diameter.

In addition, the design of coastal structures should consider not only the stability of the trunk at its final constructed stage. Other key aspects should also be considered: singular elements such as round-heads and toes, non standard environmental forcing such as oblique waves and the stability during the construction phase (see CIRIA et al. (2007), van Gent & van der Werf (2010), Hofland et al. (2014), van Gent (2014), van Gent & van der Werf (2014) and Mulders et al. (2015)).

2.1.3. Stability of slopes with a berm

van Gent (2013) presents a design method for rubble mound structures with a static stable berm, where only reduced movement is allowed. This method is based on the modified formulae from van der Meer (1988) adapted by van Gent et al. (2003) (see Equations 2.13 and 2.14). The main equations of this method are presented below and divided between the upper slope and the lower slope (which includes the damage to the horizontal berm):

For the upper slope stability:

$$\frac{H_s}{\Delta D_{n50}} = \left(\frac{1}{\gamma_{berm,up}\gamma_{pos}}\right)^{0.2} c_{pl} P^{0.18}\left(\frac{S}{\sqrt{N}}\right)^{0.2}\left(\frac{H_s}{H_{2\%}}\right)\left(\xi_{m-1,0}\right)^{-0.5} \tag{2.17}$$

For the lower slope stability:

$$\frac{H_s}{\Delta D_{n50}} = \frac{1}{\gamma_{berm,low}} c_{pl} P^{0.18}\left(\frac{S}{\sqrt{N}}\right)^{0.2}\left(\frac{H_s}{H_{2\%}}\right)\left(\xi_{m-1,0}\right)^{-0.5} \tag{2.18}$$

where:

H_s (m): significant wave height.

Δ (-): relative buoyant density.

D_{n50} (m): median nominal diameter.

c_{pl} (-): 8.4, plunging coefficient ($\sigma = 0.7$).

$\gamma_{berm,up}$ (-): reduction factor (see Equation 2.19).

γ_{pos} (-): reduction factor (see Equation 2.20).

$\gamma_{berm,low}$ (-): reduction factor (see Equations 2.21 and 2.22).

P (-): notional permeability.

S (-): damage level parameter.

$\xi_{m-1,0}$ (-): surf similarity parameter using the spectral wave period $T_{m-1,0}$.

$T_{m-1,0}$ (-): spectral wave period equal to m_{-1}/m_0.

N (-): number of incident waves.

α (°): slope angle.

$$\gamma_{berm,up} = 1 - 0.15\xi_{m-1,0}\left(\frac{B}{H_s}\right)^{0.3} \quad \text{with} \quad \gamma_{berm,up} \geq 0 \tag{2.19}$$

$$\gamma_{pos} = \left(0.25 + 0.125\cot\alpha\left(1 + \frac{h_b}{H_s}\right)\right)^5 \quad \text{with} \quad 0 \leq \gamma_{pos} \leq 1 \tag{2.20}$$

$$\gamma_{berm,low} = 1 - 0.12\frac{B}{H_s}\frac{h_b}{H_s} \quad \text{for} \quad h_b/H_s \geq 0 \tag{2.21}$$

$$\gamma_{berm,low} = 1 - 0.02\xi_{m-1,0}\frac{B}{H_s}\left|\frac{h_b}{H_s}\right| \quad \text{for} \quad h_b/H_s \leq 0 \tag{2.22}$$

where:

B (m): berm width.

h_b (m): berm level w.r.t. SWL (positive is submerged, negative is emerged).

2.2. Damage characterization methods

This section presents the main contributions on damage characterization definitions and parameters. The various developments on damage characterization concepts are divided below into three main groups. Firstly, the percentage of moved units over the total units in the armour (Hudson 1959); secondly, the eroded volume and area associated with the number of moved units (Thompson & Shuttler (1975), Broderick (1984) and van der Meer (1988)); and thirdly, the erosion depth of the armour (Melby & Kobayashi (1998), Hofland et al. (2011) and Hofland et al. (2014)).

2.2.1. Percentage of moved units

Hudson (1959) introduces for the first time a damage parameter in the stability of armoured slopes under wave action, since Iribarren (1938) did not include any damage consideration in his formulae. This damage parameter is defined as *"the percentage of armour units displaced from the cover layer"* and represented as D.

The Hudson Formula was initially calibrated (trough parameter K_D) for a *no-damage* limit, defined as the conditions when less than 1% of the armour units have moved ($D < 1\%$) due to the wave action. Later, the Hudson formulae also included calibrations of K_D for larger damage levels, allowing the reduction of the armour units when a certain movement of the armour units is allowed.

This damage parameter D represents a development on the damage characterization concepts but also include significant limitations. The first limitation of the parameter D is that the damage is no included in the formula directly but only through a calibration parameter. The second limitation is that this damage parameter is function of the type and volume of the armour layer considered, leading to significantly different percentages of moved units when the same erosion is produced in structures with wider or narrower armour layers.

Parameter summary from Hudson (1959):

$$D\ (\%) = \frac{\text{Number of moved units in the armour}}{\text{Total number of units in the armour}} \tag{2.23}$$

Damage limits summary from Hudson (1959):

No-damage limit ⇒ Less than 1% of moved units in the armour ($D < 1\%$).

According to CIRIA et al. (2007), the percentage of moved units (N_d) is obtained considering the armour units moved within a reference area. This area can be defined as the total armour volume (as in Hudson (1959) or between two levels and over a certain width.

$$N_d\ (\%) = \frac{\text{Number of moved units in a reference area of the armour}}{\text{Total number of units in a reference area of the armour}} \tag{2.24}$$

2.2.2. Number of moved units

Thompson & Shuttler (1975) work on the stability of rip-rap provides relevant contributions to the study of damage characterization. The author defines first that the damage caused by the impact of a random sequence of waves over a randomly placed agglomeration of material is in consequence a random process with a expected mean value. Thus, this author presents the statistical uncertainties associated with the study of stability and damage to structures under wave attack.

Furthermore, Thompson & Shuttler (1975) introduces a damage parameter to be calculated from the comparison of profile surveys before and after a given test run. This parameter is defined as *"the number of D_{50} sized spherical stones eroded from a $9D_{50}$ width slope"* and represented as N_Δ. This author also defines that *no-damage* limit is the point from which the increase in damage increases significantly with increasing wave height, although it does not provide further details regarding this lower limit. Furthermore, *failure* is reached when the erosion of the armour leaves the filter exposed, defined as when a hole with a diameter $D_{50}/2$ is observed in the armour down to the filter layer, measured with a hand held gauge with a hemispherical foot of $D_{50}/2$ diameter. More precisely, failure was determined if the $D_{50}/2$ diameter foot could touch the filter layer at any location (inside or outside the measurement grid) after a sequence of 500 waves, whether or not filter material was eroded.

Parameter summary from Thompson & Shuttler (1975):

$$N_\Delta\ (\text{Number of units}) = \frac{V_e \rho_B}{\rho_s \left(\frac{\pi}{6} D_{50}^3\right)} \tag{2.25}$$

where:

V_e (m^3): eroded volume.

ρ_B (kg/m^3): bulk density of the eroded volume.

ρ_s (kg/m^3): apparent mass density of the rock.

D_{50} (m): median diameter.

Damage limits summary from Thompson & Shuttler (1975):

No-damage limit ⇒ Point at which erosion increases significantly with increasing wave height.

Failure limit ⇒ Filter layer becomes exposed through a hole of $D_{50}/2$ diameter.

Broderick (1984) also contributed to the damage characterization concepts while working on the stability of rip-rap. The damage parameter, calculated from the comparison of averaged profile surveys before and after a given test run, is defined as *"the erosion volume per unit length, made dimensionless by the cube-root squared of the median stone mass divided by the density"* and represented as D' (currently known as the S parameter). Considering Equation 2.5, this parameter can be re-written as *the eroded volume made dimensionless by the nominal median diameter*. For this author, *no-damage (or zero-damage)* limit is defined as D' (or S) $= 2$, since this is the lowest value which can be consistently detected in the survey data. The *failure* limit in this case is reached when the erosion of the armour leaves the filter exposed, without an extension threshold for the filter exposure.

Parameter summary (Broderick 1984):

$$D'(=S) \text{ (Number of units)} = \frac{A_e}{\left(\frac{M_{50}}{\rho_s}\right)^{2/3}} = \frac{A_e}{D_{n50}^2} \tag{2.26}$$

where:

A_e (m^2): eroded area.

M_{50} (kg): median mass.

ρ_s (kg/m^3): apparent mass density of the rock.

D_{n50} (m): nominal median diameter.

Damage limits summary (Broderick 1984):

No-damage limit ⇒ $S = 2$ (lowest value consistently detected in survey data).

Failure limit ⇒ Filter layer becomes exposed.

van der Meer (1988) incorporates in his formulae for the stability of slopes facing wave action (see Section 2.1.2) a damage parameter equal to the one described in Broderick (1984) as *"the eroded volume made dimensionless by the nominal median diameter"* and represented as S. For the *no-damage* limit (named as start of damage), the criterion from Hudson (1959) leads to erosion values of S between 1 and 3, which is also aligned with the limit proposed by Broderick (1984). The *failure* limit is defined as the value of S when the filter layer becomes exposed and varies between 8 and 17 for different slopes.

Parameter summary from van der Meer (1988):

$$S \text{ (Number of units)} = \frac{A_e}{D_{n50}^2} \tag{2.27}$$

where:

A_e (m^2): eroded area.

D_{n50} (m): nominal median diameter.

Damage limits summary from van der Meer (1988):

No-damage limit ⇒ S between 1 and 3 (based in Broderick (1984), Hudson (1959)).

Failure limit ⇒ S between 8 and 17 (filter layer becomes exposed).

Furthermore, the number of moved units (N_{od}) is obtained considering the armour units moved within a strip of breakwater slope of one D_{n50} width. Two similar equations for this parameter are shown below (CIRIA et al. (2007)).

$$N_{od}\ (\%) = \frac{\text{Number of moved units in a breakwater strip of one } D_{n50} \text{ width}}{D_{n50}} \tag{2.28}$$

$$N_{od}\ (\%) = \frac{\text{Number of moved units in a breakwater section}}{\text{Section width}/D_{n50}} \tag{2.29}$$

2.2.3. Eroded depth

Melby & Kobayashi (1998) introduced innovative concepts for the characterization of damage in rubble mound coastal structures, defining three new dimensionless parameters to characterize the damage and remaining strength: *erosion depth* E, *erosion length* L and *cover depth* C (see Figure 2.3 and Equations 2.30, 2.31 and 2.32). In addition, this author defines the concept of *failure* limit as when a hole with a diameter D_{n50} is observed in the armour down to the filter layer. Furthermore, Melby & Kobayashi (1998) uses the damage parameter S with a different definition compared with van der Meer (1988), considering the average of the damage calculated in each individual profile instead of the damage calculated with the averaged profile (which is the mean of all individual profiles).

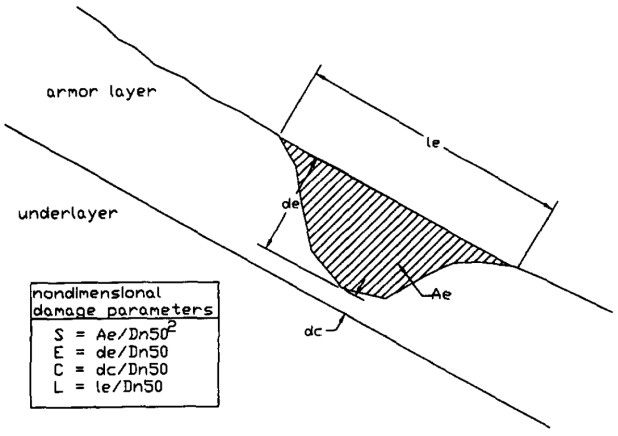

Figure 2.3: Damage parameters E, L, C and S (Melby & Kobayashi 1998).

Parameter summary from Melby & Kobayashi (1998):

$$E\ (\text{Erosion depth in units}) = \frac{d_e}{D_{n50}} \tag{2.30}$$

$$L\ (\text{Erosion length in units}) = \frac{l_e}{D_{n50}} \tag{2.31}$$

$$C\ (\text{Cover depth in units}) = \frac{d_c}{D_{n50}} \tag{2.32}$$

where:

d_e (m): erosion depth.

l_e (m): erosion length.

d_c (m): cover depth.

D_{n50} (m): nominal median diameter.

Damage limits summary from Melby & Kobayashi (1998):

Failure limit ⇒ Filter layer becomes exposed through a hole of $1D_{n50}$ diameter.

Hofland et al. (2011) further develop the concept of the dimensionless erosion depth parameter (E), distinguishing 2D and 3D parameters. For 2D conditions such as conventional trunk alignments, E_{2D} is obtained from the initial and final averaged profiles over a given characterization width. For 3D conditions such as non-conventional structures and roundheads, $E_{3D,m}$ is obtained in a given characterization area from the initial and final 3D surveys averaged with a circular moving average of mD_{n50} diameter. Hofland et al. (2014) and Disco (2012) applied these new damage parameters for the characterization of rounheads, an example of structure which cannot be characterized using conventional damage parameters.

Regarding the *no-damage* limit, it is considered when one unit is moved in a strip of $1D_{n50}$ width ($N_{od} = 1$). In addition, the *failure* limit is defined based on Thompson & Shuttler (1975) as when locally a minimum armour thickness of 0 is observed. The author remarks the importance of taking into account the implications of evaluating damage from a mean profile, where a safety margin should be included to account for local deviations of the mean value (averaged profile).

Parameter summary from Hofland et al. (2011):

$$E_{2D}\ \text{(Erosion depth in units)} = \frac{\max\left(\langle e\rangle_w\right)}{D_{n50}} \tag{2.33}$$

$$E_{3D,m}\ \text{(Erosion depth in units)} = \frac{\max\left(\langle e\rangle_{mD_{n50}}\right)}{D_{n50}} \tag{2.34}$$

where:

$\langle e\rangle_w$ (m): erosion depth averaged over the width denoted by.

$\langle e\rangle_{mD_{n50}}$ (m): erosion depth averaged over an area of mD_{n50} diameter.

D_{n50} (m): nominal median diameter.

Damage limits summary from Hofland et al. (2011):

No-damage limit ⇒ One unit is moved in a strip of $1D_{n50}$ width.

Failure limit ⇒ Locally a minimum armour thickness of 0 is observed.

2.3. Physical modelling techniques

This section addresses two different aspects related with physical modelling. Firstly, it is described the most important guidelines and criteria to be taken into account when using physical modelling as a research technique. Secondly, the measuring techniques used for damage characterization by Hudson (1959), Thompson & Shuttler (1975), Broderick (1984), van der Meer (1988), Melby & Kobayashi (1998) and Hofland et al. (2011) are summarized.

2.3.1. Guidelines

For the design of physical modelling tests, Hughes (1993) defines the main aspects to be taken into account. More recently, (Wolters et al. 2009) and (Frostick et al. 2011) are also references for physical modelling experiments. Martín-Hidalgo et al. (2014) and Martín-Soldevilla et al. (2015) have the aim of improving the characterization of real storms through theoretical models, while (de Leau 2017) evaluates the accuracy of such theoretical models compared with classic storm characterization methods used in physical modelling.

Based on Hudson et al. (1979), Hughes (1993) divides the 11 similitude rules for designing physical models of rubble mound structures into 5 fundamental requirements. These requirements include the following parameters.

d (m): water depth at the toe of the structure.

g (m/s^2): gravitational acceleration.

H (m): wave height.

l_a (m): characteristic linear dimension of the armour unit (e.g. unit diameter).

V_w (m/s): water velocity in the vicinity of the cover layer.

α (°): seaside slope angle measured from the horizontal.

β (°): incident wave angle.

Δ (-): shape of the armour unit.

θ (°): bottom slope seaward of the structure.

L (m): wave length.

μ (kg/(ms)): dynamic viscosity of the water in the vicinity of the breakwater.

ϵ_a (m): characteristic linear dimension of the armour unit surface roughness.

ρ_a (kg/m^3): mass density of the armour units.

ρ_w (kg/m^3): mass density of water in vicinity of the breakwater.

First requirement:
Rubble-mound structure models must be geometrically undistorted in length scale.

$$\left(\frac{l_a}{h}\right)_p = \left(\frac{l_a}{h}\right)_m \tag{2.35}$$

$$\left(\frac{H}{L}\right)_p = \left(\frac{H}{L}\right)_m \tag{2.36}$$

$$\left(\frac{h}{L}\right)_p = \left(\frac{h}{L}\right)_m \tag{2.37}$$

$$(\alpha)_p = (\alpha)_m \tag{2.38}$$

$$(\beta)_p = (\beta)_m \tag{2.39}$$

$$(\Delta)_p = (\Delta)_m \tag{2.40}$$

$$(\theta)_p = (\theta)_m \tag{2.41}$$

Second requirement:
Flow hydrodynamics in a rubble-mound structure model must conform to the Froude criterion.

$$\left(\frac{V_w}{\sqrt{g l_a}}\right)_p = \left(\frac{V_w}{\sqrt{g l_a}}\right)_m \tag{2.42}$$

Third requirement:
Rubble-mound structure models must have turbulent flow conditions throughout the primary armour.

$$\left(\frac{V_w l_a}{\mu \rho_w}\right)_p = \left(\frac{V_w l_a}{\mu \rho_w}\right)_m \tag{2.43}$$

Since the following relationship cannot be achieved, this requirement is considered reasonably fulfilled when the Reynolds number in the model is larger than a given threshold. According to various authors this lower limit is located around $3{\cdot}10^4$ (Hughes 1993) (see Equation 2.44 where ν (m/s^2) is the kinematic viscosity of the water in the model and l_a the median nominal diameter).

$$R_e = \frac{\sqrt{gH} l_a}{\nu} > 3 \cdot 10^4 \tag{2.44}$$

Forth requirement:
The relative mass density relationship in the prototype must be maintained in the model.

$$\left(\frac{\rho_w}{\rho_a - \rho_w}\right)_p = \left(\frac{\rho_w}{\rho_a - \rho_w}\right)_m \tag{2.45}$$

Fifth requirement:
The effects of surface roughness of the armour units in the prototype must be the same in the model.

$$\left(\frac{\epsilon_a}{l_a}\right)_p = \left(\frac{\epsilon_a}{l_a}\right)_m \tag{2.46}$$

2.3.2. Measuring tools

The measuring techniques used for damage characterization according to the different authors have significantly evolved throughout time. Hereafter the main characteristics of these measuring campaigns are presented.

Hudson (1959)

The stability tests were done in a concrete flume 1.5 m wide, 1.2 m deep and 36 m long where the regular incident waves were measured with a resistive gauge. The profile measurements were done using a sounding rod with a circular foot equal to one-half the average diameter of the armour units. Nevertheless, no information is provided regarding the spacing and resolution of the measurements.

Thompson & Shuttler (1975)

The tests were done in a flume 1.2 m wide (divided into a calibration channel and a test channel of 0.65 m wide each), 45 m long and maximum working depth of 0.61 m. Irregular incident waves were measured with a resistive gauge in the calibration channel. The profile measurements were done using a surface profiler with a hemispherical foot with a diameter of one-half the median diameter of the armour units ($D_{50}/2$). The surveys measured the levels before and after the test runs over a square grid (in plan view) with points separated D_{50}, from which 10 sections (covering a $9D_{50}$ width of slope) were obtained.

Broderick (1984)
The tests were done in two different flumes (large flume: 4.6 m wide, 6.1 m deep and 193.5 m long. short flume: and 4.6 m wide, 6.1 m deep and 193.5 m long), on which regular and irregular wave action were generated. The profile measurements were done before and after each run, although no information is provided regarding the measurement instrumentation.

van der Meer (1988)
Almost all tests were done in a flume 1.0 m wide, 1.2 m deep and 50 m long with compensation for the reflected wave at the wave board. Irregular waves were measured by two wave gauges separated one-quarter of wave length, allowing to distinguish the incident and reflected wave spectra. The profile measurements were done using a surface profiler on a computer-controlled carriage with nine gauges separated 0.10 m, measuring along the slope every 0.04 m. Nevertheless, no information is provided regarding the shape and size of the surface profiler foot or regarding how the the damage values of parameter S are obtained from the measured profiles.

Melby & Kobayashi (1998)
The tests were done in a flume 1.52 wide, 2.0 deep and 61.1 m long without compensation for the reflected wave at the wave board. In this flume, two identical structures were build in each half of the flume (0.76 m wide each structure). Irregular waves were measured by three wave gauges in front of the wave board, allowing to distinguish the incident and reflected wave spectra. The profile measurements were done using a surface profiler with eight profiling arms with a lateral spacing of 0.05 m between arms, with the center-line of the profiler located at the center-line of each of the 0.76 m structures. The profiler arms had a spheroid foot with a diameter of one-half the nominal median diameter of the armour units ($D_{n50}/2$).

Hofland et al. (2011)
The measurements considered in this paper were obtained from tests carried out in wave flumes (2D conditions) and wave basins (3D conditions), where irregular waves were generated. Profile measurements were done following two methods: first, fully automated mechanical profiler with 9 gauges; second, with Digital Stereo Photography technique with a grid resolution of 1 mm.

2.4. Climate change adaptation alternatives

This section presents the existing contributions on the impacts of climate change on coastal structures and the possible adaptation alternatives. Firstly, it is described the expected changes on the loads acting on coastal structures in climate change scenarios; secondly, it is described the previous contributions on alternatives for the upgrading of coastal structures facing such increased loads.

2.4.1. Climate change impacts

The study of climate change has developed significantly in the last years, being the Fifth Assessment Report from the Intergovernmental Panel on Climate Change (IPCC 2013) the main reference on climate change research. This source presents the most complete set of observations and predictions covering causes, consequences and mitigation measures. An important conclusion regarding climate change and sea level rise is that even if there are scenarios where global temperatures are stabilized (see Figure 2.4), global sea level will continue to rise in all future scenarios (see Figure 2.5).

Semedo et al. (2013) presents a global model for future projections of the wave climate based on climate models and the climate change scenarios from IPCC (2013). Furthermore, Weisse et al. (2014) evaluates the past and future changes in extreme sea level in European coasts. This last author defines the change in the mean sea level as the main contribution for the increase of extreme sea levels, ahead of changes in wind waves and storm surges patterns. It is also highlighted that shallower areas are specially sensitive to changes in sea levels, since this could increase the tidal range and incident wave height. Thus, it is described the need of evaluating increased loads acting on coastal structures and implementing adaptation strategies.

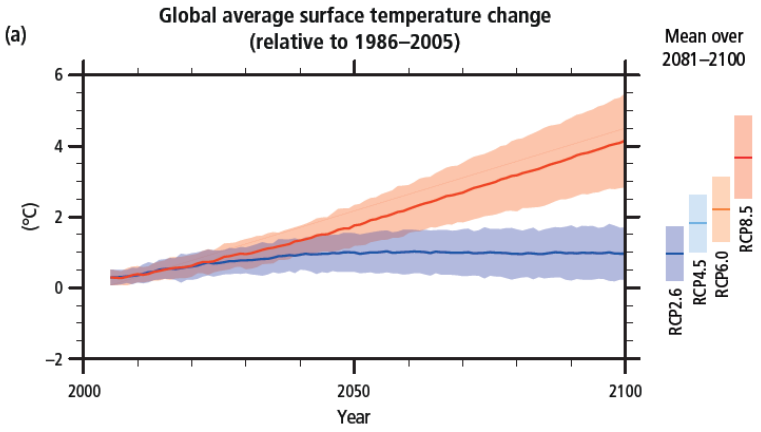

Figure 2.4: Global average temperature, scenarios RCP8.5 (red) and RCP2.6 (blue) (IPCC 2013).

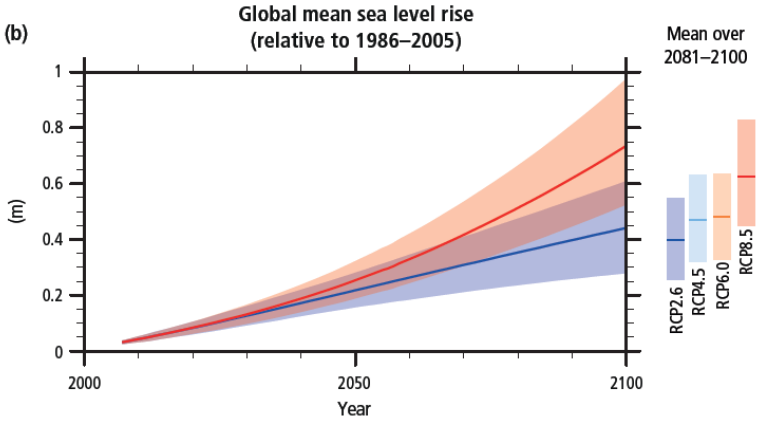

Figure 2.5: Global mean sea level rise, scenarios RCP8.5 (red) and RCP2.6 (blue) (IPCC 2013).

Isobe (2013) focuses on the impacts of climate change on coastal structures, mainly the impact of sea level rise. Special attention is placed again on shallow water areas, where sea level rise increases not only the water depth but also the incident wave height. Additionally, it is described four consequences of increased loads on coastal structures such as increase of run-up height and overtopping volumes or the reduction in stability of rubble mound and vertical breakwaters. Considering this, it is highlighted the importance of implementing adaptation strategies such as raising the crown height or increasing the weight of armour units. These upgrading measures are also required to be economically feasible, so national adaptation strategies need to establish long-term planning able to ensure that safety levels are maintained throughout time and financial limitations are overcome.

2.4.2. Upgrading alternatives

Burcharth et al. (2014) presents a study on various upgrading alternatives for rock armoured revetments as part of adaptation strategies facing climate change. These adaptation strategies are justified with the need of maintaining (or increasing) safety levels of coastal structures in current and future scenarios. This author evaluates a number of alternatives using desk tools and accounting for two consequences of climate change: sea level rise and an increase in storm intensity. The upgrading alternatives were divided into the conditions where a raise in the crest level is allowed (see Figure 2.6) and where a raise in the crest level is not allowed (see Figure 2.7). Among all the alternatives, the simplest solutions proven to be the most cost-effective (e.g. extra armour layer or front berm). Nevertheless, these conclusions were done using desk tools only and it is recommended to validate such upgrading alternatives with physical models.

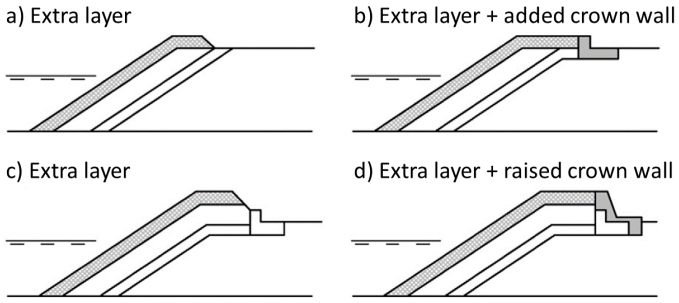

Figure 2.6: Upgrading of coastal structures with an increase in the crest level (Burcharth et al. 2014).

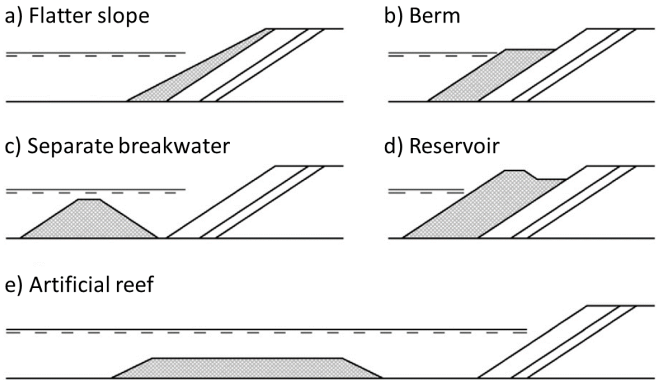

Figure 2.7: Upgrading of coastal structures with no increase in the crest level (Burcharth et al. 2014).

Koftis et al. (2015) evaluates upgrading alternatives for coastal structures facing climate change scenarios, considering two existing structures in Greece: one emerged and one submerged breakwater. In the case of the existing emerged breakwater, the stability of the armour in the climate change scenario would be fulfilled while the overtopping volumes would not be acceptable. In the case of the existing submerged breakwater, the stability of the armour in the climate change scenario would be fulfilled while the wave transmission would not be acceptable. Thus, according to the authors the impact of sea level rise was proven to be more critical than the increase of the incident wave heights. Considering this need of upgrade, various alternatives are evaluated according to cost-effectiveness criteria. In the case of the emerged breakwater, the most cost-effective upgrade was to add a front berm.

van Gent (2013) presents the formulae for the design of breakwaters with a berm (see Section 2.1.3), where this structure is recommended for the upgrade of structures facing climate change scenarios. In addition, van Gent & Lim (2016) also presents the addition of a front berm as an upgrading alternative, due to its flexibility and cost-effectiveness. Due to the existing uncertainties in the forecast of future climate change scenarios, it can be economically attractive to design structures that could be easily adapted in the future. This would produce cost-effective designs able to cope with any future climate change scenario.

3

Theoretical development

The aim of this chapter is to introduce the theoretical concepts, parameters and methods to be used in the damage characterization of coastal structures. The first sections addresses the summary of all definitions to be considered in the damage characterization methods. The second section establishes the damage concepts to be considered, the third section establishes the damage parameters to be used, while the fourth introduce the importance of the measuring techniques in damage characterization.

3.1. Definitions

This first section presents the basic definitions to be considered for damage characterization of coastal structures (see Chapter 2 for the references). In the first sub-section the damage parameters (S, E_{2D} and $E_{3D,m}$) are described into detail, including the procedure for their calculation. In the second sub-section it is highlighted four fundamental aspects that influence significantly the results of damage characterization.

3.1.1. Parameters

The first damage parameter considered in S, as defined by Broderick (1984) and van der Meer (1988) (see Equation 3.1). This damage parameter is widely used and describes the damage to the structure as the number of units eroded in the width-averaged profile. The process for obtaining this damage parameter is described in more detail in Figure 3.1.

$$S \text{ (Number of units)} = \frac{A_e}{D_{n50}^2} \tag{3.1}$$

where:

A_e (m^2): eroded area.

D_{n50} (m): nominal median diameter.

The following two parameters (E_{2D} and $E_{3D,m}$) are considered as defined by Hofland et al. (2011) (see Equations 3.2 and 3.3). These two parameters estimate the damage to the structure considering the maximum erosion depth perpendicular to the slope. The distinction between them is that for E_{2D} this erosion depth is measured in the width-averaged profile, while for $E_{3D,m}$ this erosion depth is obtained as the maximum erosion depth recorded at any point of the structure. In addition, for $E_{3D,m}$ the initial profile and the profile after the test are averaged with a circular spatial moving average with mD_{n50} diameter. The process for obtaining these two damage parameters is described in more detail in Figures 3.2 and 3.3.

$$E_{2D} \text{ (Erosion depth in units)} = \frac{\max\left(\langle e\rangle_w\right)}{D_{n50}} \tag{3.2}$$

$$E_{3D,m} \text{ (Erosion depth in units)} = \frac{\max\left(\langle e\rangle_{mD_{n50}}\right)}{D_{n50}} \tag{3.3}$$

where:

$\langle e\rangle_w$ (m): erosion depth averaged over the width denoted by w.

$\langle e\rangle_{mD_{n50}}$ (m): erosion depth averaged over an area of mD_{n50} diameter.

D_{n50} (m): nominal median diameter.

In this thesis the strengths of innovative damage parameters such as E_{2D} and $E_{3D,m}$ will be evaluated in order to allow more accurate and versatile damage characterizations of coastal structures compared to the use of traditional damage parameters (S). Section 3.3 addresses the introduction of innovative damage parameters in more detail.

3.1.2. Method components

The use of the previous described traditional (S) and innovative (E_{2D} and $E_{3D,m}$) damage parameters is dependent on four components that define the damage characterization method. This means that the damage parameter itself does not provide all required information but it must be combined with these 4 components shown below.

Damage limits

The first element that should be considered in the damage characterization of coastal structures are the damage concepts and limits. Concepts such as damage initiation, intermediate damage and failure should be unified and precisely described for each damage characterization method and damage parameter. Currently, such definitions are not available and the existing damage limits were established based on various different arguments influenced by low resolution and low accuracy measuring techniques. Section 3.2 addresses this component.

Characterization width

The second element that should be considered in the damage characterization of coastal structures is the characterization width. The width to be considered for damage measurements should be clearly defined, since it affects the measured damage in all damage parameters. Currently, there is no definition of the width that should be considered and the effect that it has in the damage characterization results. Section 3.2 addresses this component.

Measuring technique

The third element that should be considered in the damage characterization of coastal structures are the measuring techniques. Damage characterization methods should describe the measuring techniques to be used and their influence in the results, in both measured values and associated variability. Currently, the measuring techniques to be used and their effect on the measuring results are not defined. Section 3.4 addresses this component.

Post processing

The fourth element that should be considered in the damage characterization of coastal structures is the post processing. The steps followed in the post processing on the measured data should be defined in order to contribute to the quality of the characterization and avoid deviations in the results. Currently, there is no description of the post processing steps for the damage characterization of coastal structures. Section 3.4 addresses this component.

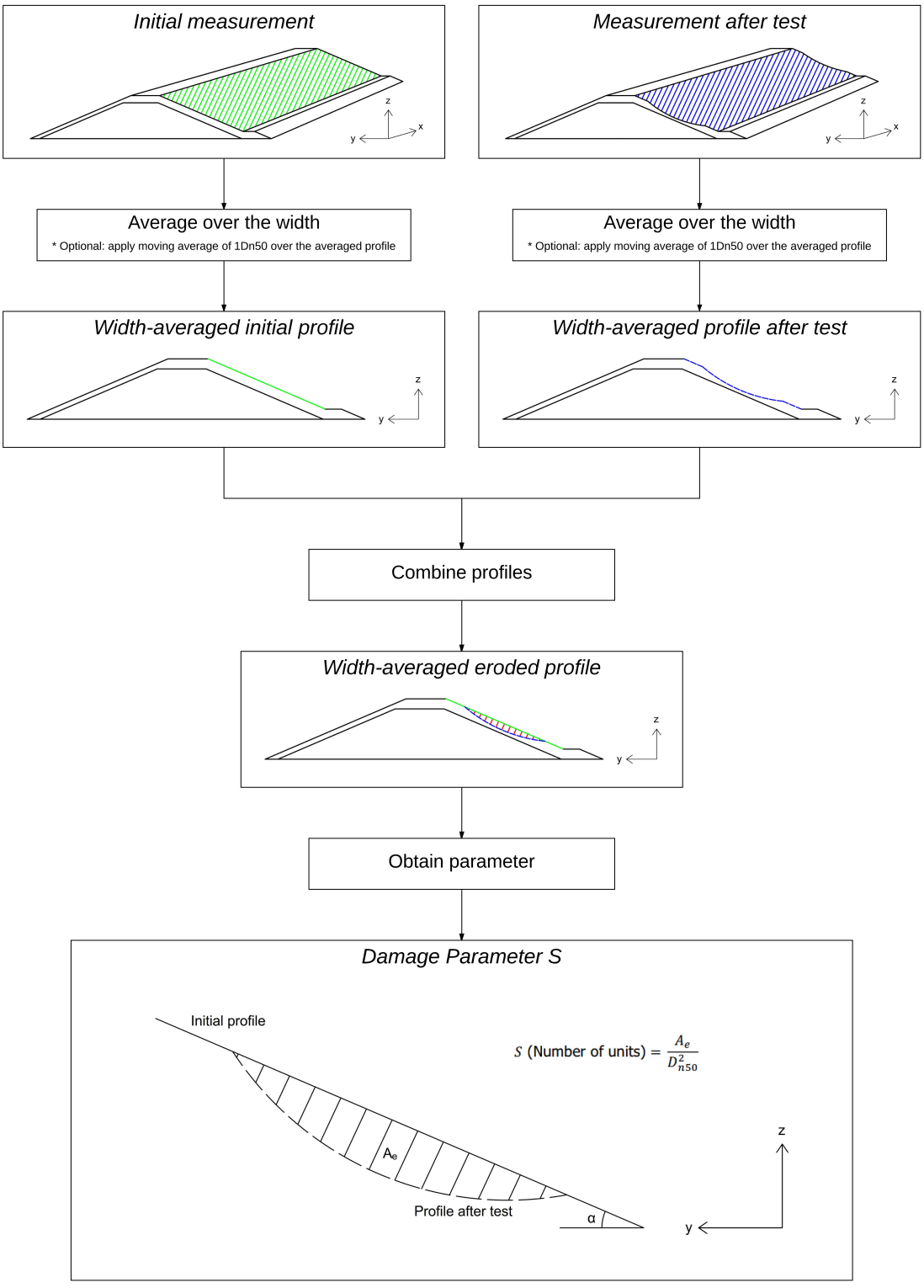

Figure 3.1: Process for obtaining S damage parameter.

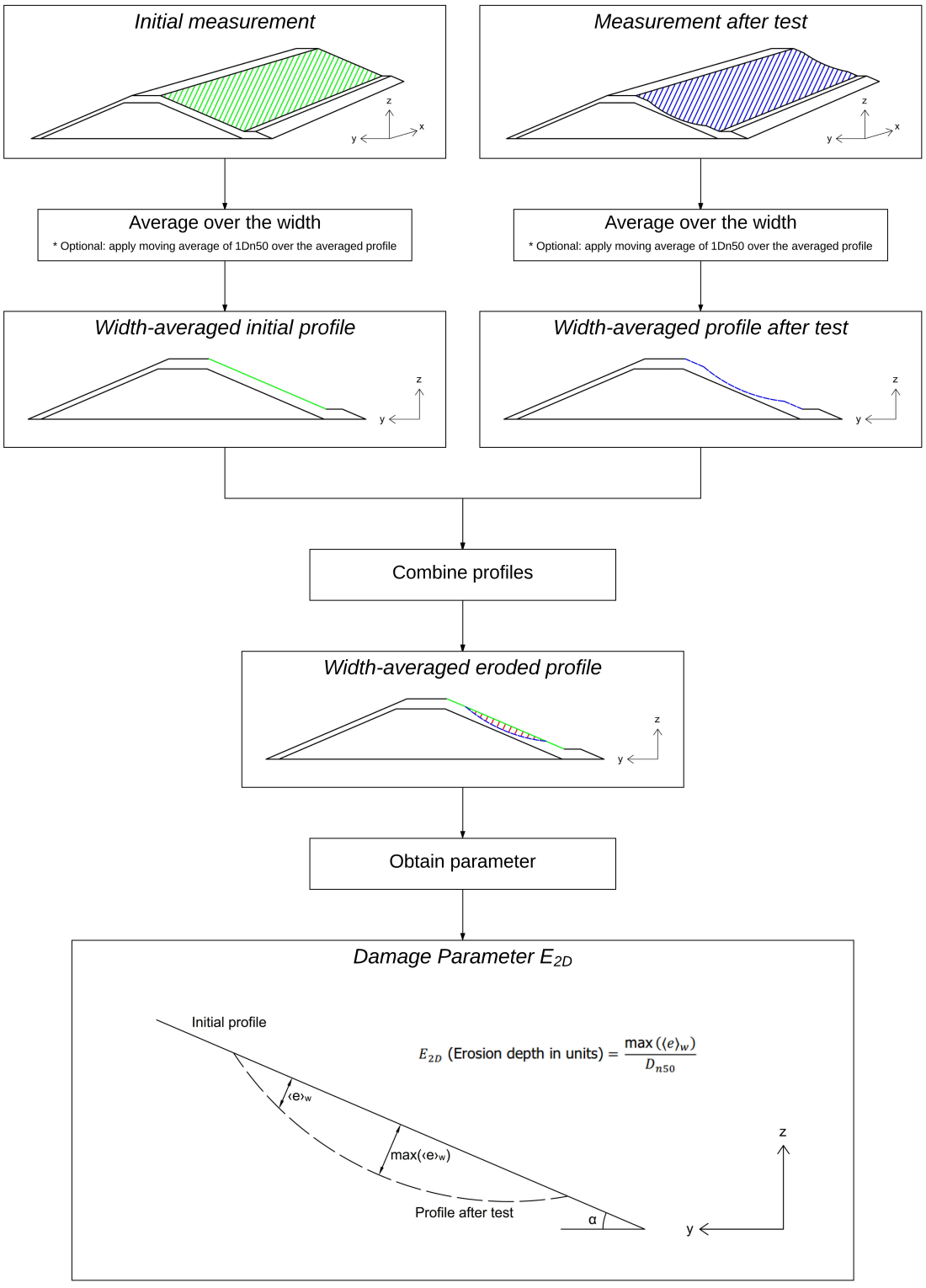

Figure 3.2: Process for obtaining E_{2D} damage parameter.

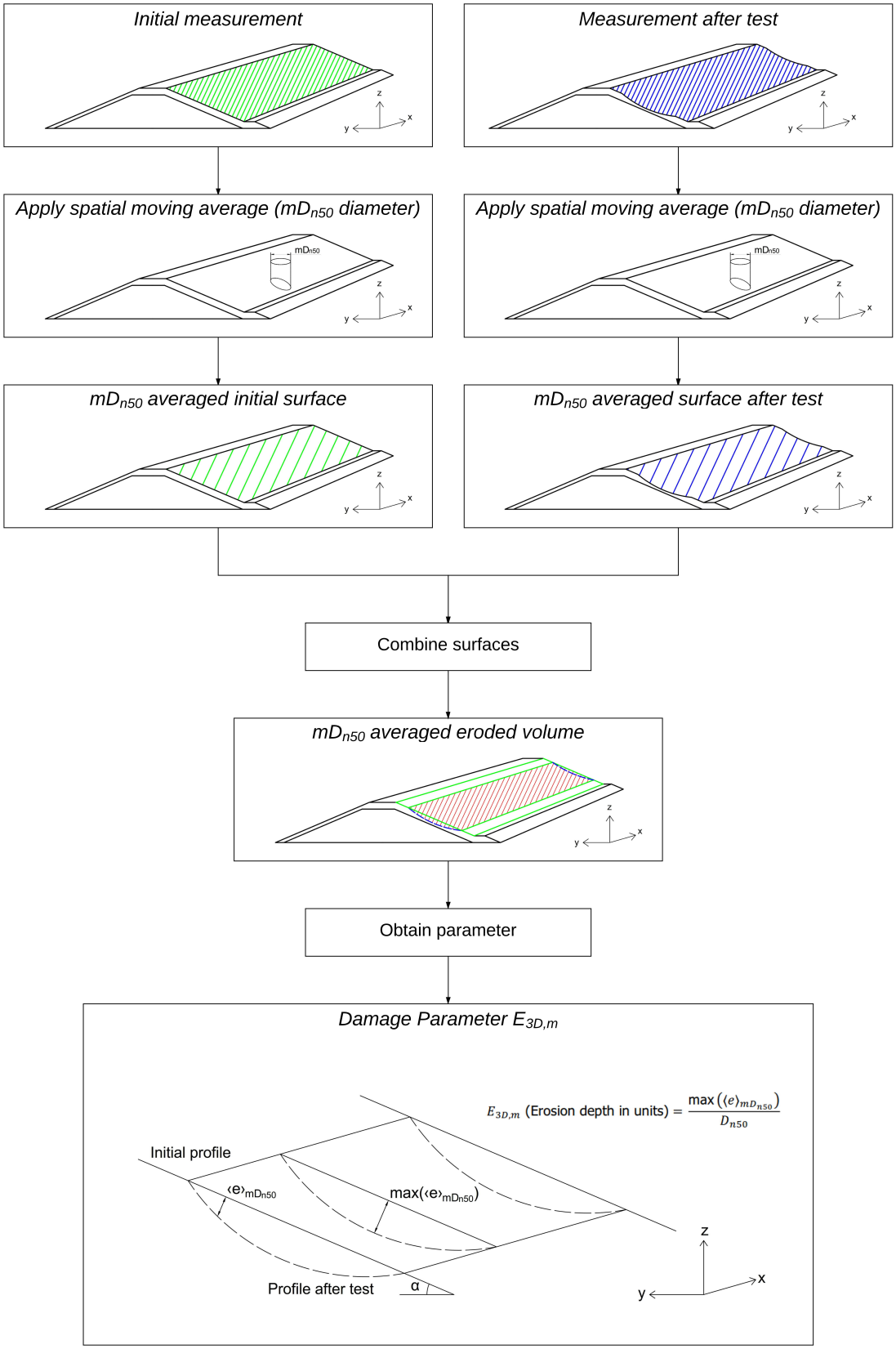

Figure 3.3: Process for obtaining $E_{3D,m}$ damage parameter.

3.2. Establishing damage concepts

This section initiates the discussion regarding sub-question 1 (How can we establish and validate unified concepts of ”damage initiation”, ”intermediate damage” and ”failure” in rubble mound structures?). As described in the previous section, these damage definitions should be established considering the width of the structure used in the damage characterization. Thus, the characterization width and damage limits are addressed in more detail in the next two sections.

3.2.1. Characterization width

This aspect is addressed given that the use of different characterizations widths in the assessment of a given coastal structure would lead to different damage results for all damage parameters and would influence the definitions of damage limits. Frostick et al. (2011) recommends the use of characterization widths larger than 15-20 rock diameters in order to achieve representative results, but does not discusses the influence it has in the measured damage. Thus, such influences of the characterization width are going to be evaluated and a range of suitable characterization widths will be recommended.

The influence of the characterization width is expected to be different in damage parameters which evaluate width-averaged profiles (S and E_{2D}) compared to damage parameter that evaluates the maximum erosion ($E_{3D,m}$). In one hand, in the case of S and E_{2D} a larger characterization width would lead to a reduction of the measured damage since the damage to certain areas will be hidden by the accretion in other areas. In the other hand, in the case of $E_{3D,m}$ a larger characterization width would lead to an increase of the probability of observing a larger maximum erosion depth.

All these influences are evaluated in Section 6.1.1 together with the recommendations for defining the most suitable width for damage characterization in coastal structures.

3.2.2. Damage limits

This study aims to establish unified damage limits for the characterization of coastal structures such as damage initiation, intermediate damage and failure. The damage limits of parameter S (currently the most used damage parameter for rock armoured slopes), were established by Broderick (1984) and van der Meer (1988) based on low resolution and low accuracy measurements and only qualitative definitions of the exposure of the filter layer. Thompson & Shuttler (1975), Melby & Kobayashi (1998) and Hofland et al. (2011) provides better descriptions of failure of coastal structures, describing more precisely the extent of exposed filter layer which represents the failure of the structure.

Thus, the need for better characterization of coastal structures and the current availability of high resolution and accuracy measurement techniques demands an update of the descriptions of damage limits. These damage limits will be validated by measurements with Digital Stereo Photography, which can offer a complete and detailed survey of the structure with a 1 mm resolution.

Based on the contributions found in literature and the need of establishing unified concepts for damage characterization, the following damage limits are proposed for a $2D_{n50}$ thick rock armoured slopes:

- **Damage initiation:** defined as the condition where a circular hole of $1D_{n50}$ diameter and a depth of $1D_{n50}$ is observed in the armour layer.
- **Intermediate damage:** defined as the condition where a circular hole of $1D_{n50}$ diameter and a depth of $1.5D_{n50}$ is observed in the armour layer.
- **Failure limit:** defined as the condition where a circular hole of $1D_{n50}$ diameter and a depth of $2D_{n50}$ is observed in the armour layer.

For rock armoured slopes with a different armour thickness nD_{n50}, these limits can be generalized as follows:

- **Damage initiation:** defined as the condition where a circular hole of $1D_{n50}$ diameter and a depth of $1D_{n50}$ is observed in the armour layer.
- **Intermediate damage:** defined as the condition where a circular hole of $1D_{n50}$ diameter and a depth of $1.5D_{n50}$ is observed in the armour layer.
- **Failure limit:** defined as the condition where a circular hole of $1D_{n50}$ diameter and a depth of nD_{n50} is observed in the armour layer.

The previously established damage limits are validated in Section 6.1.2 taking into account the physical modelling tests described in Chapter 4 and Chapter 5.

3.3. Establishing damage parameters

This section initiates the discussion regarding sub-question 2 (How can we establish and validate an universal damage parameter able to accurately characterize the the response and remaining strength of rubble mound structures?). Two innovative damage parameters are proposed in order to significantly improve the characterization of coastal structures: the erosion depths E_{2D} and $E_{3D,m}$ (see Section 3.1.1 for their definitions).

The E_{2D} parameter is obtained from the structure width-averaged profiles measured before and after a given test run in a given characterization width (see Figure 3.2). This is obtained from the "xyz" measurements being the coordinates "x" perpendicular to the wave direction, "y" parallel to the wave direction and "z" the vertical direction. When averaging over "x", an "yz" width-averaged profile is obtained. Low resolution traditional measurements such as mechanical profilers could also generate similar results but with less accurate results and more variability (see Section 3.4). In order to reduce the noise in the measurements, a moving average with a length of $1D_{n50}$ is applied in all the profiles. From the comparison of these initial and final width-averaged profiles, the maximum erosion depth perpendicular to the slope is obtained and normalized by the nominal median diameter as shown in Equation 3.2.

The $E_{3D,m}$ parameter is obtained directly from the structure "xyz" measurements before and after a given test run in a given characterization width (see Figure 3.3). These "xyz" survey data is processed applying a moving circular average with a diameter of mD_{n50}. From the comparison of these initial and final "xyz" averaged data, the maximum erosion depth perpendicular to the slope is obtained and normalized by the nominal median diameter as shown in Equation 3.3.

These two damage parameters are validated in Section 6.2 in combination with the damage limits discussed in the previous section.

3.4. Measuring techniques

This section initiates the discussion regarding sub-question 3 (How can we validate the increase in reliability of physical modelling tests results based on innovative and higher accuracy testing and measuring techniques?). The use of different measuring techniques is considered as an important factor that influences the results of a given damage characterization method. It will be discussed the impact in the results when using high resolution and high accuracy measurements techniques compared with low resolution and low accuracy tools used in traditional surveys. In addition, post processing steps such as the application of moving averages are going to be briefly evaluated.

Regarding measuring techniques it is discussed the influence in the characterization of coastal structures when using traditional measuring equipment such as mechanical profilers compared to high resolution and high accuracy techniques such as Digital Stereo Photography. The fundamental differences between such methods is the fact that traditional techniques are not able to capture the damage in all the structure surface, leaving damaged areas unnoticed. In contrast, high resolution techniques are able to measure the state of the whole structure surface and capture all the erosion areas.

These high resolution measuring techniques present a number of advantages for the damage characterization of coastal structures. First, it allows the introduction of innovative and precise damage parameters such as $E_{3D,m}$ (as described in Section 3.3) and allows the improvement in the damage limits definitions (as described in Section 3.2.2). Second, for parameters obtained from width-averaged profiles such as S and E_{2D}, high resolution surveys which captures the state of the whole structure surface are able to reduce the variability and uncertainty in the damage characterization results.

Regarding post processing steps, the effects of tools such as moving averages used for calculating traditional (S) and innovative (E_{2D} and $E_{3D,m}$) damage parameters are described. Such tools are recommended in order to reduce the noise present in the measurement results and capture more precisely the damage to the structure. Nevertheless, the extent to which these tools are used should be defined and uniform in order to not alter the fundamental outcome of the damage measurements.

These aspects are considered in Section 6.3 after the processing of the data obtained from the physical modelling tests with Digital Stereo Photography surveys.

4

Physical modelling test set-up

This chapter presents the set-up for the physical modelling tests carried out during this thesis. The first section describes the criteria taken into account during the planning of the physical modelling tests carried out at Uporto and Deltares. The set-up used in the Uporto deep water tests (carried out in a wave basin) is described in the second section, while the set-up used in the Deltares shallow water tests (carried out in a wave flume) is described in the third section. The fourth section describes the technique used for measuring damage, the Digital Stereo Photography.

4.1. Test planning

The physical modelling tests considered in this thesis were planned with the aim of obtaining the better validation data for the research questions discussed in the previous chapters. This planning was done before both test campaigns, with the aim of optimizing the quality of measured data as well as allowing the large number of tested conditions and repetition tests. The justification of the test conditions considered in both set-ups is briefly described below.

4.1.1. UPorto deep water tests

The Uporto deep water tests were carried out in a wave basin (see Section 4.2), and the set-up was based on coastal areas with wave conditions which are not depth-limited. Thus, conditions where the increase in the water level due to climate change would be linked to a change in the overtopping discharge were studied. Such test conditions allowed to evaluate the influence that the change in overtopping discharge has in the measured damage.

The selected set-up consisted of a low-crested rubble mound structure with a permeable core, a 1:2 slope and no foreshore. This set-up allowed the acquisition of a large amount of data in a very wide structure, allowing the validation of damage characterization concepts, parameters and methods in the following conditions:

- Currently sea level and sea level rise scenarios (in not depth-limited conditions)
- Cumulative and non-cumulative damage
- Long-crested waves and short-crested waves

4.1.2. Deltares shallow water tests

The Deltares shallow water tests were carried out in a wave flume (see Section 4.3), and the set-up was based on shallow coastal areas with wave conditions which are depth-limited. Thus, conditions where the increase in the water level due to climate change would be directly linked to a change in the incident wave height at the toe of the structure were studied.

This set-up allowed to expand significantly the conditions tested in Uporto, including a non-overtopped rubble mound structure with an impermeable core, a 1:3 slope and a foreshore. In addition, the main particularity of these tests for shallow coastal areas is that the generated wave was equal for all test runs, and only the change in the water depth at the toe of the structure defined the incident wave height. This way, the effect of the sea level rise in the damage to the structure was clearly represented. Thus, this set-up provided a large amount of complementary data given the number of tests carried out, which allowed the testing of different slope configurations and a number of repetition tests. The testing conditions included the following:

- Currently sea level and sea level rise scenarios (in depth-limited conditions)
- Cumulative and non-cumulative damage
- Adaptation alternatives: straight slope and four berm configurations
- Damage variability: repetition tests

Thus, the planning of both test campaigns were made in order to allow the generalization of the conclusions to be made on damage characterization of coastal structures and adaptation alternatives for climate change scenarios. In the next sections, the characteristics of these two physical modelling tests are described in more detail.

4.2. UPorto deep water tests set-up

The UPorto deep water tests were carried out in a wave basin at the Hydraulics Laboratory of the Faculty of Engineering of the University of Porto. This wave basin is shown in Figure 4.1 before one of the test runs.

Figure 4.1: Wave basin used for the UPorto tests.

The model set-up used in the UPorto test runs is shown in Figure 4.2, where it can be identified the four measurement locations: front slope, rear slope, roundhead and overtopping tank. In this thesis, only the damage to the front slope is considered. The cross-sections of the trunk are shown in Figures 4.3 and 4.4.

Incident wave heights were not depth-limited since no foreshore was present in this model. The model scale was 1:35 (considering reference wave climate in the Portuguese Algarve) according to Froude criterion. In this model, sufficiently large Reynolds ($Re>3{\cdot}10^4$) ensured turbulent conditions and reduced scale effects (see Section 2.3.1). In addition, the wave generation equipment included active compensation for the reflected wave at the wave board.

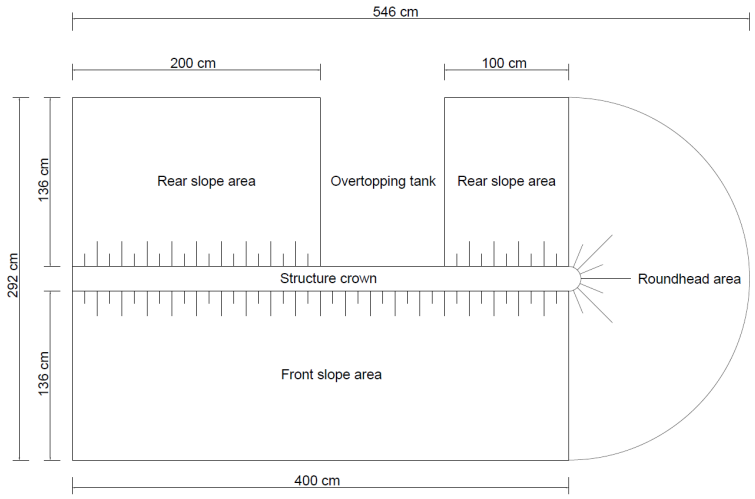

Figure 4.2: Plan view of the UPorto set-up.

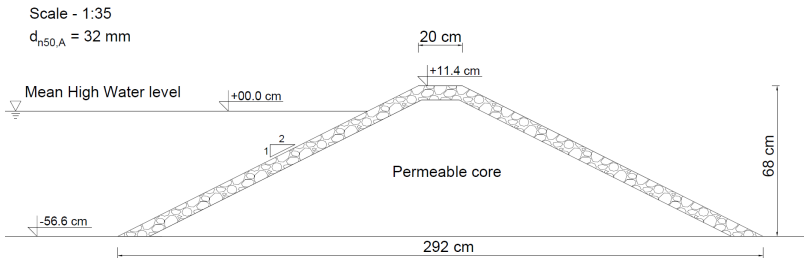

Figure 4.3: Cross-section UPorto set-up - with front slope and rear slope.

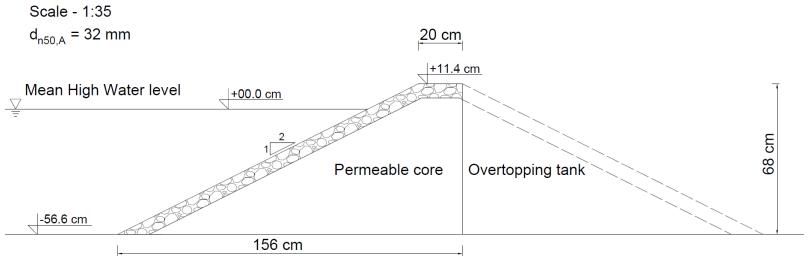

Figure 4.4: Cross-section UPorto set-up - with front slope and overtopping tank.

The main characteristics of the the model are:

- Model scale: 1:35
- Structure slope: 1:2 rock slope
- Structure total height: 0.68 m
- Structure composition: $2D_{n50}$ rock armour layer over a permeable core
- Armour gradation characteristics: D_{n50} = 32.0 mm and D_{n85}/D_{n15} = 1.25
- Core gradation characteristics: D_{n50} = 11.6 mm
- Water levels: 0.566 m for tests with MHW, 0.589 m for tests with MHW+SLR
- Freeboards: 0.114 m for tests with MHW, 0.091 m for tests with MHW+SLR

The gradation of the armour material was determined through the weighting of various samples of stones and transformed to median nominal diameter D_{n50} according to Equation 2.5. The gradation of the core material was determined by sieve analysis and transformed to median nominal diameters according to Equation 2.6. See Appendix G for more details.

The test planning included 16 test runs divided into four series briefly described below. A summary of the tested conditions are shown in Table 4.1, where it is described the type of damage (cumulative or non-cumulative), the type of waves (long-crested or short-crested), the water depth (h), the test condition (Cond.), the wave height (H_s) and the peak wave period (T_p).

- **Series 1:** cumulative damage with constant sea level and long-crested waves
- **Series 2:** non-cumulative damage with constant sea level and long-crested waves
- **Series 3:** cumulative damage with increased sea level and long-crested waves
- **Series 4:** cumulative damage with constant sea level and short-crested waves

Table 4.1: UPorto test conditions

Series	Run	Damage	Waves	h (m)	Cond.	H_s (m)	T_p (s)
S1	R1	Cum.	Long-crested	MHW - 0.566	60%	0.071	1.29
	R2	Cum.	Long-crested	MHW - 0.566	80%	0.094	1.58
	R3	Cum.	Long-crested	MHW - 0.566	100%	0.118	1.87
	R4	Cum.	Long-crested	MHW - 0.566)	120%	0.142	2.18
S2	R1	Non-cum.	Long-crested	MHW - 0.566	80%	0.094	1.58
	R2	Non-cum.	Long-crested	MHW - 0.566	100%	0.118	1.87
	R2r	Non-cum.	Long-crested	MHW - 0.566	100%	0.118	1.87
	R3	Non-cum.	Long-crested	MHW - 0.566	120%	0.142	2.18
S3	R1	Cum.	Long-crested	MHW - 0.566	60%	0.071	1.29
	R2	Cum.	Long-crested	MHW - 0.566	80%	0.094	1.58
	R3	Cum.	Long-crested	MHW+SLR - 0.589	100%	0.118	1.85
	R4	Cum.	Long-crested	MHW+SLR - 0.589	120%	0.142	2.15
S4	R1	Cum.	Short-crested	MHW - 0.566	60%	0.071	1.29
	R2	Cum.	Short-crested	MHW - 0.566	80%	0.094	1.58
	R3	Cum.	Short-crested	MHW - 0.566	100%	0.118	1.87
	R4	Cum.	Short-crested	MHW - 0.566	120%	0.142	2.18

The calibration of wave conditions were done without and with the structure, and the latter was considered in the test runs. The incident and reflected waves were measured with wave probes placed at a distance of one wave length from the toe of the structure. For tests with long-crested waves, an array of 4 aligned wave probes were used (see Figure 4.5). For tests with short-crested waves, a group of 6 wave probes were used in a CERC6 array (Davis & Regier 1977).

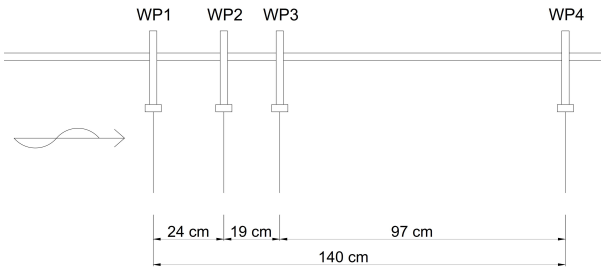

Figure 4.5: Probes distances used in the UPorto tests for long-crested waves.

4.3. Deltares shallow water tests set-up

The Deltares shallow water tests were carried out in the Western Scheldt Flume of Deltares, Delft. This wave flume is shown in Figure 4.6.

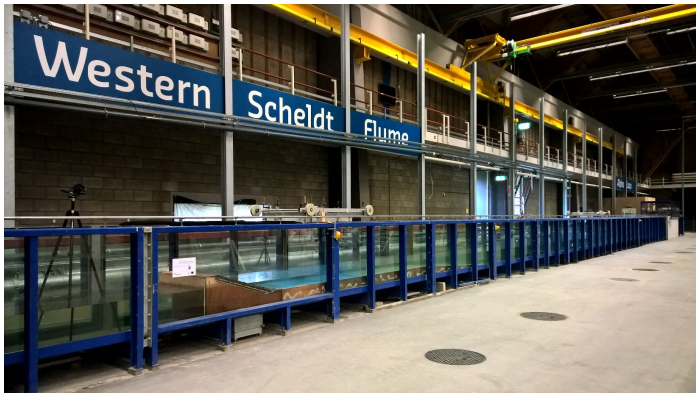

Figure 4.6: Wave flume used in the Deltares tests.

The model set-up used in the Deltares test runs is shown in Figure 4.7. During these tests, only the damage to the front slope was evaluated. Figure 4.8 presents the cross-section of the first structure to be tested: a 1:3 straight rock slope over a impermeable core. Figures 4.9, 4.10, 4.11 and 4.12 present four variations of berms added to the staight slope. These variations include the berm width ($10D_{n50}$ and $5D_{n50}$) and the berm height (at 100% and 80% water level).

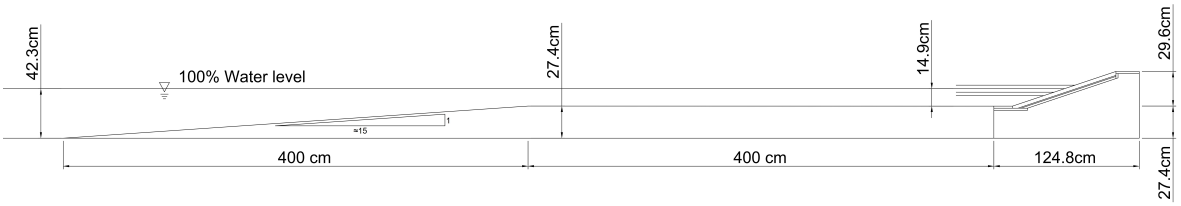

Figure 4.7: Deltares model set-up.

Incident wave heights were depth-limited since a 8 metres long foreshore was present in this model. The model scale was 1:42 (considering reference wave climate in the Dutch Wadden sea) according to Froude criterion. In this model, moderate Reynolds ($Re>1{\cdot}10^4$) did not ensure turbulent conditions so small scale effects were expected (see Section 2.3.1). In addition, the wave generation equipment included active compensation for the reflected wave at the wave board.

The main characteristics of the the model are:

- Model scale: 1:42
- Structure slope: 1:3 rock slope
- Structure total height: 0.296 m
- Structure composition: $2D_{n50}$ rock armour layer over a filter and impermeable core
- Armour gradation characteristics: D_{n50} = 16.3 mm and D_{n85}/D_{n15} = 1.25
- Filter gradation characteristics: D_{n50} = 9.4 mm
- Water levels at toe: from 0.089 m for 60% tests to 0.179 m for 120% tests.
- Freeboards: from 0.207 m for 60% tests to 0.117 m for 120% tests.

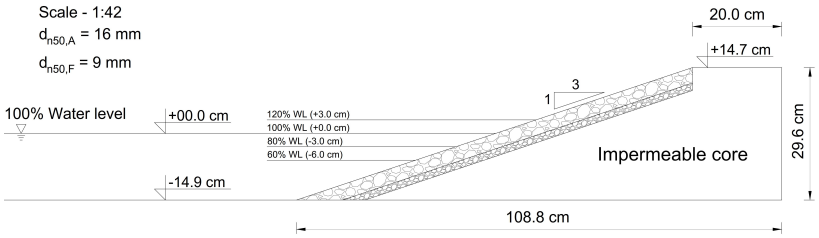

Figure 4.8: Cross-section Deltares set-up - straight slope.

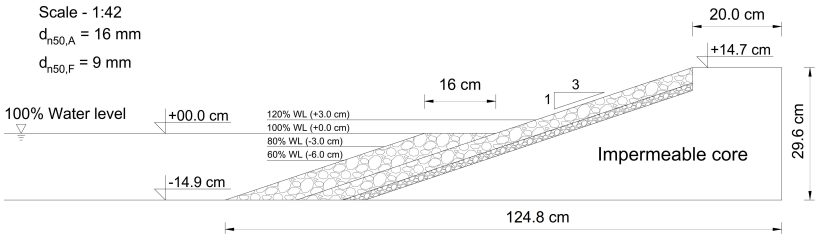

Figure 4.9: Cross-section Deltares set-up - slope with a berm $10d_{50}$ wide at the 100% water level.

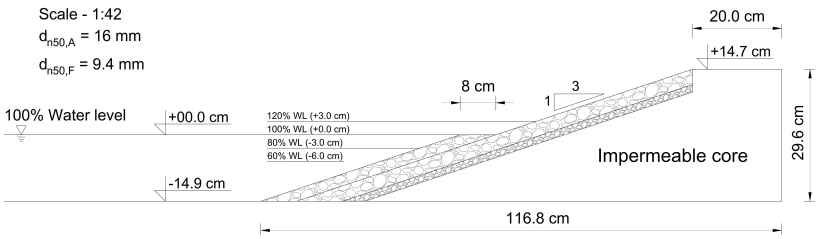

Figure 4.10: Cross-section Deltares set-up - slope with a berm $5d_{50}$ wide at the 100% water level.

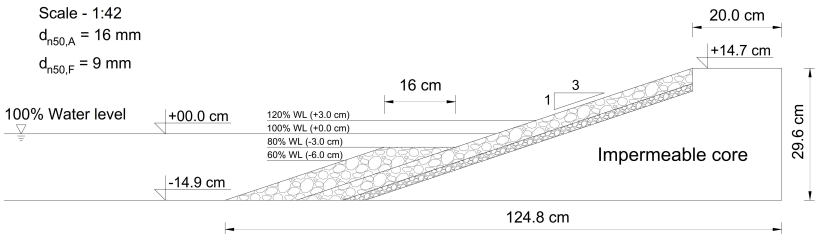

Figure 4.11: Cross-section Deltares set-up - slope with a berm $10d_{50}$ wide at the 80% water level.

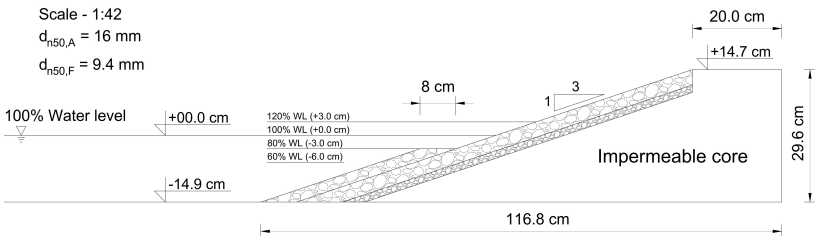

Figure 4.12: Cross-section Deltares set-up - slope with a berm $5d_{50}$ wide at the 80% water level.

The gradation of the armour and filter material was determined through the weighting of various samples of stones and transformed to median nominal diameter D_{n50} according to Equation 2.5. See Appendix G for more details. In addition, the filter material was fixed with poli-pox glue over the impermeable core, which was built with an wooden structure.

The test planning included 41 runs divided into six series briefly described below. A summary of the tested conditions are shown in Table 4.2, where the type of damage (cumulative or non-cumulative), the berm width (B), the berm level (d_b), the water depth at the toe of the structure (h_T), the test condition (Cond.), the generated wave height ($H_{s,g}$), the wave height at the toe of the structure ($H_{s,T}$) and the peak wave period (T_p) are described.

- **Series 1:** straight slope with cumulative damage (5 realizations: S1a, S1b, S1c, S1d, S1e)
- **Series 2:** straight slope with non-cumulative damage (5 realizations: S2a, S2b, S2c, S2d, S2e)
- **Series 3:** slope with a berm $10D_{n50}$ wide at the 100% water level with cumulative damage
- **Series 4:** slope with a berm $5D_{n50}$ wide at the 100% water level with cumulative damage
- **Series 5:** slope with a berm $10D_{n50}$ wide at the 80% water level with cumulative damage
- **Series 6:** slope with a berm $5D_{n50}$ wide at the 80% water level with cumulative damage

Table 4.2: Deltares test conditions

Series	Run	Damage	B (m)	d_b (m)	h_T (m)	Cond.	$H_{s,g}$ (m)	$H_{s,T}$ (m)	T_P (s)
S1	R1	Cum.	-	-	0.089	60%	0.087	0.037	1.27
	R2	Cum.	-	-	0.119	80%	0.087	0.050	1.27
	R3	Cum.	-	-	0.149	100%	0.087	0.062	1.27
	R4	Cum.	-	-	0.179	120%	0.087	0.074	1.27
S2	R1	Non-cum.	-	-	0.149	100%	0.087	0.062	1.27
S3	R1	Cum.	$10D_{n50}$	100%	0.089	60%	0.087	0.037	1.27
	R2	Cum.	$10D_{n50}$	100%	0.119	80%	0.087	0.050	1.27
	R3	Cum.	$10D_{n50}$	100%	0.149	100%	0.087	0.062	1.27
	R4	Cum.	$10D_{n50}$	100%	0.179	120%	0.087	0.074	1.27
S4	R1	Cum.	$5D_{n50}$	100%	0.089	60%	0.087	0.037	1.27
	R2	Cum.	$5D_{n50}$	100%	0.119	80%	0.087	0.050	1.27
	R3	Cum.	$5D_{n50}$	100%	0.149	100%	0.087	0.062	1.27
	R4	Cum.	$5D_{n50}$	100%	0.179	120%	0.087	0.074	1.27
S5	R1	Cum.	$10D_{n50}$	80%	0.089	60%	0.087	0.037	1.27
	R2	Cum.	$10D_{n50}$	80%	0.119	80%	0.087	0.050	1.27
	R3	Cum.	$10D_{n50}$	80%	0.149	100%	0.087	0.062	1.27
	R4	Cum.	$10D_{n50}$	80%	0.179	120%	0.087	0.074	1.27
S6	R1	Cum.	$5D_{n50}$	80%	0.089	60%	0.087	0.037	1.27
	R2	Cum.	$5D_{n50}$	80%	0.119	80%	0.087	0.050	1.27
	R3	Cum.	$5D_{n50}$	80%	0.149	100%	0.087	0.062	1.27
	R4	Cum.	$5D_{n50}$	80%	0.179	120%	0.087	0.074	1.27

The calibration of the wave conditions was done with the foreshore and without the structure, using a metallic wave dumper in order to reduce the reflected wave. The incident and reflected waves were measured at two locations: at 0.5 m from the toe of the structure on foreshore and at 18 m from the toe of the structure (10 m before the start of the 8 metres long foreshore). The measurement of the waves in both locations was done with 3 aligned wave probes as shown in Figure 4.13.

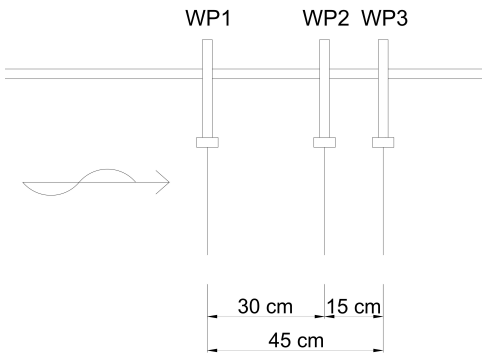

Figure 4.13: Probes distances used in the Deltares tests.

4.4. Measuring technique

Both during the UPorto and Deltares tests, the measurement of damage to the armour layer was done using the Digital Stereo Photography technique. This method included the following equipment provided by Deltares (see Figure 4.14). The description of this method and main steps can be found in Hofland et al. (2011) and Raaijmakers et al. (2012).

- A – Markers base plate: fixed origin of coordinates for the 3D reconstruction and comparison between test runs, to be kept fixed during the complete testing period.
- B – Additional markers: reference points for the 3D reconstruction, to be randomly placed before each measurement and removed after it.
- C – Cameras: two digital cameras with a fixed distance between each other.
- D – Laptop: used for obtaining the pairs of images and carrying out the post-processing.

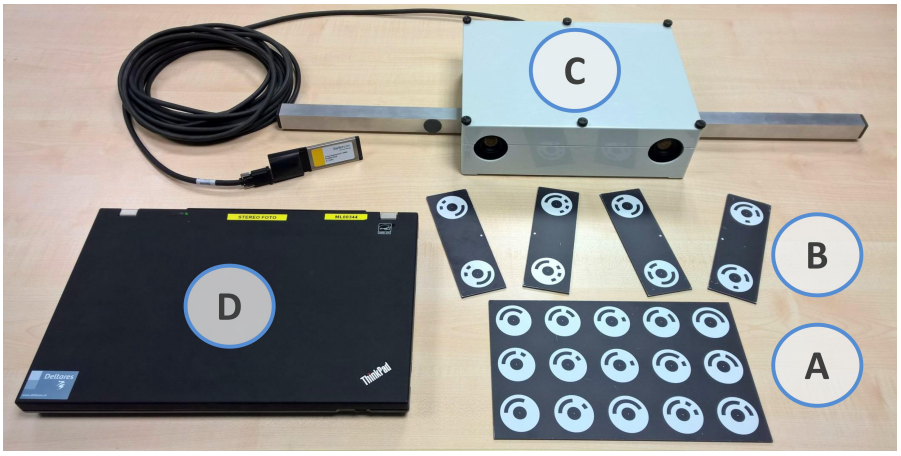

Figure 4.14: Digital Stereo Photography equipment.

5

Physical modelling test results

Following the realization of the two physical modelling test campaigns, a summary of the main results from the Uporto and Deltares tests are presented in the first and second sections. A first discussion on the main results of the two test campaigns, and a comparison with literature data is presented in the third section. Further analysis of these results are presented in Chapter 6 and Chapter 7, where the research questions of this thesis are answered.

5.1. Uporto deep water test results

This section presents the results from the Uporto deep water tests described in Section 4.2, which was composed by a total of 16 test runs divided into 4 test series.

The damage to the structure was measured with the Digital Stereo Photography (see in Section 4.4). Figure 5.1a illustrates the initial conditions of a given test series while Figure 5.1b shows the state of the structure after a given test run. The damage for each test run was obtained as the difference between the initial measurement (before test series for cumulative damage test series or before individual test runs for non-cumulative test series) and the measurement after the given test run, as shown in Figure 5.2. All damage plots from the UPorto tests are shown in Appendix A.

Table 5.1 presents the measured damage for each test run, considering the damage parameters previously discussed in Chapter 3 (S, E_{2D}, $E_{3D,1}$ and $E_{3D,5}$). These damage parameters were only determined for the front slope, which in this section includes the total 100 D_{n50} width of the front slope area (see Figure 4.2). For the damage parameters calculated for a 25 D_{n50} width and measured incident wave conditions, see Appendix H. In addition, the damage to the roundhead, to the rear slope and the overtopping measurements are not considered in this thesis.

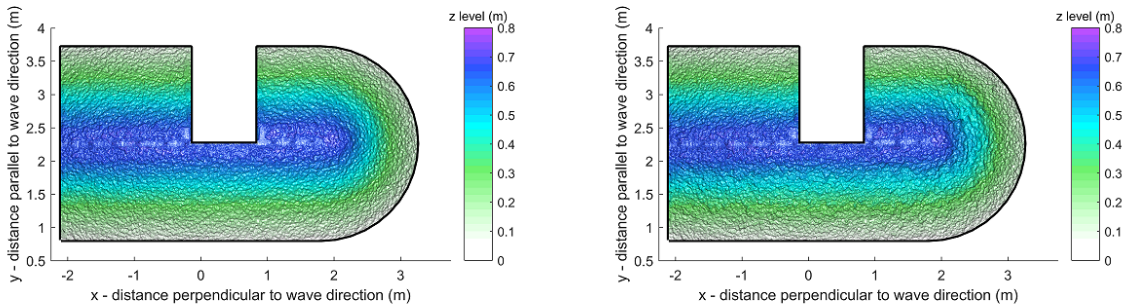

(a) Series 1 - initial conditions.

(b) Series 1 - After run 3.

Figure 5.1: UPorto damage measurements - Series 1.

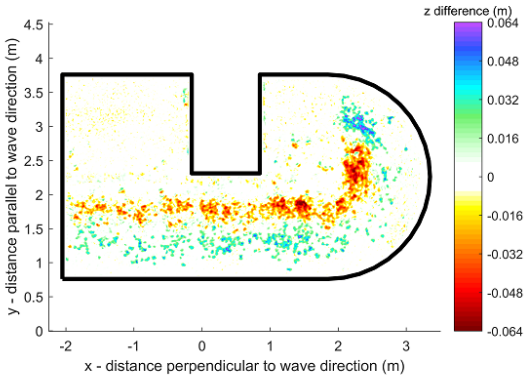

Figure 5.2: UPorto tests Series 1 - z difference: after test run 3 compared with initial.

Table 5.1: UPorto test results

Series	Run	Damage	Waves	h (m)	Cond.	S	E_{2D}	$E_{3D,1}$	$E_{3D,5}$
S1	R1	Cum.	Long-crested	MHW	60%	0.1	0.02	0.94	0.12
	R2	Cum.	Long-crested	MHW	80%	1.1	0.20	1.20	0.48
	R3	Cum.	Long-crested	MHW	100%	3.4	0.49	1.57	1.06
	R4	Cum.	Long-crested	MHW	120%	12.9	1.08	1.95	1.46
S2	R1	Non-cum.	Long-crested	MHW	80%	0.6	0.11	1.12	0.43
	R2	Non-cum.	Long-crested	MHW	100%	2.6	0.27	1.23	0.82
	R2r	Non-cum.	Long-crested	MHW	100%	3.7	0.47	1.81	1.21
	R3	Non-cum.	Long-crested	MHW	120%	12.7	0.98	1.98	1.53
S3	R1	Cum.	Long-crested	MHW	60%	0.4	0.04	1.12	0.21
	R2	Cum.	Long-crested	MHW	80%	1.4	0.13	1.08	0.51
	R3	Cum.	Long-crested	MHW+SLR	100%	1.5	0.18	1.22	0.52
	R4	Cum.	Long-crested	MHW+SLR	120%	8.9	0.70	2.08	1.63
S4	R1	Cum.	Short-crested	MHW	60%	0.0	0.02	0.77	0.06
	R2	Cum.	Short-crested	MHW	80%	0.4	0.08	0.83	0.25
	R3	Cum.	Short-crested	MHW	100%	1.4	0.22	1.18	0.70
	R4	Cum.	Short-crested	MHW	120%	4.0	0.44	1.85	1.05

The damage profiles for the 4 test series are presented in Figures 5.3, including a 90% confidence interval for the mean value. The mean damage was obtained from the total 100 D_{n50} width of the model. The confidence bounds were obtained dividing the width of the model into 10 equal sections with a width of 10 D_{n50}, applying a student-t distribution with critical t-value of 1.833 ($\delta = \pm 1.833 \cdot \sigma/\sqrt{10}$).

The analysis of these damage data is described in more detail in Chapter 6 and Chapter 7. Nevertheless, a brief analysis will be made here regarding the differences between cumulative (Series 1) and non-cumulative (Series 2) damage. In Figure 5.4a the non-cummulative damage results from Series 2 are compared with the incremental damage of each test run from Series 1 (which is obtained as the damage recorded between a given test run and the previous test). In this case, it can be seen that the non-cummulative results leads to larger erosion of the rebuilt structure (Series 2), while the cumulative tests show less damage to the already damaged structure (Series 1). In contrast, in Figure 5.4b the non-cummulative damage results from Series 2 are compared with the standard damage of each test run from Series 1 (which is obtained as the damage recorded between a given test run and the initial conditions for the series). In this case both cumulative and non-cumulative results shows a similar damage. Furthermore, Deltares test results (see Section 5.2) also shows small variations (from 0% to 5% in measured damage according to both S and $E_{3D,5}$ parameters) between cumulative (Series 1) and non-cumulative (Series 2) measured damage. Thus, according to the UPorto and Deltares test results, both testing methods presented similar damage results for rock armoured slopes.

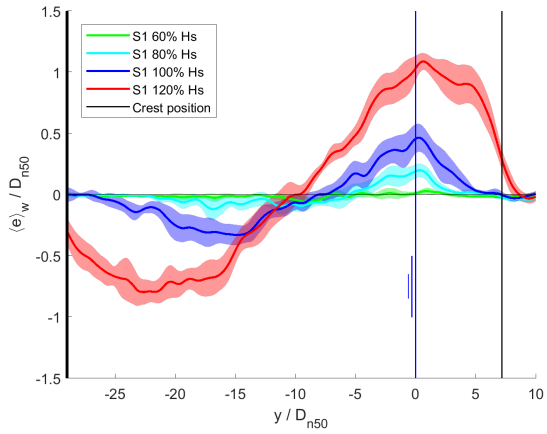

(a) Series 1: non-cumulative damage, constant level.

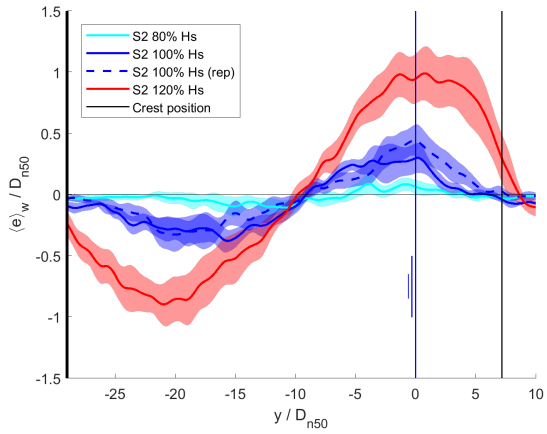

(b) Series 2: cumulative damage, constant level.

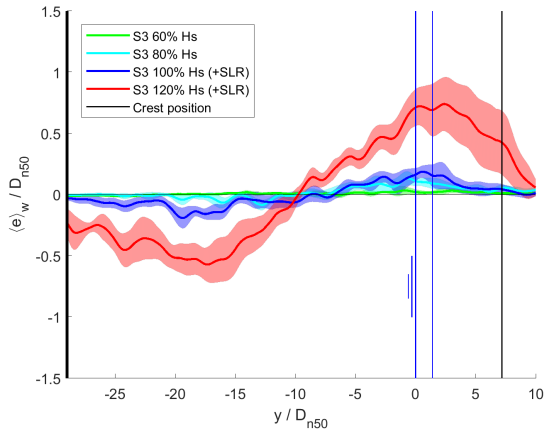

(c) Series 3: non-cumulative damage, increased level.

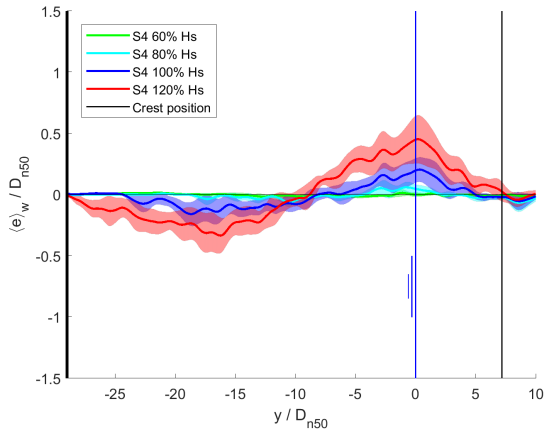

(d) Series 4: short-crested waves.

Figure 5.3: UPorto tests - Series 1-2-3-4 damage profiles with 90% confidence bounds for the mean.

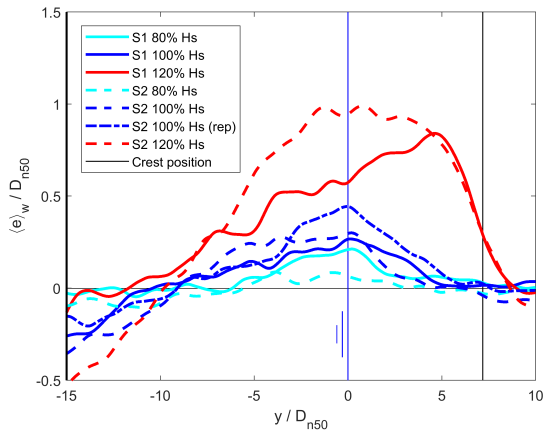

(a) Incremental damage: compared with previous test.

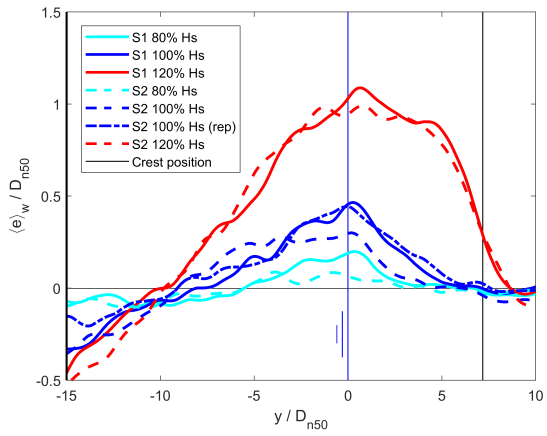

(b) Standard damage: compared with initial conditions.

Figure 5.4: UPorto tests - Analysis of cumulative (Series 1) and non-cumulative (Series 2) damage.

5.2. Deltares shallow water test results

This section presents the results from the Deltares shallow water tests described in Section 4.3, which was composed by 41 test runs divided into 6 test series.

The damage to the structure was measured with the Digital Stereo Photography (see Section 4.4). Figure 5.5a illustrates the initial conditions of a given test series while Figure 5.5b shows the state of the structure after a given test run. The damage for each test run was obtained as the difference between the initial measurement (before test series for cumulative damage test series or before individual test runs for non-cumulative test series) and the measurement after the given test run, as shown in Figure 5.6. All damage plots from the Deltares tests are shown in Appendix B.

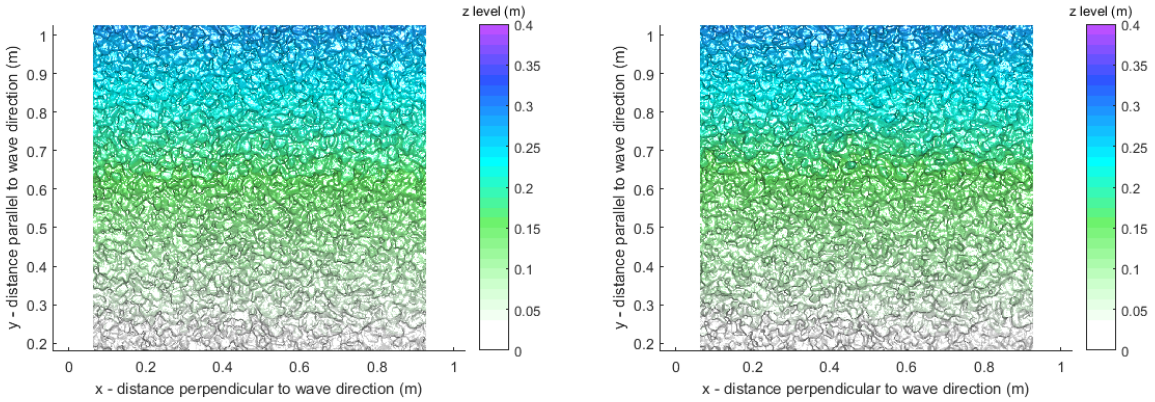

(a) Series 1a - initial conditions.

(b) Series 1a - After run 3.

Figure 5.5: Deltares damage measurements - Series 1a.

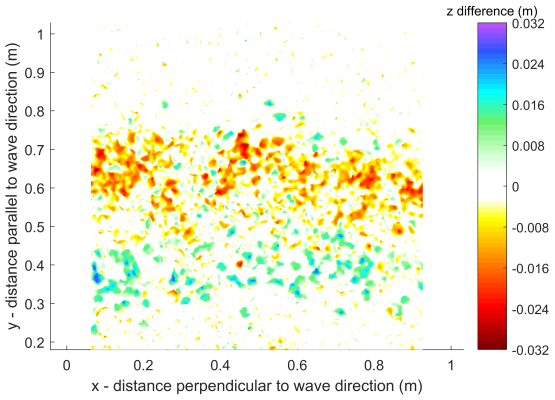

Figure 5.6: Deltares tests Series 1a - z difference: after test run 3 compared with initial.

Table 5.2 presents the measured damage for each test run considering the damage parameters previously discussed in Chapter 3 (S, E_{2D}, $E_{3D,1}$ and $E_{3D,5}$). These damage parameters were calculated considering the erosion of the front slope, and in this section includes the total 54 D_{n50} width of the model. For the damage parameters calculated for a 27 D_{n50} width and measured incident wave conditions, see Appendix H.

In addition, the damage to the configurations with a berm can be evaluated at the lower slope (which includes the horizontal berm) and the upper slope. This damage for the upper and lower slope are presented in Table 5.3 considering the damage parameters S and $E_{3D,5}$.

Table 5.2: Deltares test results

Series	Run	Damage	B (m)	d_b (m)	Cond.	S	E_{2D}	$E_{3D,1}$	$E_{3D,5}$
S1a	R1	Cum.	-	-	60%	0.2	0.07	1.03	0.18
	R2	Cum.	-	-	80%	1.3	0.13	1.07	0.31
	R3	Cum.	-	-	100%	4.3	0.45	1.46	0.66
	R4	Cum.	-	-	120%	10.9	0.83	2.00	1.25
S1b	R1	Cum.	-	-	60%	0.3	0.05	1.11	0.16
	R2	Cum.	-	-	80%	0.8	0.19	1.05	0.41
	R3	Cum.	-	-	100%	3.5	0.41	1.39	0.68
	R4	Cum.	-	-	120%	11.6	1.03	2.30	1.48
S1c	R1	Cum.	-	-	60%	0.3	0.06	1.12	0.19
	R2	Cum.	-	-	80%	0.5	0.14	1.12	0.30
	R3	Cum.	-	-	100%	3.5	0.38	1.54	0.69
	R4	Cum.	-	-	120%	11.4	0.93	1.98	1.17
S1d	R1	Cum.	-	-	60%	0.2	0.04	1.01	0.15
	R2	Cum.	-	-	80%	0.9	0.17	1.27	0.35
	R3	Cum.	-	-	100%	3.8	0.45	1.51	0.89
	R4	Cum.	-	-	120%	12.0	1.04	2.43	1.37
S1e	R1	Cum.	-	-	60%	0.3	0.11	1.10	0.16
	R2	Cum.	-	-	80%	0.9	0.15	1.22	0.36
	R3	Cum.	-	-	100%	3.2	0.35	1.36	0.71
	R4	Cum.	-	-	120%	11.0	0.99	1.94	1.27
S2a	R1	Non-cum.	-	-	100%	3.0	0.39	1.73	0.68
S2b	R1	Non-cum.	-	-	100%	4.5	0.48	1.53	0.84
S2c	R1	Non-cum.	-	-	100%	4.0	0.41	1.49	0.71
S2d	R1	Non-cum.	-	-	100%	3.3	0.35	1.32	0.74
S2e	R1	Non-cum.	-	-	100%	2.2	0.31	1.46	0.73
S3	R1	Cum.	$10D_{n50}$	100%	60%	0.1	0.03	1.13	0.18
	R2	Cum.	$10D_{n50}$	100%	80%	1.1	0.15	1.11	0.28
	R3	Cum.	$10D_{n50}$	100%	100%	2.0	0.25	1.35	0.44
	R4	Cum.	$10D_{n50}$	100%	120%	2.5	0.25	1.35	0.38
S4	R1	Cum.	$5D_{n50}$	100%	60%	0.4	0.08	0.93	0.15
	R2	Cum.	$5D_{n50}$	100%	80%	0.8	0.13	1.07	0.32
	R3	Cum.	$5D_{n50}$	100%	100%	2.9	0.51	1.40	0.81
	R4	Cum.	$5D_{n50}$	100%	120%	4.8	0.58	1.40	0.86
S5	R1	Cum.	$10D_{n50}$	80%	60%	0.7	0.11	1.09	0.22
	R2	Cum.	$10D_{n50}$	80%	80%	0.7	0.14	1.09	0.28
	R3	Cum.	$10D_{n50}$	80%	100%	0.9	0.16	1.24	0.25
	R4	Cum.	$10D_{n50}$	80%	120%	4.6	0.45	1.30	0.74
S6	R1	Cum.	$5D_{n50}$	80%	60%	0.3	0.04	0.97	0.17
	R2	Cum.	$5D_{n50}$	80%	80%	1.0	0.14	1.11	0.28
	R3	Cum.	$5D_{n50}$	80%	100%	3.2	0.31	1.35	0.68
	R4	Cum.	$5D_{n50}$	80%	120%	4.7	0.53	1.51	0.74

Table 5.3: Deltares test results - slope with a berm - lower and upper slope

Series	Run	S TOTAL	S Lower	S Upper	$E_{3D,5}$ TOTAL	$E_{3D,5}$ Lower	$E_{3D,5}$ Upper
S3	R1	0.1	0.1	0.0	0.18	0.18	0.01
	R2	1.1	1.1	0.0	0.28	0.28	0.02
	R3	2.0	1.7	0.3	0.44	0.44	0.20
	R4	2.5	1.5	1.0	0.38	0.38	0.38
S4	R1	0.4	0.4	0.0	0.15	0.15	0.03
	R2	0.8	0.8	0.0	0.32	0.32	0.08
	R3	2.9	2.8	0.1	0.81	0.81	0.18
	R4	4.8	2.9	1.9	0.86	0.86	0.53
S5	R1	0.7	0.6	0.1	0.22	0.22	0.04
	R2	0.7	0.6	0.1	0.28	0.28	0.11
	R3	0.9	0.6	0.3	0.24	0.24	0.18
	R4	4.6	1.2	3.4	0.74	0.31	0.74
S6	R1	0.3	0.2	0.1	0.17	0.17	0.03
	R2	1.0	0.7	0.3	0.28	0.28	0.20
	R3	3.2	1.2	2.0	0.68	0.37	0.68
	R4	4.7	0.1	4.6	0.74	0.24	0.74

The damage profiles for the 6 test series are shown below, including a 90% confidence interval for the mean value. Figure 5.7 shows all the damage profiles for the Series 1 tests. In more detail, Figures 5.7a, 5.7b, 5.7c, 5.7d and 5.7e show the damage profile for each test run while Figure 5.7f shows the average damage considering the mean of the 5 realizations for that series. Thus, plots a, b, c, d and e include the mean damage obtained from the total 54 D_{n50} width of the model, while the confidence bounds were obtained dividing the width of the model into 6 equal sections with a width of 9 D_{n50}, applying a student-t distribution with critical t-value of 2.015 ($\delta = \pm 2.015 \cdot \sigma/\sqrt{6}$). Plot f includes the mean damage obtained from the combined 270 D_{n50} width of the 5 test realizations in the 54 D_{n50} wide model, and the confidence bounds were obtained dividing this combined width into 30 equal sections with a width of 9 D_{n50}, applying a student-t distribution with critical t-value of 1.699 ($\delta = \pm 1.699 \cdot \sigma/\sqrt{30}$).

Figure 5.8 presents all the damage profiles for Series 2 tests. In more detail, Figures 5.8a, 5.8b, 5.8c, 5.8d and 5.8e shows the damage profile for each test run while Figure 5.8f shows the average damage considering the mean of the 5 realizations for that series. The process to obtain the mean and confidence bounds were the same as for Series 1.

The analysis of these damage data is described in more detail in Chapter 6 and Chapter 7. Nevertheless, a brief analysis will be made here regarding the variability observed in the damage in the series were repeated tests were carried out (Series 1 and Series 2). The first remark is that even if $54D_{n50}$ is wider than the section usually considered in physical modelling tests, a large scatter is observed in the results. In addition, it can be also observed that when a combined test width of $270D_{n50}$ is considered (see Figures 5.7f and 5.8f), the mean damage value can be estimated more precisely and the difference between damage levels can be distinguished with a large level of confidence (e.g. $\pm 0.12D_{n50}$ for $54D_{n50}$ tests and $\pm 0.05D_{n50}$ for $270D_{n50}$ tests when considering 120% damage results).

Furthermore, two additional conclusions can be drawn. First, it can be seen that increased water levels allowed larger waves acting on the structure (given the same wave generated offshore in all test runs) and consequently much larger damage was recorded on the structure. Second, it can be observed that in the Deltares tests (1:3 slope in shallow water) the maximum damage in 100% and 120% tests is located approximately $5D_n50$ above the water level, while for the UPorto tests (1:2 slope in deep water) the maximum damage in 100% and 120% tests is located around the water level.

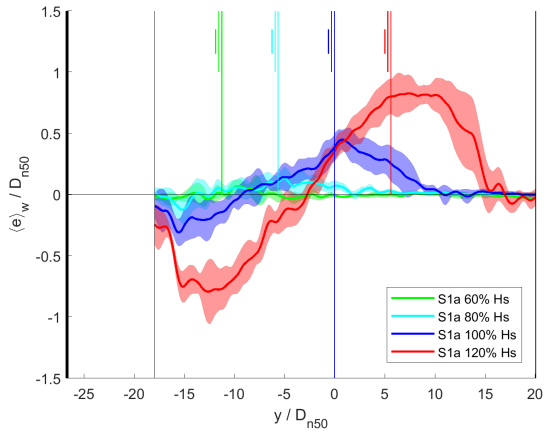

(a) Series 1a: cumulative damage tests.

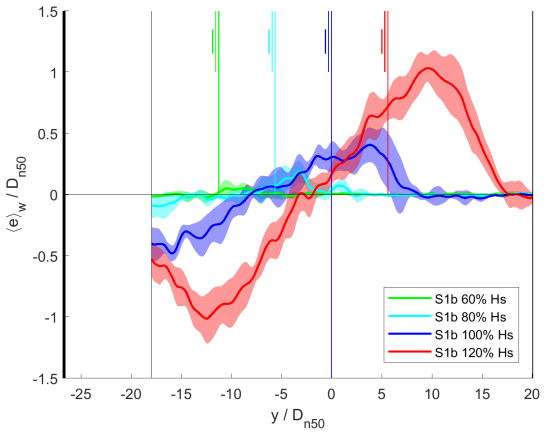

(b) Series 1b: cumulative damage tests.

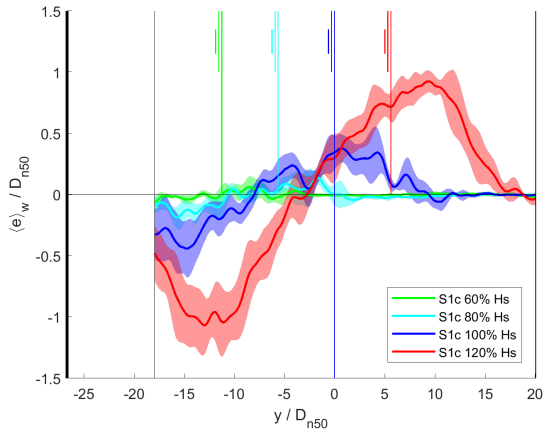

(c) Series 1c: cumulative damage tests.

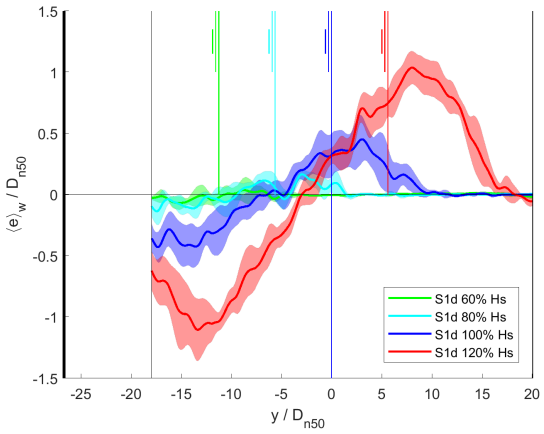

(d) Series 1d: cumulative damage tests.

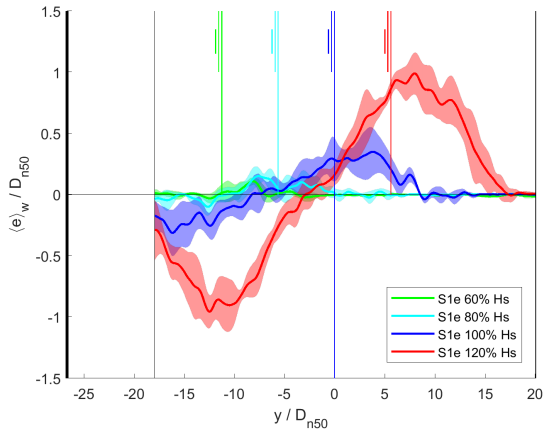

(e) Series 1e: cumulative damage tests.

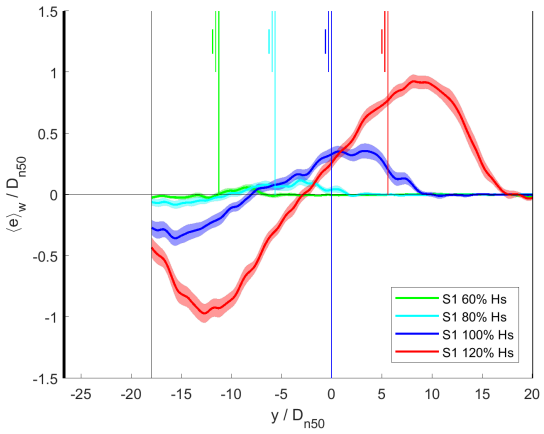

(f) Series 1 average: mean S1a, S1b, S1c, S1d, S1e.

Figure 5.7: Deltares tests - Series 1 damage profiles with 90% confidence bounds for the mean.

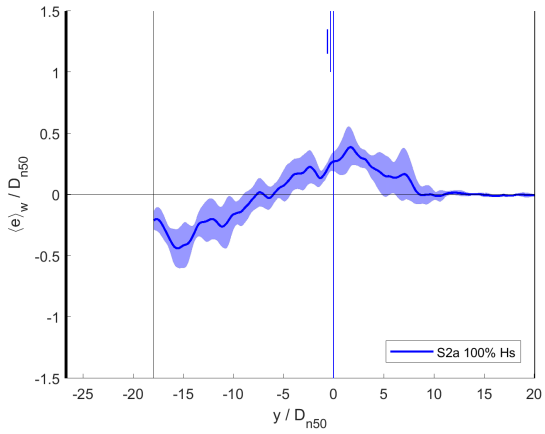

(a) Series 2a: non-cumulative damage test.

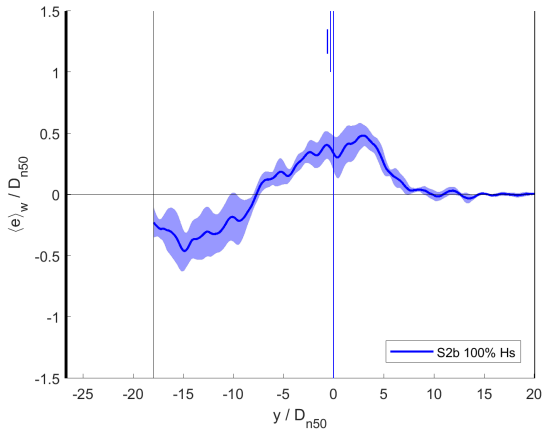

(b) Series 2b: non-cumulative damage test.

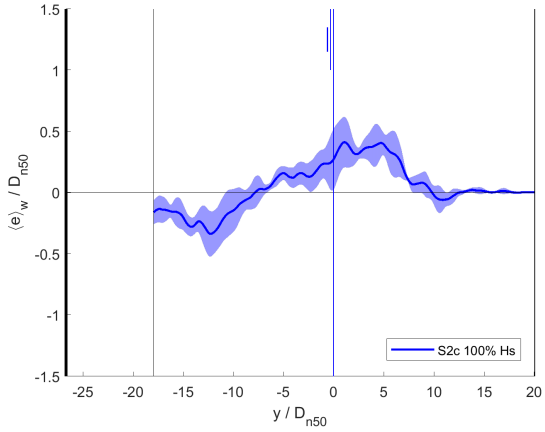

(c) Series 2c: non-cumulative damage test.

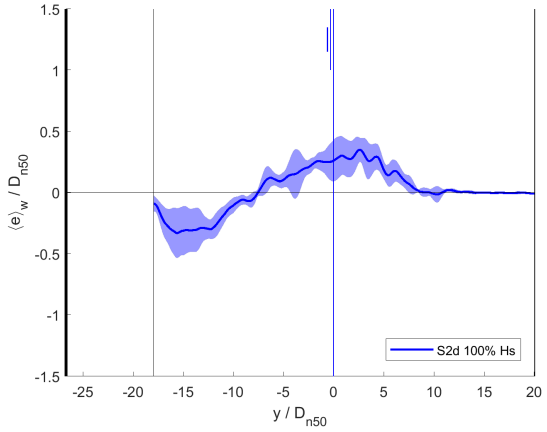

(d) Series 2d: non-cumulative damage test.

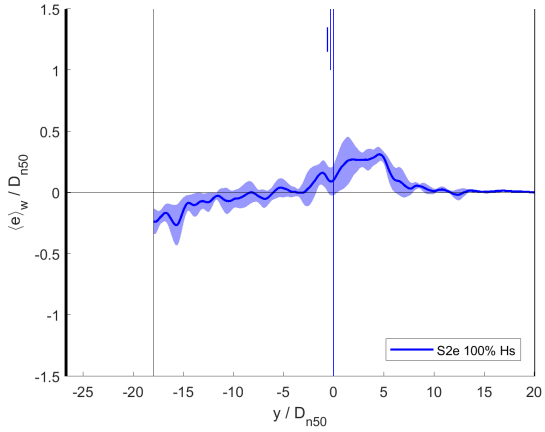

(e) Series 2e: non-cumulative damage test.

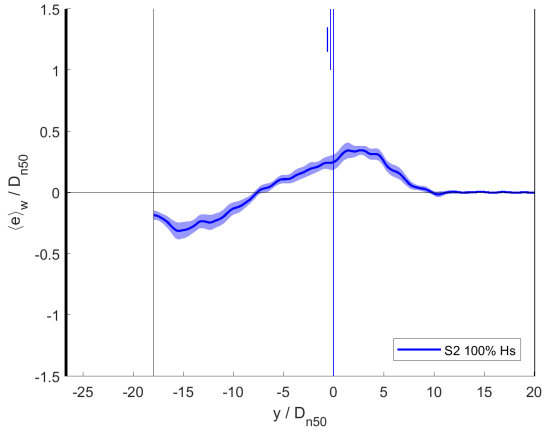

(f) Series 2 average: mean S2a, S2b, S2c, S2d, S2e.

Figure 5.8: Deltares tests - Series 2 damage profiles with 90% confidence bounds for the mean.

Figure 5.9 shows the damage profiles for the 4 test series with the presence of a berm: Series 3a (Figure 5.9a), Series 4a (Figure 5.9b), Series 5a (Figure 5.9c), Series 6a (Figure 5.9d). These series were only executed once, so the mean trend and confidence bounds were obtained in the same way the individual test series of Series 1 and 2: the mean damage obtained from the total 54D_{n50} width of the model, and the confidence bounds were obtained dividing the width of the model into 6 equal sections with a width of 9D_{n50}, applying a student-t distribution with critical t-value of 2.015 ($\delta = \pm 2.015 \cdot \sigma/\sqrt{6}$). The analysis of this damage data is described in more detail in Chapter 7.

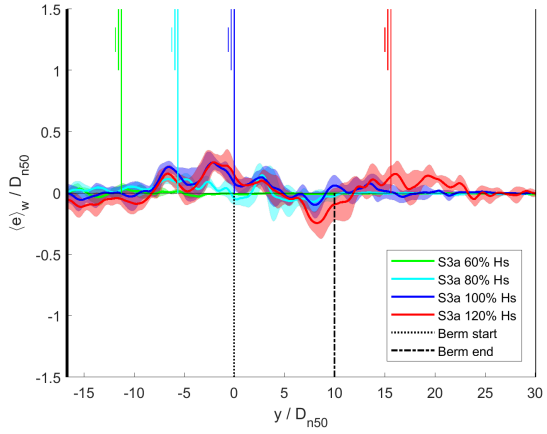

(a) Series 3a: wide (10D_{n50}) high (100% level) berm.

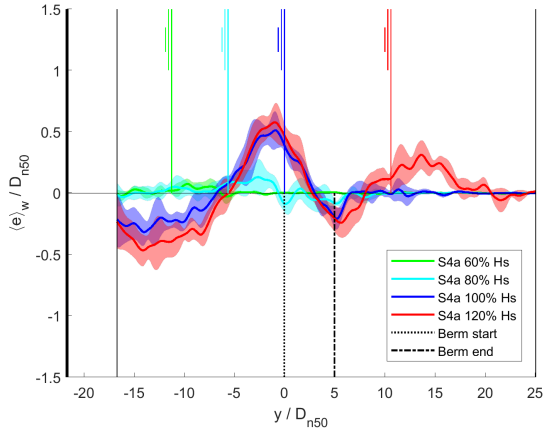

(b) Series 4a: narrow (5D_{n50}) high (100% level) berm.

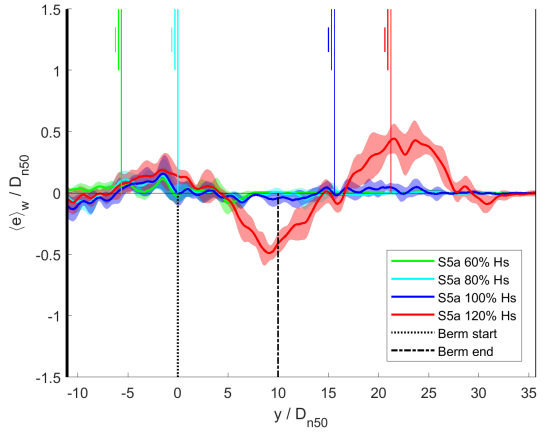

(c) Series 5a: wide (10D_{n50}) low (80% level) berm.

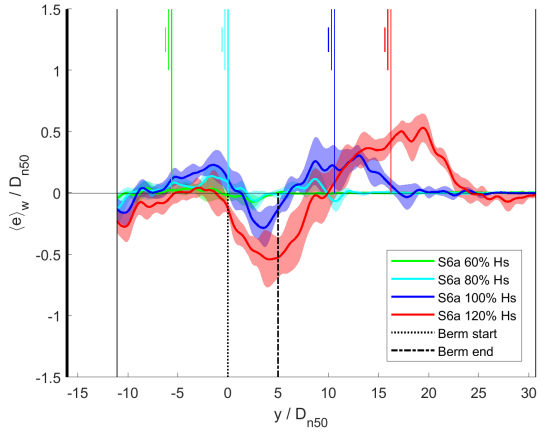

(d) Series 6a: narrow (5D_{n50}) low (80% level) berm.

Figure 5.9: Deltares tests - Series 3-4-5-6 damage profiles with 90% confidence bounds for the mean.

5.3. Test results analysis

This section briefly discusses the measured damage results in comparison with the formulae present in literature. For the comparisons regarding straight slope tests, the formulae from van der Meer (1988) and van Gent et al. (2003) were considered (see Section 2.1.2). For the comparisons of the results for the slopes with a berm, the formulae from van Gent (2013) were considered (see Section 2.1.3). Following these comparisons, various brief conclusions are drawn regarding the the variability in the measured results. In addition, it is also discussed the different test conditions used for the derivation of these formulae with respect to the ones used in the UPorto and Deltares tests.

5.3.1. Straight slope

The UPorto deep water test results are compared with the van der Meer (1988) formula (see Equations 2.8 and 2.9) in Figure 5.10. This comparison is made considering the measured damage according to the damage parameter S from Series 1, Series 2 and Series 3 (Series 4 is not considered for this comparison), summing a total of 12 test runs with a model width of 100 D_{n50}. Nevertheless, for the comparison the damage was obtained for smaller sections of 25 D_{n50}, leading to a total of 48 test results. This characterization width aspect for will be further discussed in Chapter 6. In the van der Meer (1988) formulae, the one-third wave height $H_{1/3}$ is the significant wave height to be considered and the mean period T_m is the period to be used. In addition, a permeability coefficient of P = 0.5 was considered together with a number of waves N = 1000.

Furthermore, the measured damage in the UPorto tests were cumulative without reconstruction between the 4 tests in a series (Series 1 and Series 3) and non-cumulative (Series 2). Differently, the derivation of the van der Meer (1988) formulae considered non-cumulative tests only. Regarding the wave data for the UPorto tests, it was measured as described in Section 4.2.

According to these results it can be observed that the measured damage is within the formula estimations with a 90% confidence level. It can also be observed that according to these results the difference of cumulative and non-cumulative damage measurements are not evident (Series 1 compared to Series 2). Furthermore, the tests with increased water levels (Series 3) present lower damage which is expected to be caused by the increase of the overtopping discharge. Nevertheless, it should be considered that only a reduced number of configurations were tested, so no further conclusions are made about the repeatability of the damage predicted by this formula.

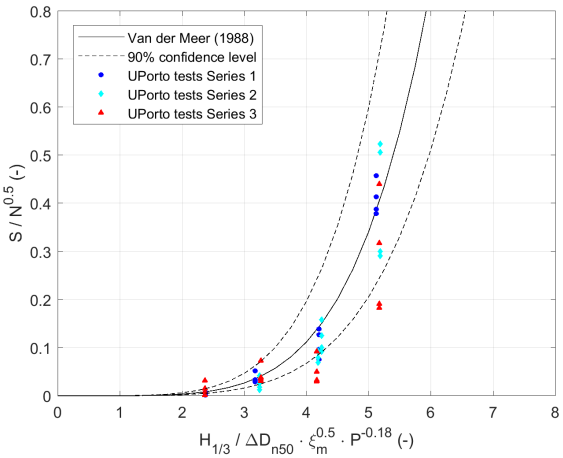

Figure 5.10: UPorto damage compared with van der Meer (1988) - plunging breaking.

The Deltares shallow water test results are compared with the van der Meer (1988) formula modified by van Gent et al. (2003) (see Equations 2.13 and 2.14) in Figure 5.11. This comparison is made considering the measured damage according to the damage parameter S from Series 1 and Series 2 (Series 3-4-5-6 with the slope with a berm are not considered for this comparison), summing a total of 25 test runs with a model width of 54 D_{n50}. Nevertheless, for the comparison the damage was obtained for smaller sections of 27 D_{n50}, leading to a total of 50 test results. This characterization width aspect for will be further discussed in Chapter 6. From these 50 test results, 20 correspond to conditions with surging breaking (runs 1 and run 2 with 60% and 80% conditions) while 30 correspond with plunging breaking (runs 3 and run 4 with 100% and 120% conditions). In the the van der Meer (1988) formula modified by van Gent et al. (2003) the one-third wave height $H_{1/3}$ is the significant wave height to be considered and the spectral wave period $T_{m-1,0}$ is the period to be used. In addition a permeability coefficient of P = 0.1 was considered together with a number of waves N = 1000.

Furthermore, the measured damage in the Deltares tests were cumulative in all test series, without reconstruction between the 4 tests in an individual series. Differently, the derivation of the van der Meer (1988) formulae and the modification by van Gent et al. (2003) considered non-cumulative tests only. Regarding the wave data for the Deltares tests, it was measured as described in Section 4.3.

According to these results (see Figure 5.11) it can be observed that the measured damage is withing the formula estimations with a 90% confidence level. Furthermore, the expected scale effects due to a reduced unit dimensions (see Section 4.3) are not evident in these results. As stated for the case of the UPorto tests, it should be considered that only a reduced number of configurations were tested, so no further conclusions are made about the repeatability of the damage predicted by this formula.

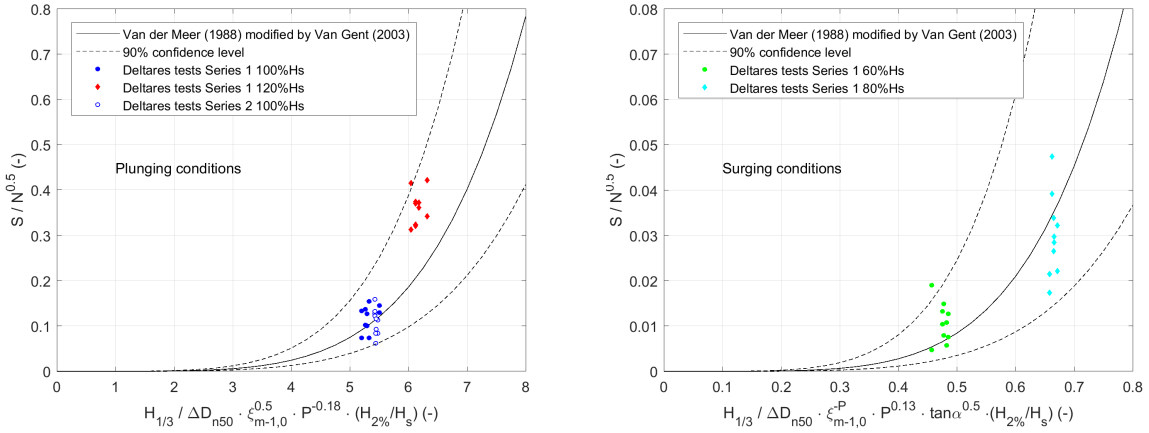

(a) Plunging breaking.

(b) Surging breaking.

Figure 5.11: Deltares damage compared with van der Meer (1988) modified by van Gent et al. (2003).

5.3.2. Slopes with a berm

The Deltares shallow water test results with berm configurations are compared with the van Gent (2013) formula (see Equations 2.17 and 2.18) in Figure 5.12. This comparison is made for the damage parameter S from Series 3-4-5-6 which include variations in the berm width and height, summing a total of 16 test runs with a model width of 54 D_{n50}. Nevertheless, for the comparison the damage was obtained for smaller sections of 27 D_{n50}, leading to a total of 32 test results. This characterization width aspect for will be further discussed in Chapter 6.

In the van Gent (2013) formula the spectral significant wave height H_{m0} is the significant wave height to be considered and the spectral wave period $T_{m-1,0}$ is the period to be used. Nevertheless, a modification to this formula was introduced here and $H_{1/3}$ is used as the significant wave height. Using $H_{1/3}$ instead of H_{m0} was considered since van Gent (2013) is derived for deep water conditions while in the Deltares tests the wave conditions were depth-limited with severe breaking taking place on the foreshore.

Furthermore, it should be considered that the tested conditions include additional differences with respect to the tests used for the derivation of the formula. The Deltares tests includes differences in the permeability (P = 0.1 while the formula was based on tests typically characterized by P = 0.5), in the slope (1:3 while the formula considers 1:2 and 1:4), in the berm level ratio (h_B / H_s up to -2 while the formula considers up to -1), in the breaking conditions (surging breaking for 60% and 80% conditions and plunging breaking for 100% and 120% tests while the formula was based on tests with plunging breaking only) and in the water depth (depth-limited wave conditions with breaking on the foreshore while the formula considers non depth-limited conditions). These differences should then be considered in the comparison between the measured and estimated damage. Regarding the wave data for the Deltares tests, it was measured as described in Section 4.3.

In addition, the Deltares tests with berm configurations had also cumulative damage measurements which is the same conditions used for the derivation of the formula by van Gent (2013). This author considers that "the observed damage is dominated by the highest waves and hardly affected by the previous test runs with lower waves", which is in line with the similar results obtained with cumulative and non-cumulative damage measurements for the straight rock slopes discussed above.

All the damage results for the test series with berm configurations are shown in Figure 5.12 with a 90% confidence level for the formula estimation. In this comparison, all the damage results are considered to be obtained in plunging conditions, since the distinction between plunging and surging conditions did not improve the confidence in the formula estimation (see Appendix I, where surging and plunging conditions are distinguished).

According to these results, it can observed that the measured damage seems rather well estimated by the van Gent (2013) formula. The largest deviations correspond to the configurations with the lowest and narrowest berm (Series 6) where the damage to the upper slope is underestimated by the formula while the damage to the lower slope is overestimated. Following these observations, a larger number of tests with berm configurations are recommended in depth-limited conditions in order to validate with more confidence the design formula in such conditions.

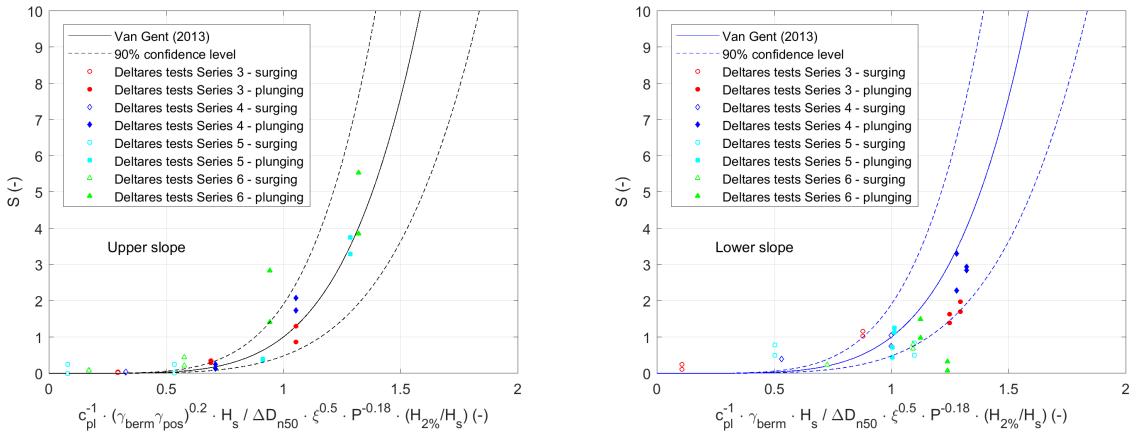

(a) Upper slope.

(b) Lower slope.

Figure 5.12: Deltares damage for slopes with a berm compared with van Gent (2013).

6

Damage characterization methods

This chapter has the aim of validating the theoretical concepts, parameters and methods for damage characterization based on the physical modelling test results (see Chapter 4 and Chapter 5 for details regarding the UPorto deep water tests and the Deltares shallow water tests). This chapter will address sub-question 1, 2 and 3 in the first, second and third section respectively. In addition, the fourth section discusses the conclusions and outcomes from these three sub-questions.

6.1. Validating damage concepts

This section addresses sub-question 1 (How can we establish and validate unified concepts of ”damage initiation”, ”intermediate damage” and ”failure” in rubble mound structures?). This section follows what has been introduced in 3.2 and is divided into two sub-sections. The first section addresses the definition of the characterization width while the second addresses the definition of the damage limits.

6.1.1. Characterization width

The validation of the most suitable characterization width for damage characterization of coastal structures was made considering the UPorto tests carried out in the wave basin and the Deltares tests carried out in a wave flume. UPorto test results will be used given its wider trunk section in an analysis considering their average values, while Deltares test results will be used given its various repetitions in an analysis considering their variability.

UPorto tests - Mean evolution

The influence of different characterization widths can be observed in Figure 6.1 for damage parameters S, E_{2D}, $E_{3D,1}$ and $E_{3D,5}$. Similar results from the Deltares tests are shown in Appendix C. The values for each characterization width are obtained as the average of all the values for that given width, being between 50 values for the $2D_{n50}$ width and 1 value for the $100D_{n50}$. This average damage is then normalized by the damage obtained for the $100D_{n50}$ characterization width.

Regarding the parameters obtained from width-averaged profiles (S in Figure 6.1a and E_{2D} in Figure 6.1b), it can be observed that the measured mean damage reduces with increased characterization width. In addition, two different behaviours for low damage and high damage conditions can be distinguished hereafter:

- **High damage conditions (100% and 120%):** S and E_{2D} damage parameters become increasingly stable with characterization widths larger than $25D_{n50}$, although considering wider sections will still affect the measured damage.
- **Low damage conditions (80%):** S and E_{2D} damage parameters do not stabilize with increased characterization widths up to widths of $100D_{n50}$. Thus, a strong characterization width effect is present in the measured damage.

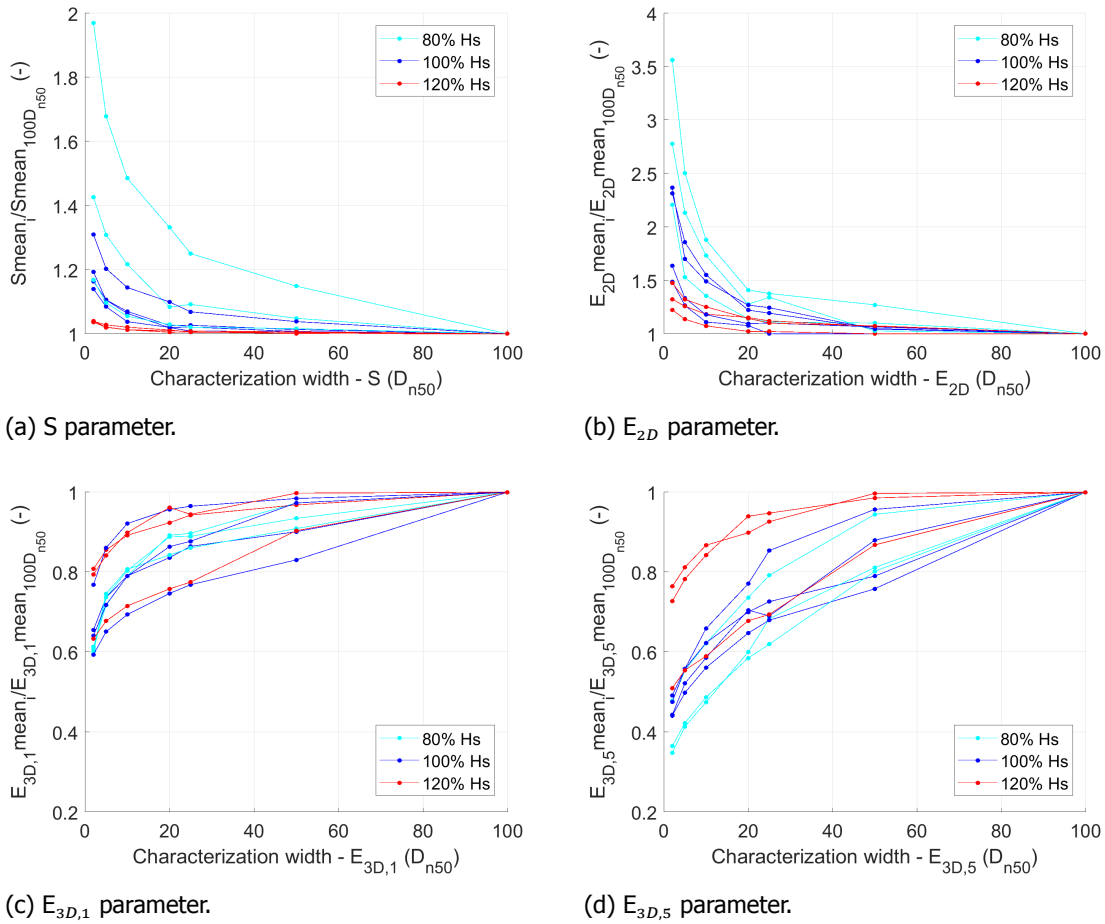

(a) S parameter.

(b) E_{2D} parameter.

(c) $E_{3D,1}$ parameter.

(d) $E_{3D,5}$ parameter.

Figure 6.1: Characterization width mean damage variation - UPorto tests Series 1-2-3.

Regarding the parameters obtained as the maximum erosion depth observed within a given characterization width ($E_{3D,1}$ in Figure 6.1c and $E_{3D,5}$ in Figure 6.1d), it can be observed that the measured damage increases with increased characterization width. For these damage parameters, there is no clear distinction between the variation in measured damage for low and high damage conditions as observed previously for S and E_{2D} parameters.

The main observation for this damage parameter $E_{3D,m}$ is that the measured damage continues to increase with increasing characterization widths. This suggests that there is no upper limit for the damage to the structure and that when considering wider structures the probability of observing a larger extreme damage will continue to increase. This length effect for the design and characterization of coastal structures should then be taken into account. Thus, the characterization width for this parameter cannot be defined only as a recommended fixed value or limit but will be described as part of a extreme value distribution for damage to coastal structures (see Section 6.2.2). All these aspects will continue to be discussed in the next sections aiming of a clear definition of suitable characterization widths considering the particularities of each damage parameter.

Deltares tests - Variability evolution

This sub-section addresses the variability of the results for each characterization width. These results are obtained from five identical realizations of Series 1, which consists of four test runs each (60%Hs, 80%Hs, 100%Hs and 120%Hs). It can be observed that the standard deviation normalized by the mean of the different damage parameters (see Figure 6.2 for damage parameters S, E_{2D}, $E_{3D,1}$ and $E_{3D,5}$) have a different behaviour, that will be briefly described below.

Regarding the parameters obtained from width-averaged profiles (S in Figure 6.2a and E_{2D} in Figure 6.2b), it can be observed that the increase in the characterization width leads to a general reduction of the variability in the measurements (although for damage parameter E_{2D} and very small damage such as the 60%Hs conditions this pattern is not clear).

Regarding the parameters obtained as the maximum erosion depth observed within a given characterization width ($E_{3D,1}$ in Figure 6.2c and $E_{3D,5}$ in Figure 6.2d), the influence of the characterization width in the variability of the results has less scatter than for S and E_{2D}. In these cases ($E_{3D,1}$ and $E_{3D,5}$) and for all damage conditions, there is a reduction of the variability with increased characterization width, specially after roughly $27D_{n50}$.

Comparing the behaviour of all damage parameters, it can be stated that $E_{3D,1}$ and $E_{3D,5}$ damage parameters presents a much smaller variability than S and E_{2D}. Thus, this variability study support the hypothesis that this $E_{3D,m}$ parameters can be considered as the reference for damage characterization.

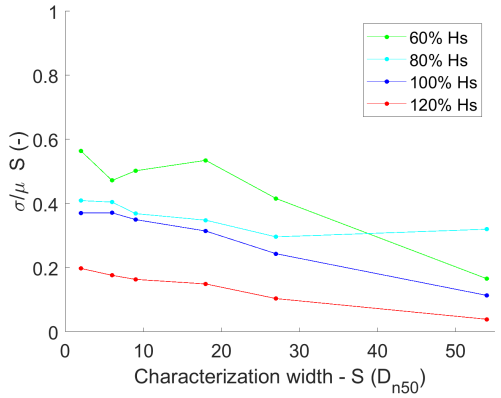

(a) S parameter.

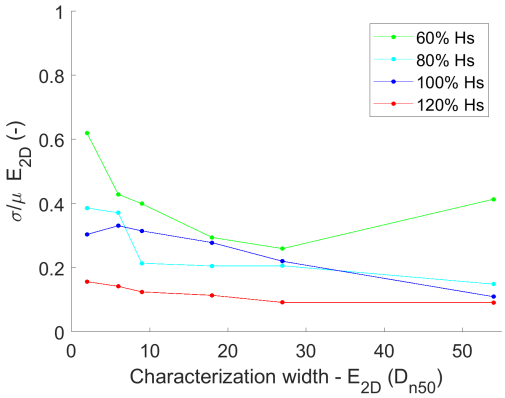

(b) E_{2D} parameter.

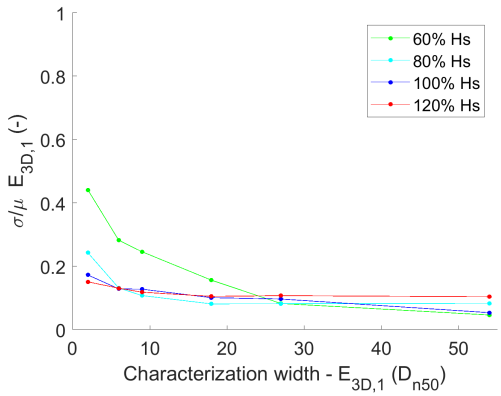

(c) $E_{3D,1}$ parameter.

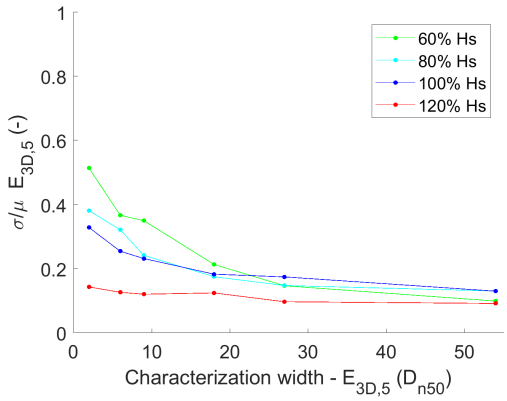

(d) $E_{3D,5}$ parameter.

Figure 6.2: Standard deviation normalized by the mean - Deltares tests Series 1.

In addition, Figure 6.3 compares the variability of cumulative and non-cumulative damage for all four damage parameters. The cumulative damage is part of Series 1 results (run 3 with 100% condition only) while non-cumulative damage is part of the single-test Series 2 results (run 1 with 100% condition). This comparison is also made based on the average deviation from the mean for each characterization width. It can be observed that, besides different damage results (see Chapter 5 for more details), both testing procedures present similar variability in the measured damage according to all damage parameters.

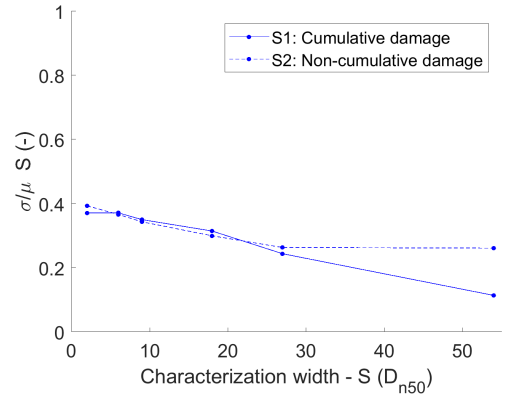

(a) S parameter.

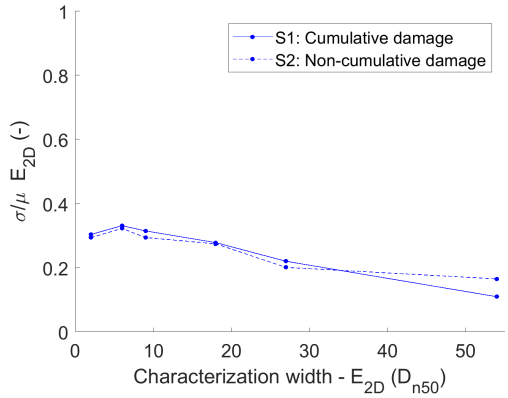

(b) E_{2D} parameter.

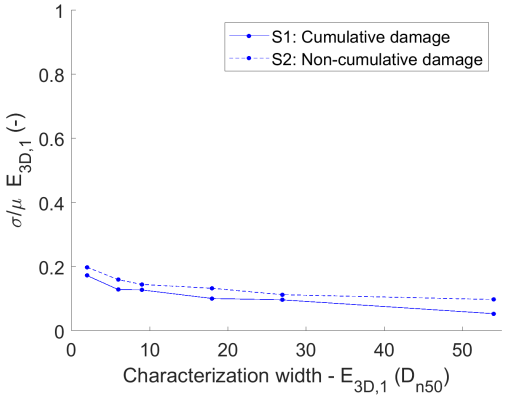

(c) $E_{3D,1}$ parameter.

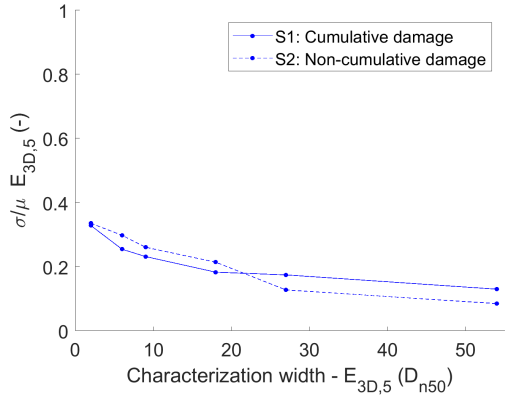

(d) $E_{3D,5}$ parameter.

Figure 6.3: Standard deviation normalized by the mean - Deltares tests Series 1 (100%) and Series 2.

Conclusions regarding characterization width

Following the previous results, it can be stated that the characterization width is an important factor in the definitions of damage to coastal structures. As it was introduced in Chapter 3 and evaluated here, the effect of the characterization width is different for the different damage parameters. Nevertheless, for the different structure configurations (UPorto and Deltares tests) the same conclusions were drawn according to the test results. In addition, in order to present recommendations for the selection of suitable characterization widths, the following criteria is considered:

- **Mean evolution:** as shown in Figures 6.1, it should be considered that different characterization widths will affect the measured damage (bias error). Thus, a suitable characterization width will be the one that shows the smallest difference in mean measured damage compared to what is obtained when considering different characterization widths.

- **Variability evolution:** as shown in Figures 6.2, it should be considered that different characterization widths will present different variability in the results when the same condition is tested repeated times (random error). Thus, a suitable characterization width will be the one that shows the smallest variability in the results.

- **Laboratory conditions:** as a third condition, the recommendations regarding the most suitable characterization widths should take into account the limited space available for physical modelling tests and the associated costs that limits the experiment dimensions. In addition, the implication of the scaling constraints which limit the possibility of reducing the units size in the armour of the structure should be taken into account. Thus, a suitable characterization width will be the one that could fit into general testing facilities without introducing scale effects.

Considering these criteria, the analysis carried out in this thesis from now on is based on a characterization width of 25-27D_{n50} for all damage parameters (S, E_{2D}, $E_{3D,1}$ and $E_{3D,5}$). In addition, for the damage parameters obtained as the maximum erosion depth observed within a given characterization width ($E_{3D,m}$), an extreme value distribution is considered in order to estimate the expected maximum damage for a structure wider than 25-27D_{n50}.

6.1.2. Damage limits

The damage limits proposed in Chapter 3 will be validated in this section considering the UPorto and Deltares physical modelling tests. These proposed limits for a 2D_{n50} thick rock armoured slopes are:

- **Damage initiation:** defined as the condition where a circular hole of 1D_{n50} diameter and a depth of 1D_{n50} is observed in the armour layer.
- **Intermediate damage:** defined as the condition where a circular hole of 1D_{n50} diameter and a depth of 1.5D_{n50} is observed in the armour layer.
- **Failure limit:** defined as the condition where a circular hole of 1D_{n50} diameter and a depth of 2D_{n50} is observed in the armour layer.

In order to characterize a given rock armoured coastal structure according to these damage limits, the parameter $E_{3D,1}$ is used as the calibration method. This $E_{3D,1}$ parameter can be described as *erosion depth measured in D_{n50} perpendicular to the slope averaged over a circular area of 1D_{n50}*, which allows to capture the damage limits describe above.

Before applying this parameter to calibrate the damage limits according to other parameters, a comparison with the currently used traditional characterization methods will be made. Such traditional methods considered slope surveys with different types of profilers (see Section 2.3.2) and the exposure of the filter layer for the failure limit: $D_{50}/2$ for Thompson & Shuttler (1975), 1D_{n50} for Melby & Kobayashi (1998) and no defined extent for the other authors (see Section 2.2). According to such methods, damage initiation and intermediate damage is based on defined parametric limits while failure is determined by the visual observation of images such as Figure 6.4 (where filter layer can be seen in white) or using cylindrical gauge with a hemispherical foot.

Figure 6.4: Deltares tests Series 1e - conditions after test run 4.

In contrast, the use of high resolution surveys such as the ones provided by Digital Stereo Photography (see Figure 6.5 for the damage measured in the structure shown in Figure 6.4) allows a more precise visualization of the state of the structure for all damage levels: damage initiation, intermediate damage and failure. In this case all the damage limits can be quantified according to the depth and extension of the damage area.

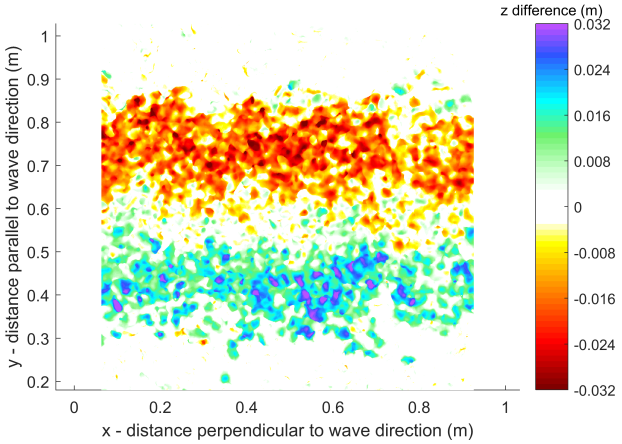

Figure 6.5: Deltares tests Series 1e - z difference: after test run 4 compared with initial.

Thus, considering the structure measurements carried out with high resolution techniques such as Digital Stereo Photography and the damage parameter $E_{3D,1}$, the proposed damage limits can be defined as:

$E_{3D,1}$ damage limits:

- **Damage initiation:** $E_{3D,1}$ = 1
- **Intermediate damage:** $E_{3D,1}$ = 1.5
- **Failure limit:** $E_{3D,1}$ = 2

From this parameter all the damage limits are calibrated for all other damage parameters, taking into account the relations shown in Figure 6.6. These figures include all the UPorto and Deltares test results for all damage parameters calculated for a characterization width of 25-27D_{n50}. Partial and complementary comparisons of these data are shown in Appendix D.

$E_{3D,5}$ damage limits:

- **Damage initiation:** $E_{3D,5}$ = 0.3
- **Intermediate damage:** $E_{3D,5}$ = 0.8
- **Failure limit:** $E_{3D,5}$ = 1.3 (90% conf.)

E_{2D} damage limits:

- **Damage initiation:** E_{2D} = 0.2
- **Intermediate damage:** E_{2D} 0.6
- **Failure limit:** E_{2D} 1.0 (90% conf.)

S damage limits:

- **Damage initiation:** S = 1
- **Intermediate damage:** S = 5
- **Failure limit:** S = 12 (90% conf.)

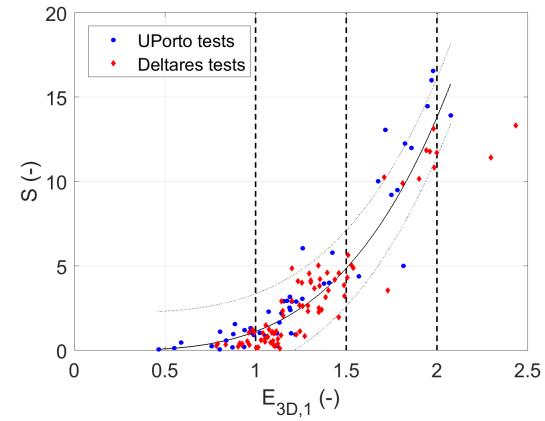

(a) $E_{3D,1}$ vs S parameters.

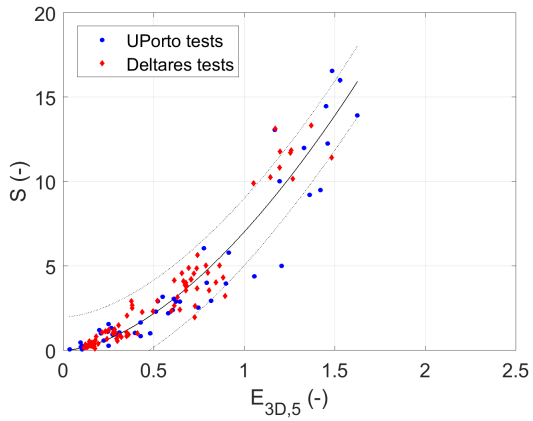

(b) $E_{3D,5}$ vs S parameters.

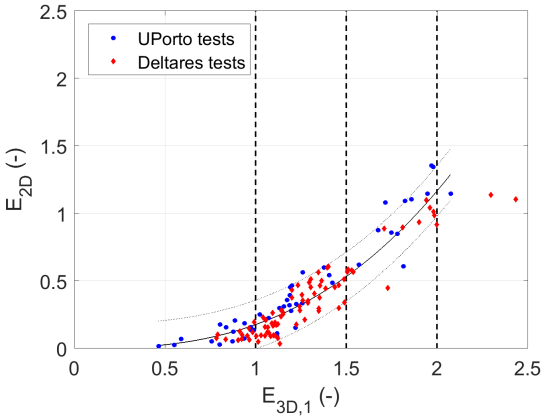

(c) $E_{3D,1}$ vs E_{2D} parameters.

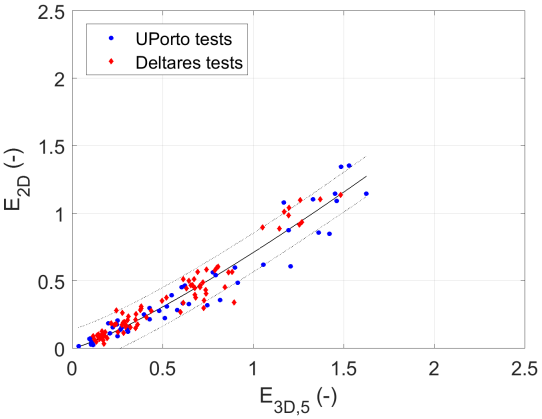

(d) $E_{3D,5}$ vs E_{2D} parameters.

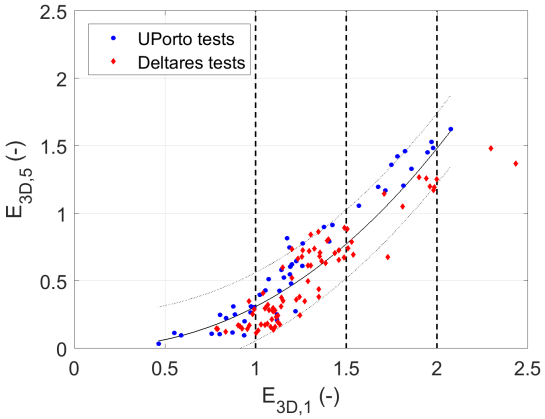

(e) $E_{3D,1}$ vs $E_{3D,5}$ parameters.

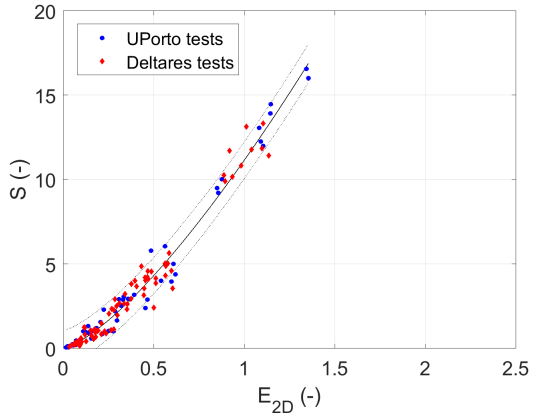

(f) E_{2D} vs S parameters.

Figure 6.6: Comparison all damage parameters.

An important remark from the previously defined calibrated damage limits is the fact that, according to the available data, they are constant for different slopes (1:2 in UPorto tests and 1:3 in Deltares tests). Nevertheless, this should be further investigated considering larger number of tests and different slope configurations in order to generalize these conclusions.

6.2. Validating damage parameters

This section addresses sub-question 2 (How can we establish and validate a universal damage parameter able to accurately characterize the response and remaining strength of rubble mound structures?). In order to provide an answer to this research question, the physical modelling test data from the Deltares shallow water tests was further analyzed. Furthermore, a characterization width of $27D_{n50}$ and the established damage limits are considered in all the analyses. Thus, the first subsection describes the analysis that leads to the validation of a suitable universal damage parameter, while the second subsection addresses the extreme distribution of damage to coastal structures.

6.2.1. Damage parameters analysis

The analysis of damage parameters is done considering hereafter four criteria to be considered for validating an universal damage parameter: bias error, random error, distinction of damage range and its values for different structures.

Bias error

The first element to be considered, the bias error in damage characterization of coastal structures, is related to the ability of the damage parameters to provide the most precise description of the state of the structure. This can be achieved with damage parameters that do not lead to hidden erosion, defined as the conditions were the damage in one location of the structure is balance by accretion in other location when considering width-averaged profiles.

Thus, the damage parameters based on width-averaged profiles (S and E_{n50}) are associated to bias error in the characterization of coastal structures while this error is not present in the damage parameters that captures the maximum erosion depth observed within a given characterization width ($E_{3D,1}$ and $E_{3D,5}$).

Random error

This second aspect, the random error in the measured damage to coastal structures, is related to the ability of damage parameters to describe the state of the structure with the smallest variability and larger confidence in the measured result. This is going to be analyzed further, in order to estimate the random error associated with each of the damage parameters.

First of all, the damage data for Series 1 (composed by four test runs of 60%, 80%, 100% and 120%) and Series 2 (composed by 1 test run of 100%) is described in the tables below. For each test run 10 observations are considered, obtained from 5 realization in a model with a width of $54D_{n50}$ (2 times the considered characterization width of $27D_{n50}$). For these five tests the following is calculated for all damage parameters: the mean (Table 6.1), the standard deviation (Table 6.2), the 80% confidence prediction interval (Table 6.3) applying a student-t distribution with critical t-value of 1.383 ($\delta = \pm 1.383 \cdot \sigma/\sqrt{10}$) and the the 80% confidence prediction interval expressed as a % of the mean (Table 6.4 and Figure 6.7). The measured damage values considered here are shown in Appendix H. Additional information of the 80% confidence prediction interval is shown in Appendix E.

From this data two conclusions can be drawn based on Table 6.4 and Figure 6.7:

- **Damage level:** it can be observed that for the most energetic wave conditions (120% in Series 1 run 4), and associated larger damage levels, all parameters present small variation for the damage prediction. For the rest of the test runs and damage levels a significant difference is observed, where damage parameters $E_{3D,1}$ and $E_{3D,5}$ leads to smaller variability while the results of E_{2D} and specially S present a large variation in the predicted damage.
- **Damage parameters:** it can be observed that damage parameter $E_{3D,1}$ presents the smallest variations in the predicted damage, followed by $E_{3D,5}$ with also small deviations. Damage parameter E_{2D} present reduced variability for large damages and large variations for smaller damages, while damage parameter S present also reduced variability for large damages but extremely large variations for smaller damages.

The previous conclusions should also be related to the test set-up considered in the Deltares tests, in order to evaluate possible laboratory effects that influenced the measured results. More precisely, the Deltares tests included a filter layer fixed with poli-pox glue which limited the damage to the armour layer and prevented the erosion to propagate towards the core of the structure. Thus, it could be expected that this test set-up would not affect lower damage conditions while for the large damage conditions the measured erosion would be constant after the armour layer are completely removed. This would then cause the variability of the large damage conditions to be smaller. Nevertheless, even for the largest wave conditions (120%), the armour layer were not removed in an area larger than $1D_{n50}$ (see measured damage according to $E_{3D,1}$ and $E_{3D,5}$ parameters and Figure 6.4) so there was no general collapse of the rock armour. Thus, according to these results the reduced variability in the measured results for large damage conditions are considered to be caused only by the nature of the damage process and not by the test set-up.

This brief study on the variability of damage parameters can then be summarized as follows: large damage conditions presents smaller variability in the results, while for small damage conditions the parameters $E_{3D,1}$ and $E_{3D,5}$ shows smaller variability than S and E_{2D}.

Table 6.1: Damage parameters Deltares tests - mean values

Parameter	S1 Run1 60%	S1 Run2 80%	S1 Run3 100%	S1 Run4 120%	S2 Run1 100% n-c
$\mathbf{E_{3D,1}}$	1.02	1.10	1.37	2.00	1.40
$\mathbf{E_{3D,5}}$	0.16	0.32	0.69	1.24	0.70
$\mathbf{E_{2D}}$	0.09	0.18	0.43	1.00	0.42
S	0.3	0.9	3.7	11.4	3.5

Table 6.2: Damage parameters Deltares tests - standard deviation

Parameter	S1 Run1 60%	S1 Run2 80%	S1 Run3 100%	S1 Run4 120%	S2 Run1 100% n-c
$\mathbf{E_{3D,1}}$	0.08	0.09	0.13	0.21	0.16
$\mathbf{E_{3D,5}}$	0.02	0.05	0.12	0.12	0.09
$\mathbf{E_{2D}}$	0.02	0.04	0.10	0.09	0.08
S	0.1	0.3	0.9	1.2	0.9

Table 6.3: Damage parameters Deltares tests - 80% confidence prediction interval

Parameter	S1 Run1 60%	S1 Run2 80%	S1 Run3 100%	S1 Run4 120%	S2 Run1 100% n-c
$\mathbf{E_{3D,1}}$	±0.12	±0.13	±0.19	±0.31	±0.23
$\mathbf{E_{3D,5}}$	±0.03	±0.07	±0.17	±0.17	±0.13
$\mathbf{E_{2D}}$	±0.03	±0.06	±0.14	±0.13	±0.12
S	±0.2	±0.4	±1.3	±1.7	±1.3

Table 6.4: Damage parameters Deltares tests - 80% confidence prediction interval respect to mean

Parameter	S1 Run1 60%	S1 Run2 80%	S1 Run3 100%	S1 Run4 120%	S2 Run1 100% n-c
$\mathbf{E}_{3D,1}$	±12%	±12%	±14%	±16%	±16%
$\mathbf{E}_{3D,5}$	±21%	±21%	±25%	±14%	±18%
$\mathbf{E}_{2D}$	±38%	±30%	±32%	±13%	±29%
S	±60%	±43%	±35%	±15%	±38%

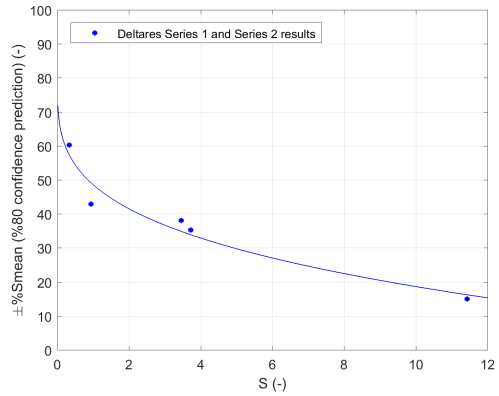

(a) S parameter.

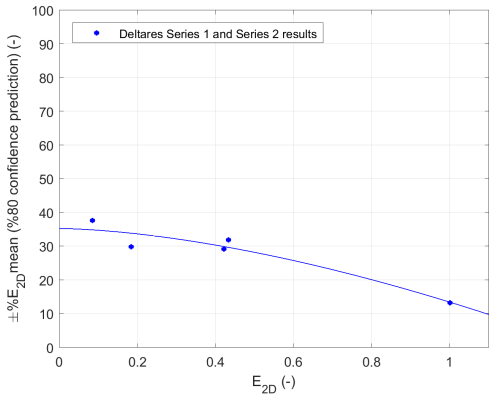

(b) E_{2D} parameter.

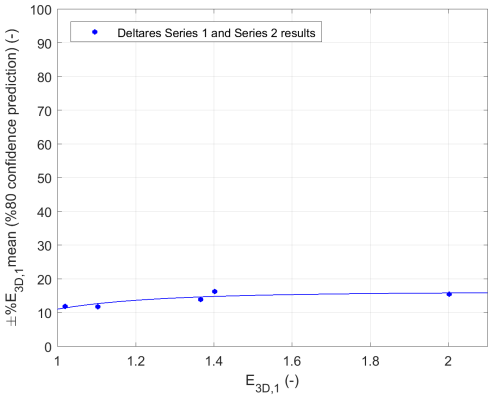

(c) $E_{3D,1}$ parameter.

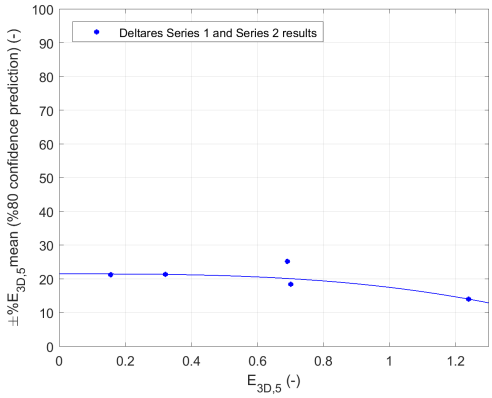

(d) $E_{3D,5}$ parameter.

Figure 6.7: Deltares tests - 80% confidence prediction interval respect to mean.

Distinction of damage range

The third element to be considered here is the ability of damage parameters to distinguish the range of damage levels between initial damage and failure. In order to address this aspect, Figure 6.8 shows the normalized damage results for all parameters in relation to the stability number ($N_s = H_{1/3}/\Delta D_{n50}$). For this comparison, the measured damage was normalized (noted with a *) in a scale where damage initiation is equal to 0 and failure is equal to 1. Equivalent plots considering the absolute measured damage are presented in Appendix J. According to these results, two conclusions will be drawn regarding the suitability of the damage to distinguish different damage levels and to be predicted from the hydrodynamic forcing ($H_{1/3}/\Delta D_{n50}$).

First, regarding the distinction of damage levels, it can be observed that parameters $E_{3D,1}$ and $E_{3D,5}$ show the continuous range of damage between damage initiation an failure while for parameters S and E_{2D} the measured damage is concentrated in certain damage levels. Regarding the predictability of damage, it can be observed that among all parameters, $E_{3D,1}$ is the one less suitable for predicting damage from the hydrodynamic forcing since it has the large scatter in the results. Thus, although $E_{3D,1}$ is used for establishing the damage limits for the characterization of coastal structures, it is less suitable for predicting damage levels. In this case the damage parameters S, E_{2D} and $E_{3D,5}$ shows more precise estimations with a narrower confidence bound for the measured results.

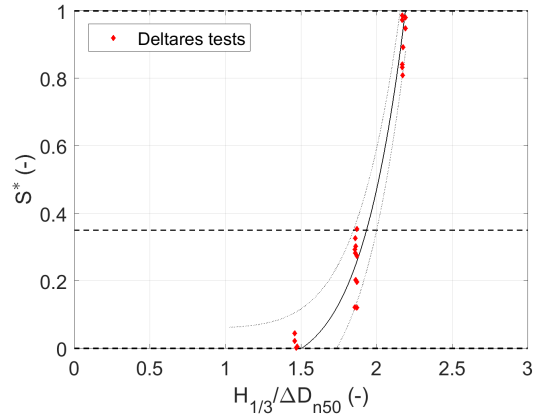

(a) S parameter.

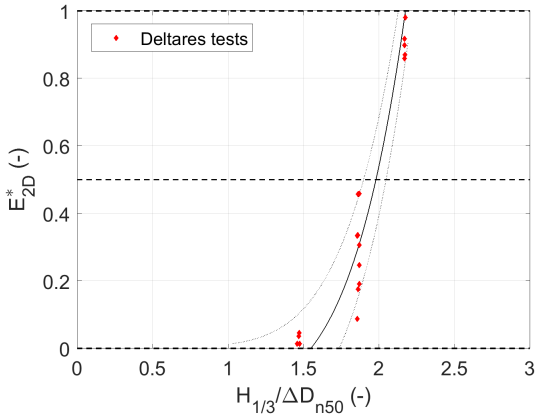

(b) E_{2D} parameter.

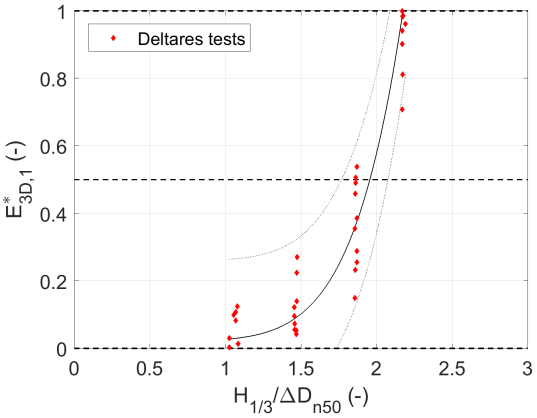

(c) $E_{3D,1}$ parameter.

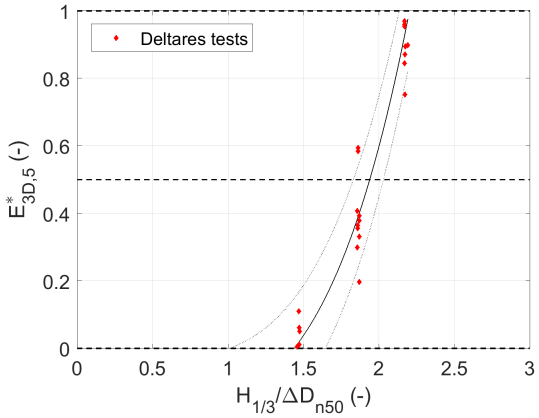

(d) $E_{3D,5}$ parameter.

Figure 6.8: Deltares tests - Normalized damage.

Values for different structures

The fourth aspect to be considered in this analysis is the suitability of damage parameters to be used in different structures. In this case different structures does not only include variations in the characteristics of the rock slope, but also 3D structures such as roundheads or slopes with a berm.

Thus, only the parameters that captures the maximum erosion depth observed within a given characterization width ($E_{3D,1}$ and $E_{3D,5}$) are suitable for describing damage to coastal structures with any geometry or 3D feature.

Conclusions on damage parameters analysis

According to the four criteria previously discussed, the damage parameter $E_{3D,5}$ is considered as the most suitable to be used as an universal damage parameter for the characterization of coastal structures based on the four reasons described hereafter:

- **Low bias error:** the damage to the structure is clearly captured, without including hidden erosion present in the parameters that consider width-averaged profiles.
- **Low random error:** this parameter describes the damage to the structure with very low variability, what increases the confidence in the measured and expected damage.
- **Distinguish damage range:** the different states of damage to the structure can be recognized according to the limits established.
- **Constant value for different structures:** for all structure configurations this parameter can be used without any modification.

6.2.2. Extreme damage distribution for $E_{3D,5}$

Following the analysis of damage parameters previously discussed, $E_{3D,5}$ parameter is analyzed in more detail, regarding its extreme distribution. Thus, the aim is to provide more information regarding the expected maximum damage that can be observed in a structure wider than the one tested in a physical model experiment. As previously discussed, damage parameters and damage limits should be defined for a typical characterization width of roughly $25D_{n50}$, but a length effect concept should be introduced in this case. This length effect can be defined as the increase in the probability that in a wider structure a larger maximum erosion depth will take place, following the same principle used in the flood risk assessment in The Netherlands (VNK 2012, 2014).

In order to define an extreme value distribution for the measured damage, the results shown in Table 6.5 are considered (five realizations of each test run from Series 1 and Series 2 with a width of $54D_{n50}$, which leads to 10 damage results for a characterization width $27D_{n50}$). In this table, also the mean value from the 10 realizations is described ($\bar{E}_{3D,5}$). These values are adjusted to a Gumbel distribution (see Equation 6.1), with the distribution parameters determined by the least square method (see non-exceddence probability and calculated distribution parameters in Table 6.5). Thus, the Gumbel extreme distribution for the maximum erosion depth measured in a characterization width of $27D_{n50}$ according to parameter $E_{3D,5}$ is shown in Figure 6.9 for the five test runs.

Table 6.5: Damage parameters Deltares tests - Measured damage for $E_{3D,5}$ parameter

Parameter	S1 Run1 60%	S1 Run2 80%	S1 Run3 100%	S1 Run4 120%	S2 Run1 100% n-c	$F_X(x)$
$\mathbf{E}_{3D,5}$	0.12	0.24	0.50	1.05	0.52	0.09
	0.13	0.28	0.60	1.14	0.61	0.18
	0.14	0.30	0.63	1.17	0.67	0.27
	0.15	0.30	0.66	1.19	0.68	0.36
	0.16	0.31	0.66	1.20	0.71	0.45
	0.16	0.31	0.68	1.25	0.73	0.55
	0.16	0.35	0.69	1.26	0.73	0.64
	0.17	0.35	0.71	1.27	0.74	0.73
	0.18	0.36	0.88	1.37	0.79	0.82
	0.19	0.41	0.89	1.48	0.84	0.91
$\bar{\mathbf{E}}_{3D,5}$	0.16	0.32	0.69	1.24	0.70	-
$\alpha_{\mathbf{E}_{3D,5}}$	0.14	0.30	0.63	1.18	0.65	-
$\beta_{\mathbf{E}_{3D,5}}$	0.02	0.05	0.13	0.12	0.09	-

$$F_X(x) = exp\left\{-exp\left\{-\left(\frac{x-\alpha}{\beta}\right)\right\}\right\} \tag{6.1}$$

where:

$F_X(x)$ (-): non-exceedance probability.

x (unit): variable value.

α (unit): location parameter.

β (unit): scale parameter.

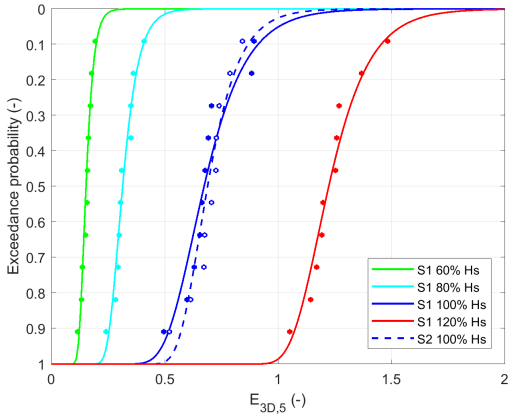

Figure 6.9: Deltares tests Gumbel damage distribution.

The exceedance probability for the damage is translated to a return width in a similar form as used for the study of extreme wave climate (see Equation 6.2). Using this expression, Figure 6.10 presents the extreme damage distribution for the $E_{3D,5}$ parameter considering the return width instead of the exceedance probability. Figure 6.10a shows the Gumbel distribution for each of the five test runs while Figure 6.10b normalizes these extreme damage distribution by the mean ($E^N_{3D,5} = E_{3D,5}/\overline{E}_{3D,5}$).

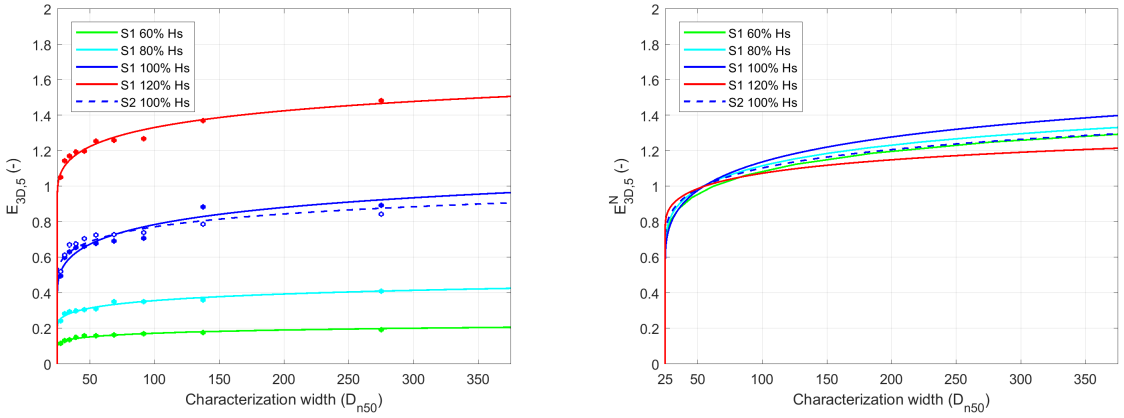

(a) Gumbel distribution.

(b) Gumbel distribution normalized by the mean.

Figure 6.10: Deltares tests Gumbel extreme damage distribution - $E_{3D,5}$ parameter.

$$R_W = \frac{\lambda}{1 - F_X(x)} \tag{6.2}$$

where:

R_W (m): return width.

λ (m): typical characterization width (27 D_{n50} for this analysis).

1 - $F_X(x)$ (-): exceedance probability.

Considering Figure 6.10, a continuous increase in the maximum erosion depth can be expected for structures wider than the characterization width of 25D_{n50} (27D_{n50} used in this analysis). Thus, this length effect for coastal structures should be further studied and included in design criteria and guidelines. Nevertheless, the results from Figure 6.10 provide different trends for the five test runs, which does not allow a general conclusion regarding this length effect. This will be briefly addressed hereafter, aiming for a more general expression for the increase of the maximum expected damage for wider structures.

Figure 6.10b normalizes the extreme damage distribution respect to the mean ($E^N_{3D,5}$), but for the various damage conditions different trends are observed. While looking into more detail to these trends, the variability in the extreme values does not show a correlation with the hydrodynamic forcing conditions and associated damage levels. Instead the different trends can be assumed to be caused by a random scatter in the measured results. Thus, all the damage results normalized by the mean (see Table 6.6) will be included to a single Gumbel extreme value distribution with the following parameters:

$$\alpha_{E^N_{3D,5}} = 0.94$$

$$\beta_{E^N_{3D,5}} = 0.12$$

Table 6.6: Damage parameters Deltares tests - Measured damage for $E^N_{3D,5}$ parameter

Parameter	S1 Run1 60%	S1 Run2 80%	S1 Run3 100%	S1 Run4 120%	S2 Run1 100% n-c
$\mathbf{E}^N_{3D,5}$	0.74	0.75	0.72	0.85	0.74
	0.85	0.89	0.87	0.92	0.88
	0.88	0.92	0.91	0.94	0.96
	0.97	0.93	0.95	0.96	0.97
	1.02	0.95	0.96	0.97	1.01
	1.02	0.97	0.98	1.01	1.03
	1.05	1.09	1.00	1.02	1.04
	1.10	1.09	1.03	1.02	1.05
	1.14	1.13	1.28	1.10	1.12
	1.24	1.28	1.29	1.20	1.20

The combined extreme distribution for the normalized damage parameter $E^N_{3D,5}$ is shown in Figure 6.11. This figure shows that a single realization of a test run for a a characterization width of 25D_{n50} is expected to present a damage of 80% the mean damage (calculated from 10 realizations) while for a structure 250D_{n50} wide a it is expected a damage of 120% the mean damage. Thus, according to this first study, the damage to a structure of 250D_{n50} wide is expected to present a damage 150% larger than the one obtained in a single realization in a 25D_{n50} characterization width.

In summary, this section used the available data in order to validate the suitability of the $E_{3D,5}$ parameter as an universal damage parameter for coastal structures. This parameter can describe more precisely the damage to the structure and remaining strength, considering four main criteria: bias error, random error, distinction of damage range and its values for different structures. In addition, this parameter should be calculated for a characterization width of roughly 25D_{n50} but must also be related to an extreme damage distribution to account for a length effect in wider structures.

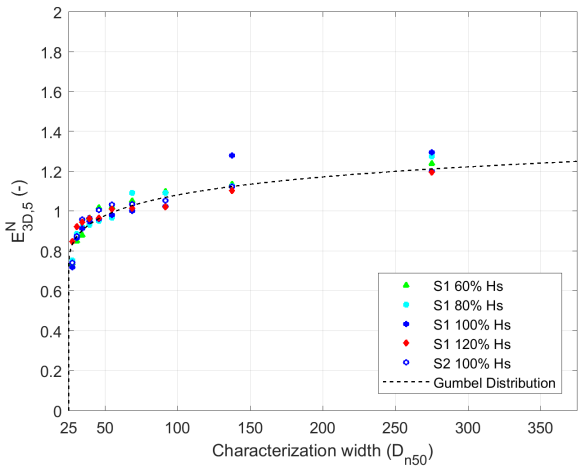

Figure 6.11: Deltares tests Gumbel extreme damage distribution - $E^N_{3D,5}$ normalized parameter.

6.3. Validating measuring techniques

This section addresses sub-question 3 (How can we validate the increase in reliability of physical modelling tests results based on innovative and higher accuracy testing and measuring techniques?). For answering this question, the effect of measuring techniques in the damage characterization of coastal structures is described considering three key aspects.

First, the use of a high resolution measuring technique such as the Digital Stereo Photography allowed the validation of more accurate damage parameters as $E_{3D,m}$ (see Section 6.2). This high definition measuring technique, together with this new parameter, can capture the state of the full structure surface in order to identify the presence of weak areas that threatens the stability of the structure.

Second, these measuring techniques eliminate the bias errors present in traditional measuring techniques associated with traditional damage parameters. In this case, the errors in the damage characterization caused by hidden erosion in width-averaged profiles can be eliminated. Then, all the erosion that takes place at any location in the structure can be captured in the damage characterization.

Third, in the case of traditional damage parameters (S) it is also expected that the use of high resolution measurements (1 mm grid) can reduce significantly the variability in the results compared with traditional measuring techniques (approx. 10 cm grid). When capturing the full structure surface with high definition measurements, width-averaged profiles will be independent of the random positions where the profiles are taken (considering for example the use of mechanical profiles, see Chapter 2) and consequently less variable.

Furthermore, the post processing steps is a significant tool that was used in the analysis. It is recommended that when considering the damage in average profiles (for damage parameters S and E_{2D}), a moving average of $1D_{n50}$ is used. In the case of the $E_{3D,m}$) damage parameters, it is necessary to use of a circular moving average for each required diameter.

Considering the three aspects discussed above, it can be concluded that innovative and high definition measuring techniques are able to improve significantly the damage characterization of coastal structures. It was shown that such techniques can provide more and more precise information about the state of the structure and the probability of failure.

6.4. Discussion of sub-questions 1, 2 and 3

In the following paragraphs, the answer to the research sub-questions 1, 2 and 3 are summarized.

Sub-question 1 was addressed in this chapter in two parts. First, defining a standard characterization width for physical modelling tests for coastal structures: $25D_{n50}$. For damage parameters that evaluate the width-averaged profiles (S and E_{2D}), this minimum width should be considered, taking into account the effects that wider test sections will have in the measured damage. For damage parameters that consider the maximum eroded depth within a characterization width ($E_{3D,1}$ and $E_{3D,5}$), this standard width should also be considered, in combination with an extreme value distribution in order to account for the increase in the probability of observing a maximum erosion in wider structures (length effect).

Second, the calibrated damage limits and damage parameters for rock armoured slopes with a thickness of $2D_{n50}$ are the following:

- **Damage initiation:** defined as the condition where a circular hole of $1D_{n50}$ diameter and a depth of $1D_{n50}$ is observed in the armour layer.

  $E_{3D,1}$ = 1

  $E_{3D,5}$ = 0.3

  E_{2D} = 0.2

  S = 1

- **Intermediate damage:** defined as the condition where a circular hole of $1D_{n50}$ diameter and a depth of $1.5D_{n50}$ is observed in the armour layer.

  $E_{3D,1}$ = 1.5

  $E_{3D,5}$ = 0.8

  E_{2D} = 0.6

  S = 5

- **Failure limit:** defined as the condition where a circular hole of $1D_{n50}$ diameter and a depth of $2D_{n50}$ is observed in the armour layer.

  $E_{3D,1}$ = 2.0

  $E_{3D,5}$ = 1.3 (90% conf.)

  E_{2D} 1.0 (90% conf.)

  S = 12 (90% conf.)

Sub-question 2 was addressed by evaluating the suitability of the different damage parameters to be used as an universal damage parameter. It was defined that $E_{3D,5}$ is the parameter that can better describe the damage and remaining strength of conventional and non-conventional structures. The key reasons for defining this parameter as the reference damage characterization parameter are the following:

- **Low bias error:** the damage to the structure is clearly captured, without including hidden erosion present in the parameters that consider width-averaged profiles.
- **Low random error:** this parameter describes the damage to the structure with very low variability, what increases the confidence in the measured and expected damage.
- **Distinguish damage range:** the different states of damage to the structure can be recognized according to the limits established.
- **Constant value for different structures:** for all structure configurations this parameter can be used without any modification.

In addition, sub-question 2 also addressed the length effect of rock armoured coastal structures, defined as the increase in the probability of observing larger damage in increasingly wider structures. According to the results from the physical modelling tests, it was observed that the measured damage for a coastal structure of $25D_{n50}$ can increase 150% for a similar structure 10 times wider. Thus, it is demonstrated that the damage characterization of coastal structures should include an extreme distribution in order to account for this length effect.

Sub-question 3 was addressed by remarking the importance of innovative and high resolution measuring techniques for delivering accurate damage characterization of coastal structures. Such techniques allow the use of the most precise damage parameters ($E_{3D,5}$), the reduction of bias errors related with hidden erosion and the reduction of random errors related with the position of the measured profiles.

7

Climate change adaptation alternatives

This chapter evaluates upgrading alternatives for coastal structures facing sea level rise cause by climate change, addressing research sub-question 4 (How can we validate the suitability of upgrading alternatives for coastal structures facing sea level rise scenarios?).

The first section discusses the influence of sea level rise on low-crested structures with non depth-limited wave conditions, following the results of the UPorto deep water tests. The second section discusses the influence of sea level rise and adaptation alternatives for non-overtopped structures with depth-limited wave conditions, following the results of the Deltares shallow water tests. The upgrading alternatives and their suitability are evaluated in the third section, while the forth section addresses the answer to research sub-question 4.

7.1. Low-crested structures

The UPorto deep water tests (see Section 4.2) considered a low-crested structure in which significant overtopping took place, specially during 100% and 120% conditions. With this set-up, the influence of sea level rise was evaluated when comparing Series 1 and Series 3 (see Table 4.1 for more details):

- **Series 1:** cumulative damage with constant sea level and long-crested waves
  - Run1: 60% wave height at MHW water level
  - Run2: 80% wave height at MHW water level
  - Run3: 100% wave height at MHW water level
  - Run4: 120% wave height at MHW water level
- **Series 3:** cumulative damage with increased sea level and long-crested waves
  - Run1: 60% wave height at MHW water level
  - Run2: 80% wave height at MHW water level
  - Run3: 100% wave height at MHW**+SLR** water level
  - Run4: 120% wave height at MHW**+SLR** water level

Thus, the comparison between both series will show the influence of the largest wave heights (100% and 120%) acting on a higher water level after identical mild storms took place (60% and 80%). This comparison is shown in Figure 7.1 where all 8 test runs are represented (the three vertical lines defines the initial water level, the increase water level and the crest position).

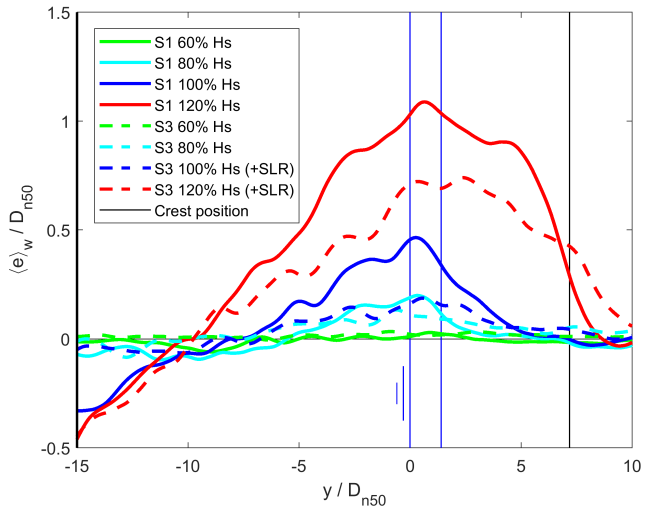

Figure 7.1: UPorto tests - comparison Series 1 and Series 3.

According to these results it can be observed that in such a low-crested structure, the rise of the water level produces an increase in the overtopping discharge which reduces the damage in the front slope. This damage to the front slope is reduced both in terms of damage area (represented by S) and depth (represented by $E_{3D,5}$) as shown in Table 7.1 for the two most energetic conditions where there was a difference in the water level. The damage parameters denoted with an overbar ($\overline{S}$ and $\overline{E}_{3D,5}$) are the mean of the damage measured in 5 independent sections with a width of $25D_{n50}$, from the single test realization with a $100D_{n50}$ wide model in both Series 1 and Series 3.

Table 7.1: Damage parameters UPorto tests - Measured damage Series 1 and Series 3

Parameter	Run	Series 1 Current sea level	Series 3 Increased sea level
$\overline{S}$	Run 3	3.5	1.6
	Run 4	13.0	8.9
$\overline{E}_{3D,5}$	Run 3	0.77	0.36
	Run 4	1.35	1.13

Nevertheless, the reduction of damage in the front slope due to increased overtopping is linked to a larger damage to the crest and rear slope. The damage to the crest can be observed in right side of the figure, while the damage to rear slope is not in the scope of the thesis (see z difference plots in Appendix A for more details).

In summary, for low-crested structures with non depth-limited wave conditions such as the one considered in the UPorto tests, the increase of the water level reduces the damage in the front slope due to an increase in the overtopping discharge. But the increase of the overtopping discharge represents a serious threat to the stability of the crest and rear slope and the continuity and safety of activities that take place in the area protected by the structure.

7.2. Upgrading alternatives results

The Deltares shallow water tests (see Section 4.3) considered a non-overtopped structure with depth-limited wave conditions caused by a 8 metres long foreshore. With this set-up, the influence of sea level rise was evaluated in all 6 test series considering the 4 test runs (see Table 4.1 for more details):

- **Run 1:** 60% water depth (which defines the 60% wave height)
- **Run 2:** 80% water depth (which defines the 80% wave height)
- **Run 3:** 100% water depth (which defines the 100% wave height)
- **Run 4:** 120% water depth (which defines the 120% wave height)

In the next sub-sections, the tests results for a straight slope and 4 variations of a slope with a berm are described. The analysis of these different slope configurations will be considered in order to define the most suitable and effective adaptation alternatives.

7.2.1. Straight slope

The straight slope configuration is represented in Figure 4.8. This structure is considered as the initial or current structure configuration, to be compared with the configurations where a berm is added. Figure 7.2 presents the averaged erosion profile for Series 1, including all 5 realizations (see the erosion profiles for all 5 realizations in Figure 5.7).

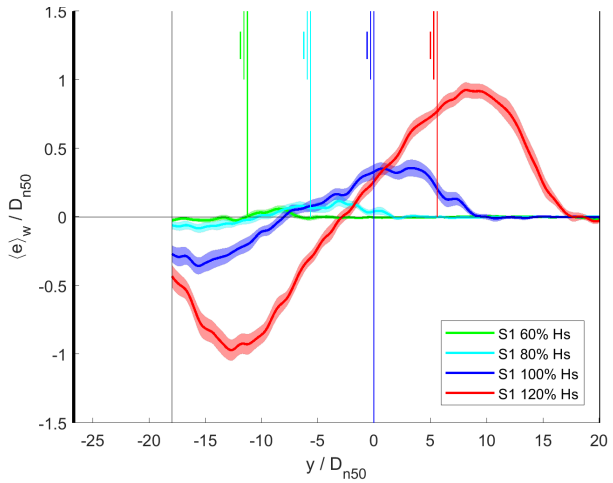

Figure 7.2: Deltares tests Series 1 (S1a, S1b, S1c, S1d, S1e) - straight slope averaged damage.

The measured damage (considering damage parameters S and $E_{3D,5}$) for the two most energetic conditions are shown below, obtained as the mean from 10 independent sections with a width of $27D_{n50}$, from the 5 test realizations with a $54D_{n50}$ wide model ($\bar{S}$ and $\bar{E}_{3D,5}$).

- **Series 1:** straight slope

  Run3:

  $\bar{S}$ = 3.7

  $\bar{E}_{3D,5}$ = 0.69

  Run4:

  $\bar{S}$ = 11.4

  $\bar{E}_{3D,5}$ = 1.24

These results show that the damage in the different test runs can be clearly distinguished when the 5 realizations of Series 1 are combined. It is then observed that the structure approaches intermediate damage after run 3 and presents almost failure after run 4 (see damage definitions Chapter 6).

7.2.2. Wide high berm

The first berm configuration is evaluated in this section, with a width of $10D_{n50}$ at the level of the 100% condition (see Figure 4.9). Figure 7.3 presents the erosion profile for Series 3a.

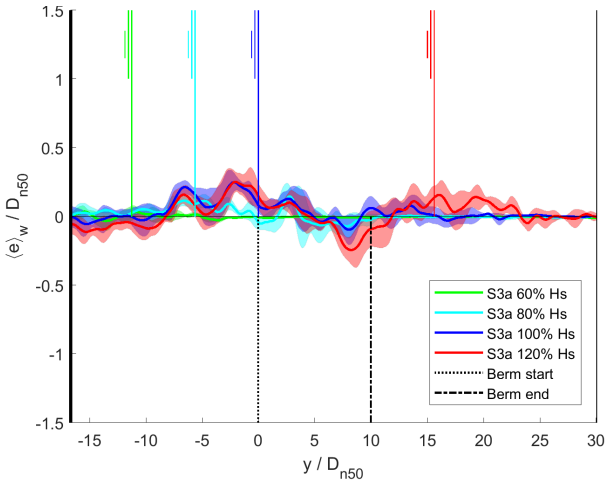

Figure 7.3: Deltares tests Series 3a - wide ($10D_{n50}$) high (100% level) berm damage profile.

The measured damage (considering damage parameters S and $E_{3D,5}$) for the two most energetic conditions are shown below, obtained as the mean from 2 independent sections with a width of $27D_{n50}$, from the single test realization with a $54D_{n50}$ wide model ($\overline{S}$ and $\overline{E}_{3D,5}$).

- **Series 3a:** wide high berm

  Run3:

  $\overline{S}$ = 2.1 (Lower slope: 1.8) (Upper slope: 0.3)

  $\overline{E}_{3D,5}$ = 0.40 (Lower slope: 0.40) (Upper slope: 0.19)

  Run4:

  $\overline{S}$ = 2.6 (Lower slope: 1.5) (Upper slope: 1.1)

  $\overline{E}_{3D,5}$ = 0.38 (Lower slope: 0.36) (Upper slope: 0.31)

These results prove that this first berm configuration reduces significantly the damage of the structure. It can be observed that both the damage area (represented by S) and depth (represented by $E_{3D,5}$) is notably smaller when compared with the straight slope configuration. The mean reduction in S is 43% for run 3 and 77% for run 4. The reduction in $E_{3D,5}$ is 42% for run 3 and 69% for run 4.

Regarding the damage location, it can be observed that the damage to the structure is spread throughout the structure for all the test runs, with larger damage at the lower slope (which includes the horizontal berm) than the upper slope.

7.2.3. Narrow high berm

The second berm configuration is evaluated in this section, with a width of $5D_{n50}$ at the level of the 100% condition (see Figure 4.10). Figure 7.4 presents the erosion profile for Series 4a.

The measured damage (considering damage parameters S and $E_{3D,5}$) for the two most energetic conditions are shown below, obtained as the mean from 2 independent sections with a width of $27D_{n50}$, from the single test realization with a $54D_{n50}$ wide model ($\overline{S}$ and $\overline{E}_{3D,5}$).

- **Series 4a:** narrow high berm

  Run3:

  $\bar{S}$ = 3.0 (Lower slope: 2.8) (Upper slope: 0.2)

  $\bar{E}_{3D,5}$ = 0.73 (Lower slope: 0.73) (Upper slope: 0.16)

  Run4:

  $\bar{S}$ = 4.8 (Lower slope: 2.9) (Upper slope: 1.9)

  $\bar{E}_{3D,5}$ = 0.83 (Lower slope: 0.83) (Upper slope: 0.48)

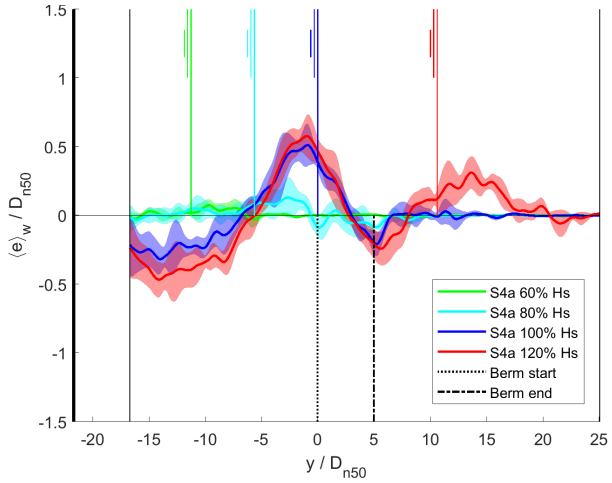

Figure 7.4: Deltares tests Series 4a - narrow ($5D_{n50}$) high (100% level) berm damage profile.

These results prove that this second berm configuration is less effective reducing the damage than the first one. For test run 3, it is shown that this configuration does not reduce the measured damage, while for test run 4 it does reduce significantly the damage obtained in the straight slope configuration. The mean reduction in S is 19% for run 3 and 58% for run 4. There is an increase in $E_{3D,5}$ of 6% for run 3 while there is a reduction of 33% for run 4.

Regarding the damage location, it can be observed that the damage to the structure is focussed on the transition between the lower slope and the horizontal berm for both run 3 and run 4.

7.2.4. Wide low berm

The third berm configuration is evaluated in this section, with a width of $10D_{n50}$ at the level of the 80% condition (see Figure 4.11). Figure 7.5 presents the erosion profile for Series 5a.

The measured damage (considering damage parameters S and $E_{3D,5}$) for the two most energetic conditions are shown below, obtained as the mean from 2 independent sections with a width of $27D_{n50}$, from the single test realization with a $54D_{n50}$ wide model ($\bar{S}$ and $\bar{E}_{3D,5}$).

- **Series 5a:** wide low berm

  Run3:

  $\bar{S}$ = 1.0 (Lower slope: 0.6) (Upper slope: 0.4)

  $\bar{E}_{3D,5}$ = 0.21 (Lower slope: 0.21) (Upper slope: 0.18)

  Run4:

  $\bar{S}$ = 4.7 (Lower slope: 1.2) (Upper slope: 3.5)

  $\bar{E}_{3D,5}$ = 0.73 (Lower slope: 0.30) (Upper slope: 0.73)

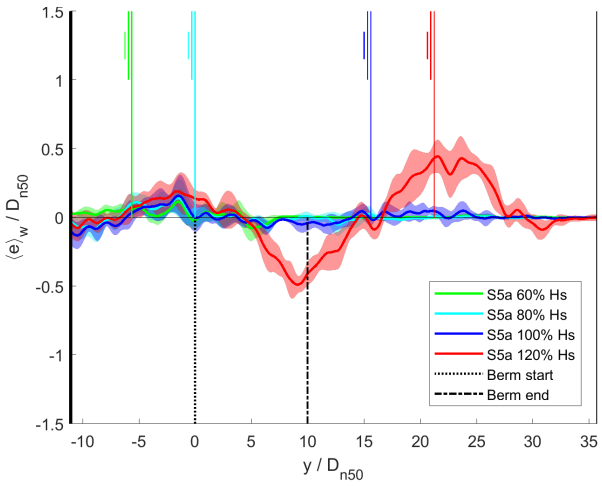

Figure 7.5: Deltares tests Series 5a - wide ($10D_{n50}$) low (80% level) berm damage profile.

These results prove that this third berm configuration is very effective reducing the damage, with a similar impact compared with the wide high berm. It is more stable than the original configuration with the straight slope, specially for test run 3 when the water level is one level above the berm. The mean reduction in S is 73% for run 3 and 59% for run 4. The reduction in $E_{3D,5}$ is 70% for run 3 and 41% for run 4.

Regarding the damage location, it can be observed that the damage to the structure with a lower berm is focussed at the transition between the lower slope and the berm up to run 3 while for run 4 the damage is clearly focussed on the upper slope.

7.2.5. Narrow low berm

The fourth berm configuration is evaluated in this section, with a width of $5D_{n50}$ at the level of the 80% condition (see Figure 4.12). Figure 7.6 presents the erosion profile for Series 6a.

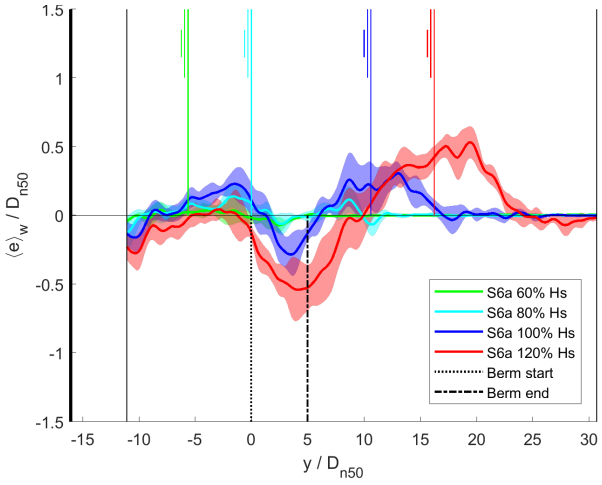

Figure 7.6: Deltares tests Series 6a - narrow ($5D_{n50}$) low (80% level) berm damage profile.

The measured damage (considering damage parameters S and $E_{3D,5}$) for the two most energetic conditions are shown below, obtained as the mean from 2 independent sections with a width of $27D_{n50}$, from the single test realization with a $54D_{n50}$ wide model ($\bar{S}$ and $\bar{E}_{3D,5}$).

- **Series 6a:** narrow low berm

  Run3:

  $\overline{S}$ = 3.3 (Lower slope: 1.2) (Upper slope: 2.1)

  $\overline{E}_{3D,5}$ = 0.53 (Lower slope: 0.33) (Upper slope: 0.53)

  Run4:

  $\overline{S}$ = 4.9 (Lower slope: 0.2) (Upper slope: 4.7)

  $\overline{E}_{3D,5}$ = 0.68 (Lower slope: 0.22) (Upper slope: 0.68)

These results prove that this fourth berm configuration is less effective reducing the damage, and similar to the narrow high berm. Nevertheless, it is more stable than the original configuration with the straight slope, with smaller damages measured as S and $E_{3D,5}$. The mean reduction in S is 11% for run 3 and 57% for run 4. The reduction in $E_{3D,5}$ is 23% for run 3 and 45% for run 4.

Regarding the damage location, it can be observed that the damage to the structure similar at the lower and upper slope for run 3 while for run 4 the damage is clearly focussed on the upper slope.

7.3. Evaluation of alternatives

This section compares the different results described above. Here, the damage parameters (S, E_{2D}, $E_{3D,1}$ and $E_{3D,5}$) are the mean values of these parameters ($\overline{S}$, $\overline{E}_{2D}$, $\overline{E}_{3D,1}$ and $\overline{E}_{3D,5}$). The first sub-section describes the reduction of the damage in slopes with a berm compared with a straight slope, while the second sub-section evaluates the differences in damage among the different berm configurations.

7.3.1. Berm configurations compared with straignt slope

As it was already described in the previous section, the slope configurations with a berm reduced significantly the damage to the structure. The damage to the straight slope and all berm configurations are shown in Figure 7.7a considering the S parameter and in Figure 7.7b considering the $E_{3D,5}$ parameter. All comparisons considering the 4 damage parameters (S, E_{2D}, $E_{3D,1}$ and $E_{3D,5}$) are shown in Appendix F.

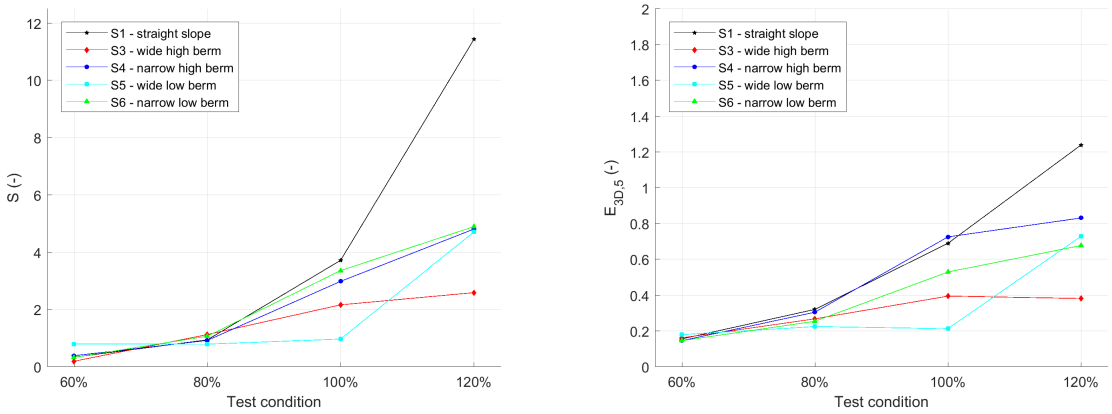

(a) S parameter.

(b) $E_{3D,5}$ parameter.

Figure 7.7: Deltares tests damage comparison - Straight slope vs Slope with a berm.

It can be observed that in the two first test conditions (60% and 80%), the berm configurations do not reduce the measured damage if compared with the results for the straight slope. Nevertheless, in the more energetic wave conditions (100% and 120%) the improvement of the stability and reduction of damage is significant when a berm is added to the front slope.

In Figure 7.8a and 7.8b the damage reduction for each berm configuration is shown for S and $E_{3D,5}$ parameters respectively. For these calculations, the damage to the straight slope is the average value obtained obtained from 10 independent sections with a width of $27D_{n50}$, from the 5 test realizations of Series 1 with a $54D_{n50}$ wide model. In a similar manner, the damage to the berm configurations is the average value obtained obtained from 2 independent sections with a width of $27D_{n50}$, from the single test realizations of Series 3-4-5-6 with a $54D_{n50}$ wide model.

In these two figures it can be observed a general reduction of the damage for the configurations with a berm, except when considering the 100% condition in Series 4. This narrow berm was severely damage when the wave action (acting at 100% water level) reach the structure at the berm level (placed at the 100% water level). In this case, the S damage was smaller than the straight slope structure while the damage depth captured by the $E_{3D,5}$ parameters was higher.

This proves the suitability of the $E_{3D,5}$ parameters to accurately characterize the damage and resistance of the structure after the impact of the waves. In this case, this parameter describes better the failure probability (defined as the exposure of the filter layer) than the parameter S.

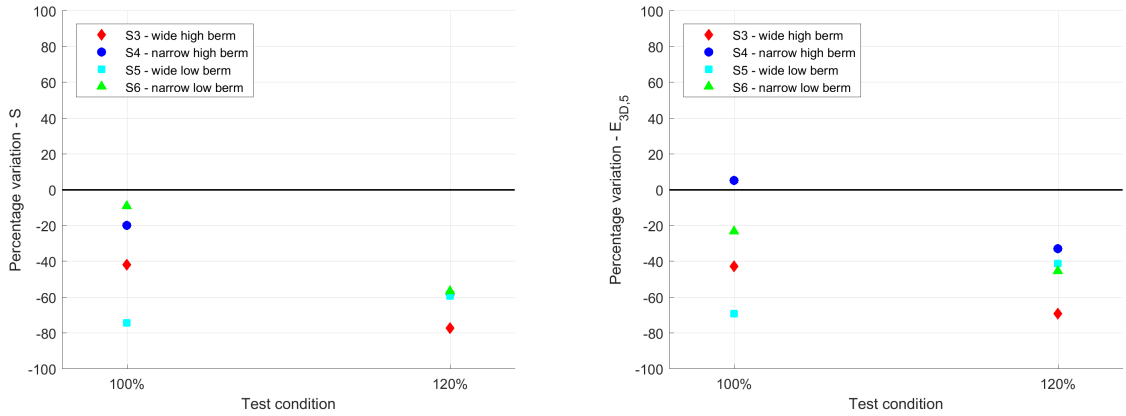

(a) S parameter.

(b) $E_{3D,5}$ parameter.

Figure 7.8: Deltares tests damage reduction for slopes with a berm.

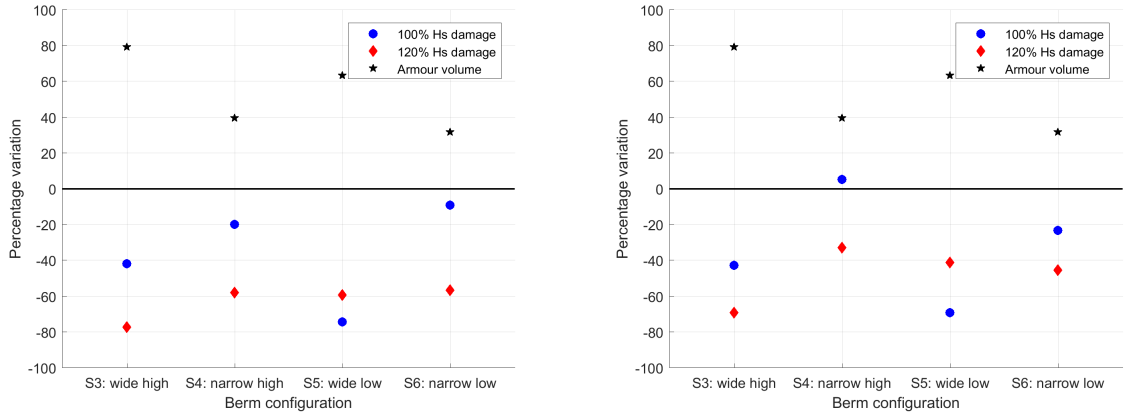

(a) S parameter.

(b) $E_{3D,5}$ parameter.

Figure 7.9: Deltares tests damage reduction and volume increase for slopes with a berm.

In addition, Figures 7.9a and 7.9b evaluate these adaptation alternatives taking into account the required increase of volume of the armour due to the berm and the associated damage reduction. It can be observed that the optimal adaptation alternative depends on two fundamental design aspects. First, the design water depth and wave height. Second, the design criteria regarding the cost of local material and the considered maintenance and repair activities.

In summary the comparison of the berm configurations with the straight slope showed that the damage to the structure is significantly reduced with the presence of a berm. It can also be observed that the most effective configurations are the wide berms positioned one level below the water level.

7.3.2. Berm configurations analysis

As it was already proven in the previous sub-section that the berm configurations reduce significantly the damage to the structure, this section analyses in more detail the damage to each berm configuration in order to assess better their effectiveness.

It was observed that in the high berms (Series 3 and Series 4), the largest damage was produced in the lower slope while for the lowest berms (Series 5 and Series 6) the largest damage took place at the upper slope. Considering the armour thickness of the two areas (thinner in the upper slope than at the lower slope), the high berms presented a larger safety margin.

In the following graphs the damage to the structure (considering S and $E_{3D,5}$ parameters) is shown in Figures 7.10a and 7.10b for the total damage, in Figures 7.11a and 7.11b for the lower slope and in Figures 7.12a and 7.12b for the upper slope.

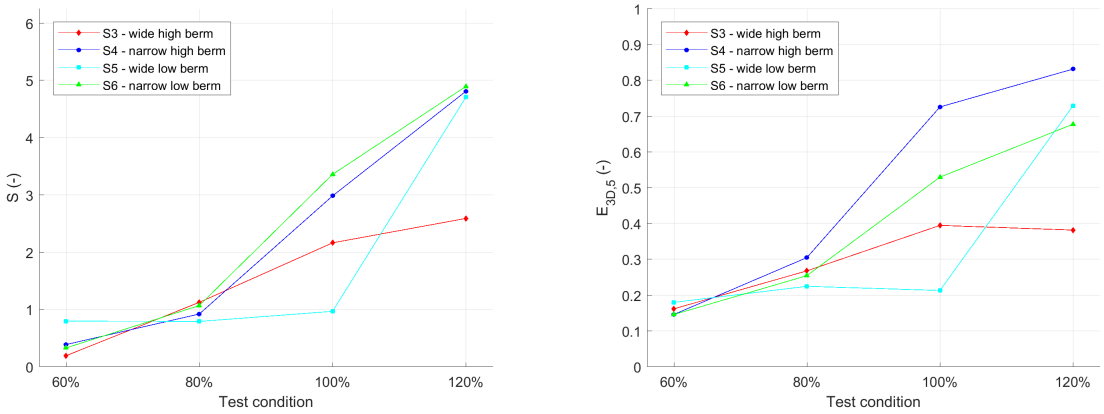

(a) S parameter.

(b) $E_{3D,5}$ parameter.

Figure 7.10: Deltares tests damage comparison - Berm configurations total damage.

Regarding the lower slope (which also includes the damage o the horizontal berm), the largest damage was measured for the high berm configurations. This seems logical since in these high berm structures the extent of the lower slope is larger and the wave action attacks it directly. Nevertheless, due to the larger thickness of the lower slope, the safety margins for these conditions are larger than compared to the same amount of damage in a much thinner layer as in the upper slope.

For the upper slope different results were observed, with much larger damage for the configurations with a lower berm. Specially for the highest water depths, the wave action attacked the upper slope without being affected by the berm. These can lead to very unsafe conditions, since the thickness of the upper layer is reduced and the same amount of damage can lead to a sooner exposure of the filter layer and consequent failure of the structure.

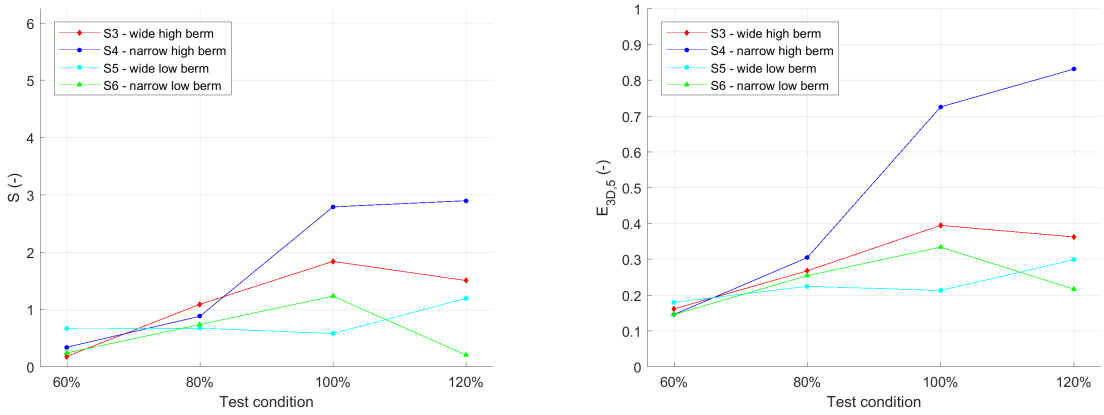

(a) S parameter. (b) $E_{3D,5}$ parameter.

Figure 7.11: Deltares tests damage comparison - Berm configurations lower slope damage.

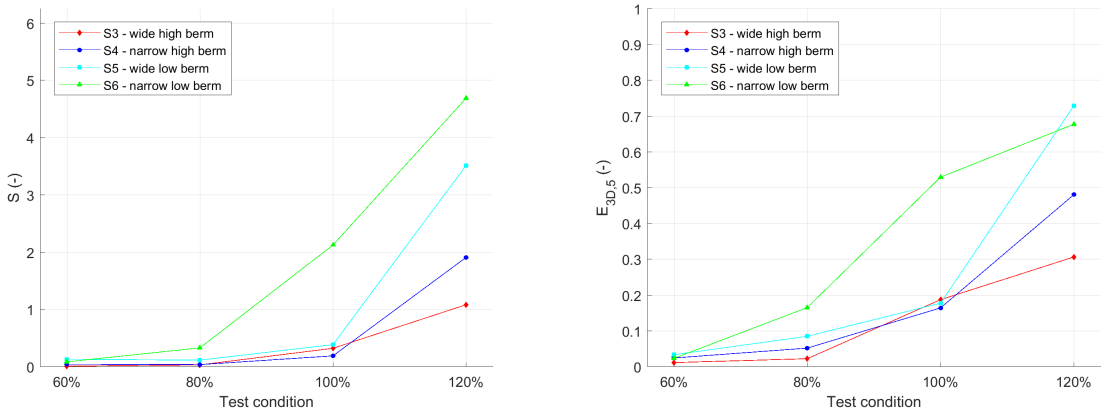

(a) S parameter. (b) $E_{3D,5}$ parameter.

Figure 7.12: Deltares tests damage comparison - Berm configurations upper slope damage.

Considering the analysis described above, it can be noted that the smallest amount of damage was measured when the berm was placed one level below the water level. Thus, the design berm level should depend on the design water level. According to the test results, the more stable conditions is reached when the berm is located one level below the water level. When considering the width of the berm, it can be also observed that the wider berms were much more stable than the narrow ones.

7.4. Discussion of sub-question 4

Sub-question 4 was addressed in this chapter, where the suitability of upgrading alternatives for coastal structures facing sea level rise scenarios where validated.

It was observed that a slope with a berm increases significantly the stability of the structure, reducing the damage caused by the impact of extreme waves and increasing its resilience in sea level rise scenarios. In such configuration, the effects on the porosity and hydrodynamic patterns were very positive for the stability of the structure. The most favourable location of the berm was observed at one level below the design water level. Furthermore, the wide configurations ($10D_{n50}$) were more effective than the narrow configurations ($5D_{n50}$). In summary, the presence of a wide berm one level below the design water level lead to reductions of up to 80% of the measured damage in both S and $E_{3D,5}$ parameters.

Regarding the damage evaluation, it was also described the suitability and accuracy of the parameter $E_{3D,5}$ to better describe the state of the upgrading structure, instead of the parameter S. It was shown that when evaluating the damage depth with $E_{3D,5}$ it is possible to better define the damage level of the structure and the failure hazard (defined as the exposure of the filter layer to the wave action). It was shown in Series 4 that the parameter $E_{3D,5}$ captures a threat to the stability of the structure which should trigger repair activities, while parameter S does not identify this situation and would lead to unsafe conditions.

Thus, berm configurations have been validated with the present measurements as an upgrading alternative to face sea level rise scenarios. For damage characterization of such non-standard coastal structures, parameter $E_{3D,5}$ is also validated as the most suitable damage parameter.

8

Conclusions and recommendations

This chapter summarizes the work developed throughout this thesis, providing the answers to the main research question and the four research sub-questions. In addition, recommendations for future studies are briefly presented.

The main research question is addressed answering first the 4 sub-questions:

> *Sub-question 1: How can we establish and validate unified concepts of "damage initiation", "intermediate damage" and "failure" in rubble mound structures?*

Sub-question 1 was addressed in two parts. First, defining a standard characterization width for physical modelling tests for coastal structures: $25D_{n50}$. For damage parameters that evaluate the width-averaged profiles (S and E_{2D}), this minimum width should be considered, taking into account the effects that wider test sections will have in the measured damage. For damage parameters that consider the maximum eroded depth within a characterization width ($E_{3D,1}$ and $E_{3D,5}$), this standard width should also be considered, in combination with an extreme value distribution in order to account for the increase in the probability of observing a maximum erosion in wider structures (length effect). Second, the calibrated damage limits and damage parameters for rock armoured slopes with a thickness of $2D_{n50}$ are the following:

- **Damage initiation:** defined as the condition where a circular hole of $1D_{n50}$ diameter and a depth of $1D_{n50}$ is observed in the armour layer.

  $E_{3D,1}$ = 1
  $E_{3D,5}$ = 0.3
  E_{2D} = 0.2
  S = 1

- **Intermediate damage:** defined as the condition where a circular hole of $1D_{n50}$ diameter and a depth of $1.5D_{n50}$ is observed in the armour layer.

  $E_{3D,1}$ = 1.5
  $E_{3D,5}$ = 0.8
  E_{2D} = 0.6
  S = 5

- **Failure limit:** defined as the condition where a circular hole of $1D_{n50}$ diameter and a depth of $2D_{n50}$ is observed in the armour layer.

  $E_{3D,1}$ = 2.0
  $E_{3D,5}$ = 1.3 (90% conf.)
  E_{2D} 1.0 (90% conf.)
  S = 12 (90% conf.)

Sub-question 2: How can we establish and validate an universal damage parameter to accurately characterize the response as well as the remaining strength of rubble mound structures?

Sub-question 2 was addressed by evaluating the suitability of the different damage parameters to be used as an universal damage parameter. It was defined that $E_{3D,5}$ is the parameter that can better describe the damage and remaining strength of conventional and non-conventional structures. The key reasons for defining this parameter as the reference damage characterization parameter are the following:

- **Low bias error:** the damage to the structure is clearly captured, without including hidden erosion present in the parameters that consider width-averaged profiles.
- **Low random error:** this parameter describes the damage to the structure with very low variability, what increases the confidence in the measured and expected damage.
- **Distinguish damage range:** the different states of damage to the structure can be recognized according to the limits established.
- **Constant value for different structures:** for all structure configurations this parameter can be used without any modification.

In addition, sub-question 2 also addressed the length effect of rock armoured coastal structures, defined as the increase in the probability of observing larger damage in increasingly wider structures. According to the results from the physical modelling tests, it was observed that the measured damage for a coastal structure of $25D_{n50}$ can increase 150% for a similar structure 10 times wider. Thus, it is demonstrated that the damage characterization of coastal structures should include an extreme distribution in order to account for this length effect.

Sub-question 3: How can we validate the increase in reliability of physical modelling tests results based on innovative and higher accuracy testing and measuring techniques?

Sub-question 3 was addressed by remarking the importance of innovative and high resolution measuring techniques for delivering accurate damage characterization of coastal structures. Such techniques allow the use of the most precise damage parameters ($E_{3D,5}$), the reduction of bias errors related with hidden erosion and the reduction of random errors related with the position of the measured profiles.

Sub-question 4: How can we validate the suitability of upgrading alternatives for coastal structures facing sea level rise scenarios?

Sub-question 4 was addressed by validating the suitability of berms as an adaptation alternative. It was observed that a slope with a berm increases significantly the stability of the structure, reducing the damage caused by the impact of extreme waves and increasing its resilience in sea level rise scenarios. In such configuration, the effects on the porosity and hydrodynamic patterns were very positive for the stability of the structure. The most favourable location of the berm was observed at one level below the design water level. Furthermore, the wide configurations ($10D_{n50}$) were more effective than the narrow configurations ($5D_{n50}$). In summary, the presence of a wide berm one level below the design water level lead to reductions of up to 80% of the measured damage in both S and $E_{3D,5}$ parameters.

Regarding the damage evaluation, it was also described the suitability and accuracy of the parameter $E_{3D,5}$ to better describe the state of the upgrading structure, instead of the parameter S. It was shown that when evaluating the damage depth with $E_{3D,5}$ it is possible to better define the damage level of the structure and the failure hazard (defined as the exposure of the filter layer to the wave action).

Thus, berm configurations have been validated with the present measurements as an upgrading alternative to face sea level rise scenarios. For damage characterization of such non-standard coastal structures, parameter $E_{3D,5}$ is also validated as the most suitable damage parameter.

After answering all research sub-questions, the main research question is addressed:

> *How can we improve the reliability in the assessment of rubble mound structures based on physical modelling in current and future scenarios by introducing accurate and universal damage characterization methods?*

The main research question can then be answered, following the validation of the damage criteria required for a precise assessment of a coastal structure (sub-question 1), the validation of an universal damage parameter for rubble mound structures (sub-question 2), the validation of the benefits of innovative measuring techniques when carrying out physical modelling tests (sub-question 3) and the validation of upgrading alternatives for climate change scenarios (sub-question 4). Thus, it can be stated that with these definitions, parameters and measuring techniques, a complete method for damage characterization of coastal structures is presented.

It was also defined how this damage characterization method can be used to precisely and accurately describe the damage to conventional and non-conventional coastal structures. Furthermore, this method was also used to describe the effects of not only current environmental forces acting on the structures but also future and more energetic scenarios. For such future scenarios, adaptation alternatives for coastal structures were evaluated and berm configurations are recommended for their upgrading.

Future research on damage characterization of coastal structures are needed in order to evaluate, adjust and generalize the conclusions made in this thesis, considering additional structure configurations and environmental loading conditions. Different configurations should include different slopes or porosity and the study of other non-conventional structures and 3D features such as roundheads. Different environmental loads should include different wave conditions (including non-breaking waves and a variety of breaking wave conditions) and water levels (including constant and changing water levels and the associate overtopping discharge).

In addition, a summary of identified key research areas still to be addressed are presented and briefly described hereafter. First, the constant damage limits observed in this thesis for different structures (slopes 1:2 and 1:3) should be further investigated given that it contradicts current design criteria. Second, the reduced difference between cumulative and non-cumulative damage measurements should be evaluated considering both rock armoured slopes and other armour units such as concrete cubes. Third, the scaling limits for physical modelling tests should also be evaluated in order to optimize the design of model set-ups, since the scale effects predicted by the existing literature were not observed in the Deltares test results. And fourth, the random behaviour of damage should be further analyzed, in special for better describing the length effect of coastal structures in order to improve the statistical tools for probabilistic design.

Future research on adaptation alternatives for coastal structures facing climate change should include the testing of not only additional upgrading solutions, but also different environmental forcing scenarios. Such different testing conditions should also include conditions where overtopping takes place and therefore the upgrading of the structure should take into account the effects at the front slope, rear slope and the activities that take place in the area protected by the structure.

Bibliography

Battjes, J. A. (1974), Computation of set-up, longshore currents, run-up and overtopping due to wind-generated waves, PhD thesis, Delft University of Technology.

Broderick, L. L. (1984), Riprap stability versus monochromatic and irregular waves, PhD thesis, Oregon State University.

Burcharth, H. F., Andersen, T. L. & Lara, J. L. (2014), 'Upgrade of coastal defence structures against increased loadings caused by climate change: A first methodological approach', *Coastal Engineering* **87**, 112 – 121.

CERC (1977), *Shore Protection Manual (3rd edition)*, Coastal Engineering Research Center, US Army Corps of Engineers, Vicksburg, MS, United States.

CERC (1984), *Shore Protection Manual (4th edition)*, Coastal Engineering Research Center, US Army Corps of Engineers, Vicksburg, MS, United States.

CIRIA, CUR & CETMEF (2007), *The Rock Manual. The use of rock in hydraulic engineering (2nd edition)*, C683 CIRIA, London, United Kingdom.

Davis, R. E. & Regier, L. A. (1977), 'Methods for estimating directional wave spectra from multi-element arrays', *Journal of Marine Research* **35**(3), 453–477.

de Leau, J. (2017), Laboratory experiments on the stability of concrete cubes. A comparison of testing methodologies, Master's thesis, Delft University of Technology.

Disco, M. J. (2012), A generic quantitative damage description for rubble mound structures. Investigation of damage to roundheads by using a 3D high-resolution measurement technique in a physical model, Master's thesis, Delft University of Technology.

Frostick, L. E., McLelland, S. J. & Mercer, T. G. (2011), *Users Guide to Physical Modelling and Experimentation: Experience of the HYDRALAB Network*, CRC Press / Balkena, Leiden, The Netherlands.

Hofland, B., Disco, M. & van Gent, M. (2014), Damage characterization of rubble mound roundheads, *in* 'Proc. CoastLab 2014', Varna, Bulgaria.

Hofland, B., van Gent, M., Raaijmakers, T. & Liefhebber, F. (2011), Damage evaluation using the damage depth, *in* 'Proc. Coastal Structures 2011', Yokohama, Japan.

Hudson, R. Y. (1959), 'Laboratory investigation of rubble-mound breakwaters', *Journal of the Waterways and Harbors Division, American Society of Civil Engineers (ASCE)* **85**(WW3), 93 – 121.

Hudson, R. Y., Herrmann, F. A., Sager, R. A., Whalin, R. W., Keulegan, G. H., Chatham, C. E. & Hales, L. Z. (1979), Coastal hydraulic models, Special report No. 5, US Army Engineer Waterways Experiment Station, Vicksburg, MS, United States.

Hughes, S. A. (1993), *Physical Models and Laboratory Techniques in Coastal Engineering*, World Scientific, Singapore.

IPCC (2013), *Climate Change 2013: The Physical Science Basis*, Cambridge University Press, Cambridge, United Kingdom and New York, NY, USA.

Iribarren, R. (1938), 'Una fórmula para el calculo de los diques de escollera', *M. Bermejillo, Pasajes, Madrid, Spain* .

Isobe, M. (2013), 'Impact of global warming on coastal structures in shallow water', *Ocean Engineering* **71**, 51 – 57. Sea Level Rise and Impacts on Engineering Practice.

Koftis, T., Prinos, P., Galiatsatou, P. & Karambas, T. (2015), An integrated methodological approach for the upgrading of coastal structures due to climate change effects, *in* 'Proc. IAHR World Congress 2015', The Hague, The Netherlands.

Martín-Hidalgo, M., Martín-Soldevilla, M. J., Negro, V., Aberturas, P. & López-Gutiérrez, J. (2014), 'Storm evolution characterization for analysing stone armour damage progression', *Coastal Engineering* **85**.

Martín-Soldevilla, M. J., Martín-Hidalgo, M., Negro, V., López-Gutiérrez, J. & Aberturas, P. (2015), 'Improvement of theoretical storm characterization for different climate conditions', *Coastal Engineering* **96**.

Melby, J. A. & Kobayashi, N. (1998), 'Progression and variability of damage on rubble mound breakwaters', *Journal of Waterway, Port, Coastal, and Ocean Engineering* **124**(6), 286 – 294.

Mulders, P., Curto, V., Zanuttigh, B., Verhagen, H. J. & Uijttewaal, W. S. (2015), 'Effects of gradation on the long-shore transport processes and reshaping of rubble mound breakwaters under construction exposed to head-on and oblique waves', *Coastal Engineering* **106**, 87 – 111.

Raaijmakers, T., Liefhebber, F., Hofland, B. & Meys, P. (2012), Mapping of 3D-bathymetries and structures using stereo photography through an air-water-interface, *in* 'Proc. CoastLab 2012', Gent, Belgium.

Semedo, A., Weisse, R., Behrens, A., Sterl, A., Bengtsson, L. & Günther, H. (2013), 'Projection of global wave climate change toward the end of the twenty-first century', *Journal of Climate* **26**(21).

Thompson, D. M. & Shuttler, R. M. (1975), Riprap design for wind-wave attack. A laboratory study in random waves, Report EX707, Hydraulic Research Station Wallingford, Oxford, United Kingdom.

van der Meer, J. W. (1988), Rock slopes and gravel beaches under wave attack, PhD thesis, Delft University of Technology.

van der Meer, J. W. (1995), Conceptual design of rubble mound breakwaters, *in* P. Liu, ed., 'Advances in Coastal and Ocean Engineering', Vol. 1, World Scientific, chapter 5, pp. 221–315.

van Gent, M. R. A. (2013), 'Rock stability of rubble mound breakwaters with a berm', *Coastal Engineering* **78**, 35 – 45.

van Gent, M. R. A. (2014), 'Oblique wave attack on rubble mound breakwaters', *Coastal Engineering* **88**, 43 – 54.

van Gent, M. R. A. & Lim, L. (2016), Incorporating effects of oblique waves in the design of coastal protection structures under sea level rise, *in* 'Proc. Singapore Sustainable Built Environment Conference 2016', Singapore.

van Gent, M. R. A., Smale, A. J. & Kuiper, C. (2003), Stability of rock slopes with shallow foreshores, *in* J. Melby, ed., 'Proc. 4th International Coastal Structures Conference Portland 2003', ASCE, Reston, VA, United States.

van Gent, M. R. A. & van der Werf, I. M. (2010), Stability of breakwaters roundheads during construction, *in* 'Proc. Coastal Engineering 2010', Shanghai, China.

van Gent, M. R. A. & van der Werf, I. M. (2014), 'Rock toe stability of rubble mound breakwaters', *Coastal Engineering* **83**, 166 – 176.

VNK (2012), VNK2 - The method in brief, Hb 1679805, VNK2 Project Office, The Netherlands.

VNK (2014), The National Flood Risk Analysis for the Netherlands, Final report, Rijkswaterstaat VNK Project Office, The Netherlands.

Weisse, R., Bellafiore, D., Menéndez, M., Méndez, F., Nicholls, R. J., Umgiesser, G. & Willems, P. (2014), 'Changing extreme sea levels along european coasts', *Coastal Engineering* **87**, 4 – 14.

Wolters, G., van Gent, M., Allsop, W., Hamm, L. & Muhlestein, D. (2009), Hydralab III: Guidelines for physical model testing of rubble mound breakwaters, *in* 'Proc. Coasts, Marine Structures and Breakwaters 2009', Institution of Civil Engineers - ICE, Edinburgh, Scotland, United Kingdom.

List of Figures

1.1 Punta Langosteira breakwater, singular coastal structure (Source: EFE). 2
1.2 Upgrading of coastal structures (based on Burcharth et al. (2014)). 3
1.3 Thesis methodology and parts. 5
1.4 Report structure and chapters. 6

2.1 Wave parameters in space and time (CIRIA et al. 2007). 7
2.2 Notional permeability coefficient (van der Meer 1988). 10
2.3 Damage parameters E, L, C and S (Melby & Kobayashi 1998). 15
2.4 Global average temperature, scenarios RCP8.5 (red) and RCP2.6 (blue) (IPCC 2013). . 20
2.5 Global mean sea level rise, scenarios RCP8.5 (red) and RCP2.6 (blue) (IPCC 2013). . . 20
2.6 Upgrading of coastal structures with an increase in the crest level (Burcharth et al. 2014). 21
2.7 Upgrading of coastal structures with no increase in the crest level (Burcharth et al. 2014). 21

3.1 Process for obtaining S damage parameter. 25
3.2 Process for obtaining E_{2D} damage parameter. 26
3.3 Process for obtaining $E_{3D,m}$ damage parameter. 27

4.1 Wave basin used for the UPorto tests. 32
4.2 Plan view of the UPorto set-up. 33
4.3 Cross-section UPorto set-up - with front slope and rear slope. 33
4.4 Cross-section UPorto set-up - with front slope and overtopping tank. 33
4.5 Probes distances used in the UPorto tests for long-crested waves. 34
4.6 Wave flume used in the Deltares tests. 35
4.7 Deltares model set-up. 35
4.8 Cross-section Deltares set-up - straight slope. 36
4.9 Cross-section Deltares set-up - slope with a berm $10d_{50}$ wide at the 100% water level. 36
4.10 Cross-section Deltares set-up - slope with a berm $5d_{50}$ wide at the 100% water level. . 36
4.11 Cross-section Deltares set-up - slope with a berm $10d_{50}$ wide at the 80% water level. . 36
4.12 Cross-section Deltares set-up - slope with a berm $5d_{50}$ wide at the 80% water level. . . 36
4.13 Probes distances used in the Deltares tests. 38
4.14 Digital Stereo Photography equipment. 38

5.1 UPorto damage measurements - Series 1. 39
5.2 UPorto tests Series 1 - z difference: after test run 3 compared with initial. 40
5.3 UPorto tests - Series 1-2-3-4 damage profiles with 90% confidence bounds for the mean. 41
5.4 UPorto tests - Analysis of cumulative (Series 1) and non-cumulative (Series 2) damage. 41
5.5 Deltares damage measurements - Series 1a. 42
5.6 Deltares tests Series 1a - z difference: after test run 3 compared with initial. 42
5.7 Deltares tests - Series 1 damage profiles with 90% confidence bounds for the mean. . 45
5.8 Deltares tests - Series 2 damage profiles with 90% confidence bounds for the mean. . 46
5.9 Deltares tests - Series 3-4-5-6 damage profiles with 90% confidence bounds for the mean. 47
5.10 UPorto damage compared with van der Meer (1988) - plunging breaking. 48
5.11 Deltares damage compared with van der Meer (1988) modified by van Gent et al. (2003). 49
5.12 Deltares damage for slopes with a berm compared with van Gent (2013). 50

6.1 Characterization width mean damage variation - UPorto tests Series 1-2-3. 52
6.2 Standard deviation normalized by the mean - Deltares tests Series 1. 53
6.3 Standard deviation normalized by the mean - Deltares tests Series 1 (100%) and Series 2. 54
6.4 Deltares tests Series 1e - conditions after test run 4. 55

6.5 Deltares tests Series 1e - z difference: after test run 4 compared with initial. 56
6.6 Comparison all damage parameters. 57
6.7 Deltares tests - 80% confidence prediction interval respect to mean. 60
6.8 Deltares tests - Normalized damage. 61
6.9 Deltares tests Gumbel damage distribution. 63
6.10 Deltares tests Gumbel extreme damage distribution - $E_{3D,5}$ parameter. 63
6.11 Deltares tests Gumbel extreme damage distribution - $E^{N}_{3D,5}$ normalized parameter. . . . 65

7.1 UPorto tests - comparison Series 1 and Series 3. 70
7.2 Deltares tests Series 1 (S1a, S1b, S1c, S1d, S1e) - straight slope averaged damage. . . 71
7.3 Deltares tests Series 3a - wide ($10D_{n50}$) high (100% level) berm damage profile. . . . 72
7.4 Deltares tests Series 4a - narrow ($5D_{n50}$) high (100% level) berm damage profile. . . . 73
7.5 Deltares tests Series 5a - wide ($10D_{n50}$) low (80% level) berm damage profile. 74
7.6 Deltares tests Series 6a - narrow ($5D_{n50}$) low (80% level) berm damage profile. 74
7.7 Deltares tests damage comparison - Straight slope vs Slope with a berm. 75
7.8 Deltares tests damage reduction for slopes with a berm. 76
7.9 Deltares tests damage reduction and volume increase for slopes with a berm. 76
7.10 Deltares tests damage comparison - Berm configurations total damage. 77
7.11 Deltares tests damage comparison - Berm configurations lower slope damage. 78
7.12 Deltares tests damage comparison - Berm configurations upper slope damage. 78

List of Tables

4.1 UPorto test conditions 34
4.2 Deltares test conditions 37

5.1 UPorto test results 40
5.2 Deltares test results 43
5.3 Deltares test results - slope with a berm - lower and upper slope 44

6.1 Damage parameters Deltares tests - mean values 59
6.2 Damage parameters Deltares tests - standard deviation 59
6.3 Damage parameters Deltares tests - 80% confidence prediction interval 59
6.4 Damage parameters Deltares tests - 80% confidence prediction interval respect to mean 60
6.5 Damage parameters Deltares tests - Measured damage for $E_{3D,5}$ parameter 62
6.6 Damage parameters Deltares tests - Measured damage for $E^{N}_{3D,5}$ parameter 64

7.1 Damage parameters UPorto tests - Measured damage Series 1 and Series 3 70

A

UPorto test results

Series 1

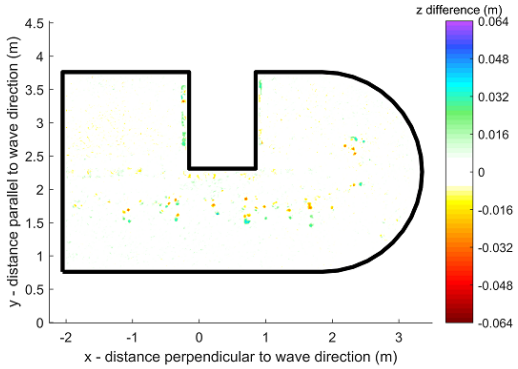

(a) z difference after run 1.

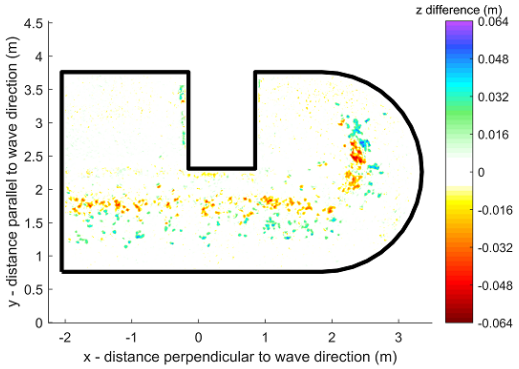

(b) z difference after run 2.

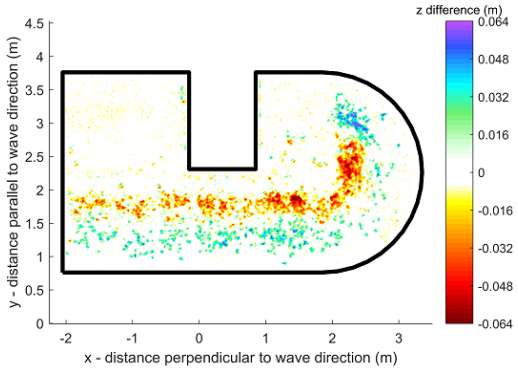

(c) z difference after run 3.

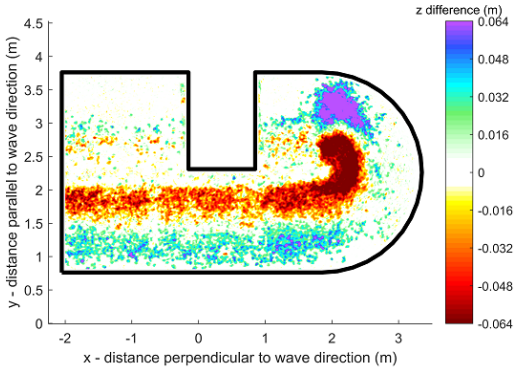

(d) z difference after run 4.

Figure A.1: UPorto tests Series 1.

Series 2

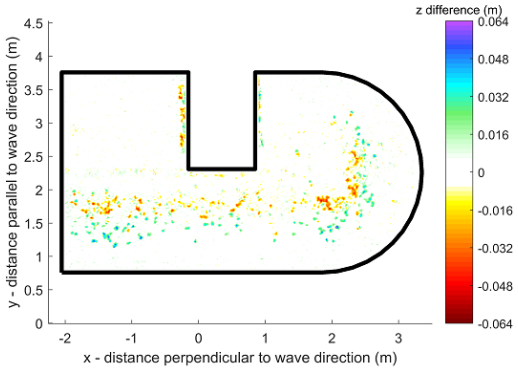

(a) z difference after run 1.

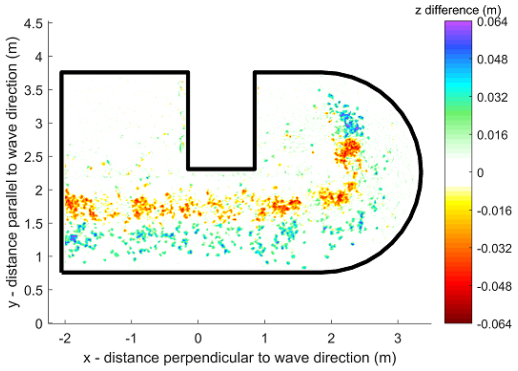

(b) z difference after run 2.

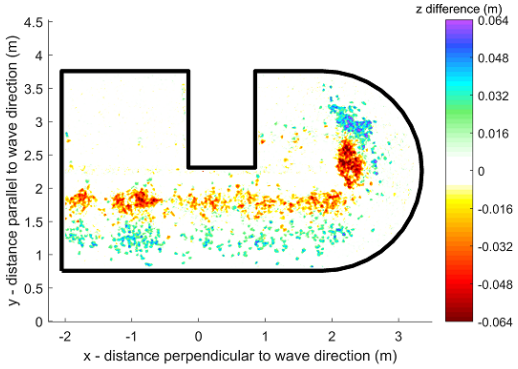

(c) z difference after run 2r.

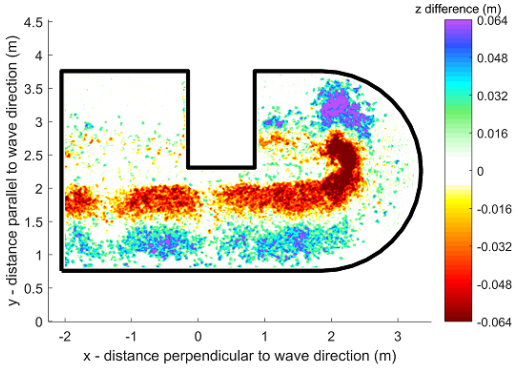

(d) z difference after run 3.

Figure A.2: UPorto tests Series 2.

Series 3

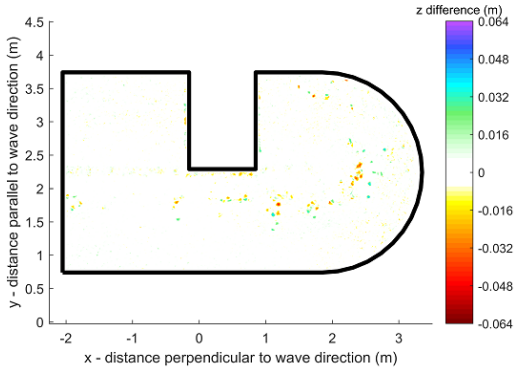

(a) z difference after run 1.

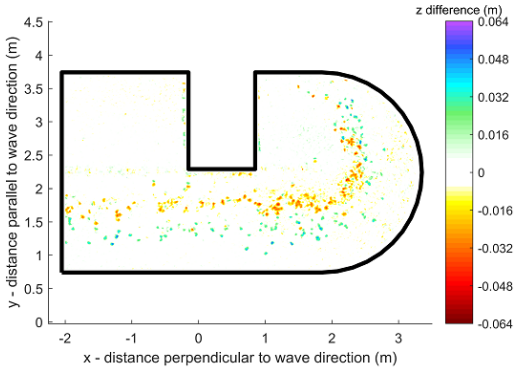

(b) z difference after run 2.

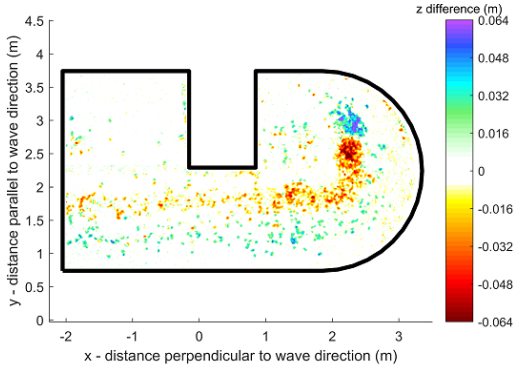

(c) z difference after run 3.

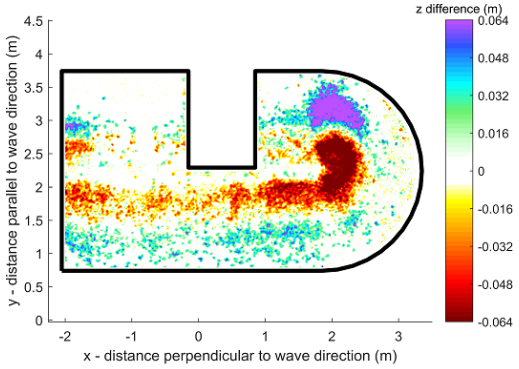

(d) z difference after run 4.

Figure A.3: UPorto tests Series 3.

Series 4

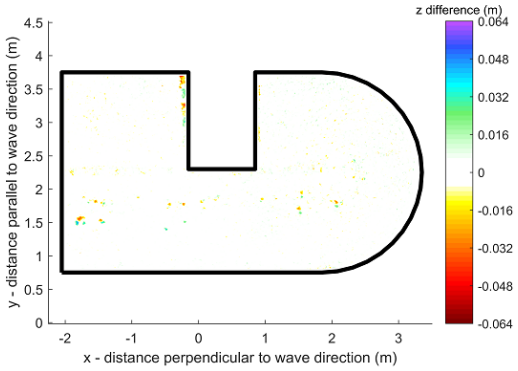

(a) z difference after run 1.

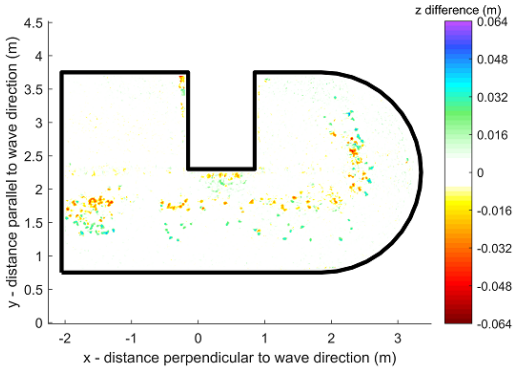

(b) z difference after run 2.

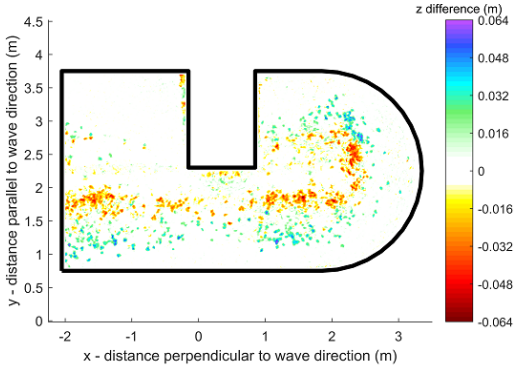

(c) z difference after run 3.

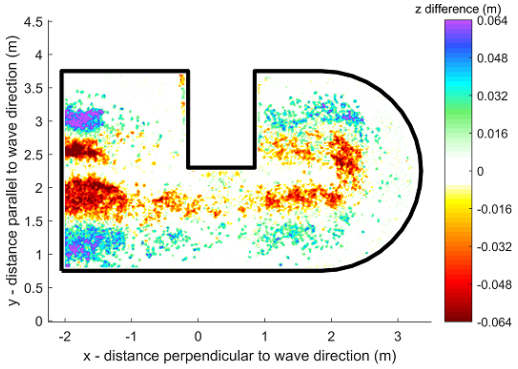

(d) z difference after run 4.

Figure A.4: UPorto tests Series 3.

B

Deltares test results

Series 1a

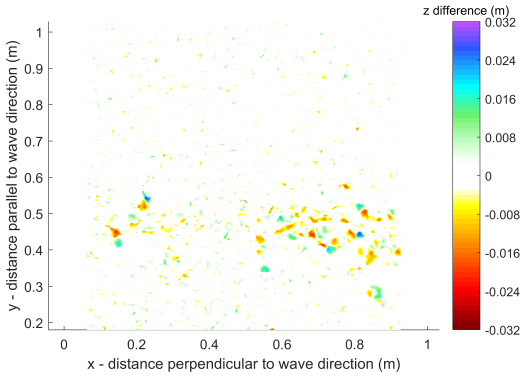

(a) z difference after run 1.

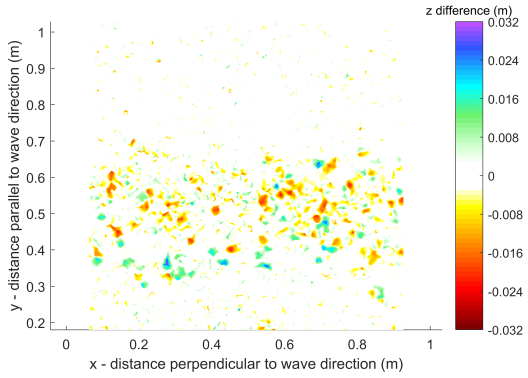

(b) z difference after run 2.

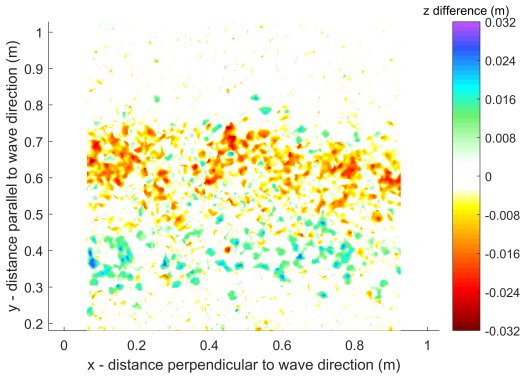

(c) z difference after run 3.

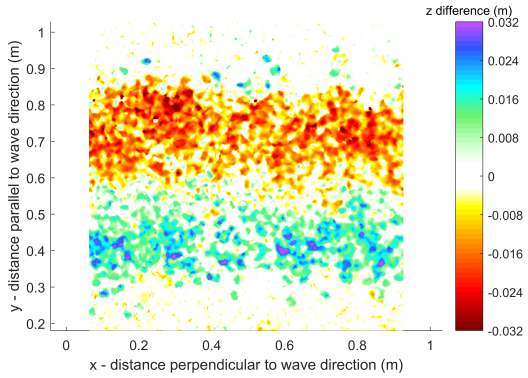

(d) z difference after run 4.

Figure B.1: Deltares tests Series 1a.

Series 1b

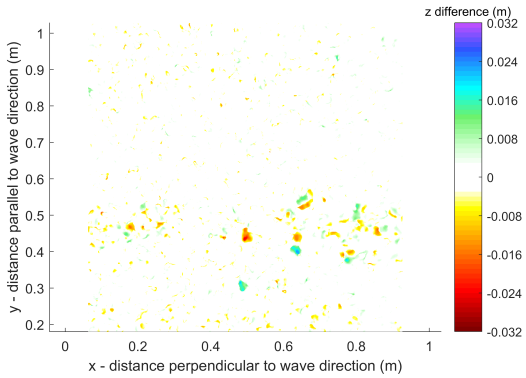

(a) z difference after run 1.

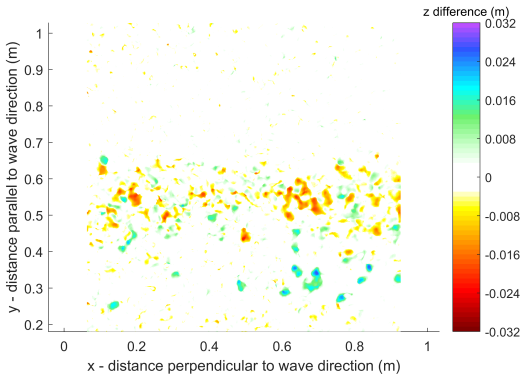

(b) z difference after run 2.

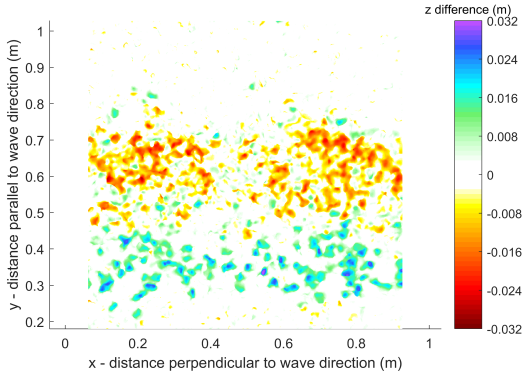

(c) z difference after run 3.

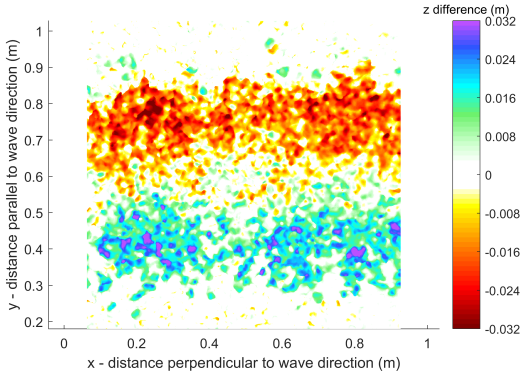

(d) z difference after run 4.

Figure B.2: Deltares tests Series 1b.

Series 1c

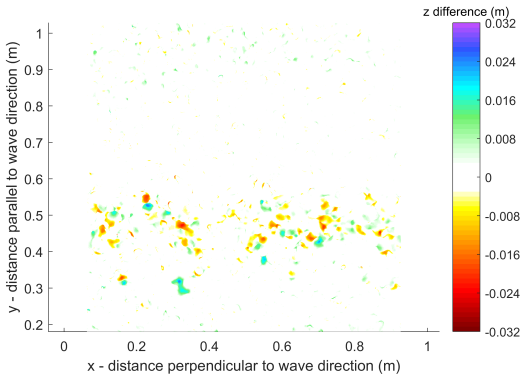

(a) z difference after run 1.

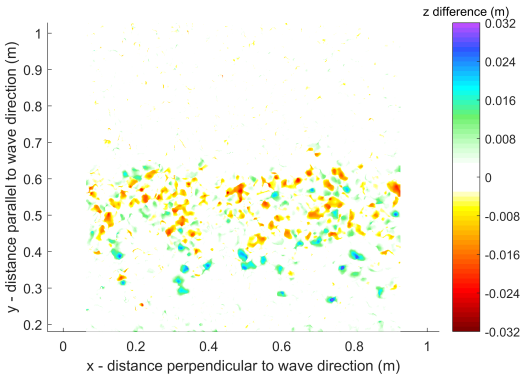

(b) z difference after run 2.

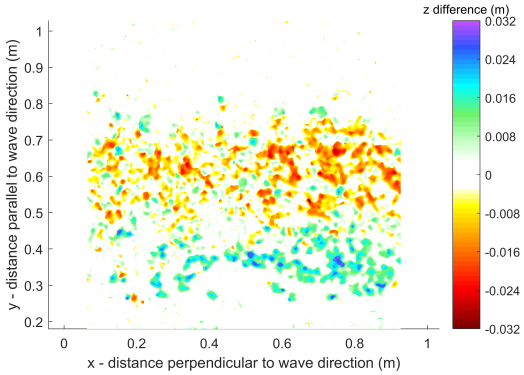

(c) z difference after run 3.

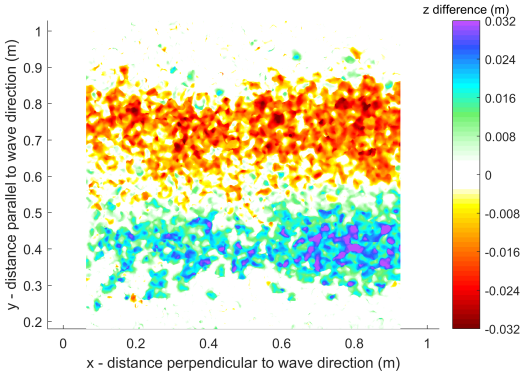

(d) z difference after run 4.

Figure B.3: Deltares tests Series 1c.

Series 1d

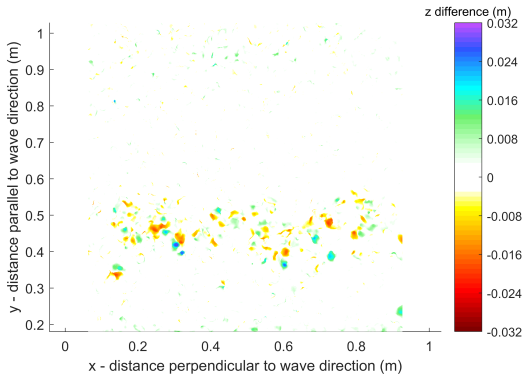

(a) z difference after run 1.

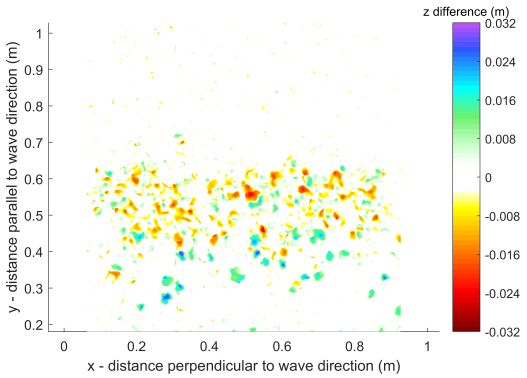

(b) z difference after run 2.

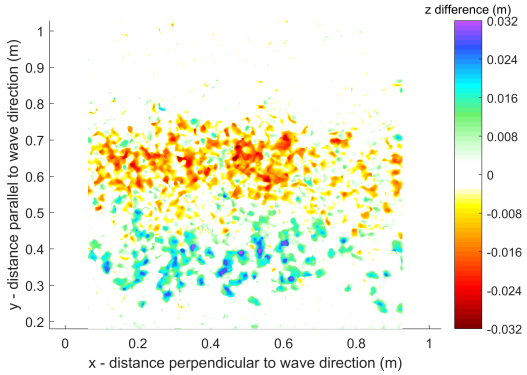

(c) z difference after run 3.

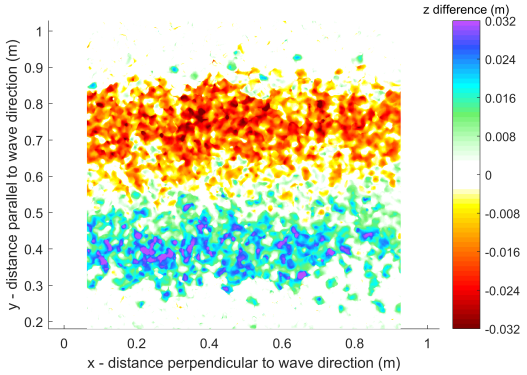

(d) z difference after run 4.

Figure B.4: Deltares tests Series 1d.

Series 1e

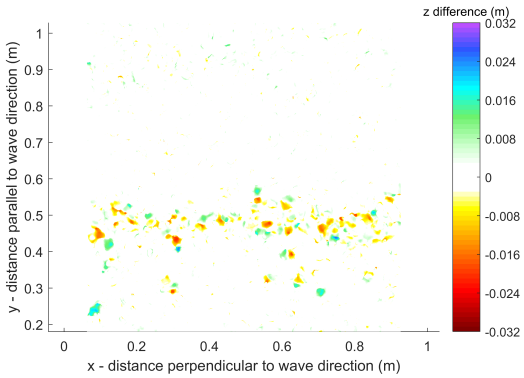

(a) z difference after run 1.

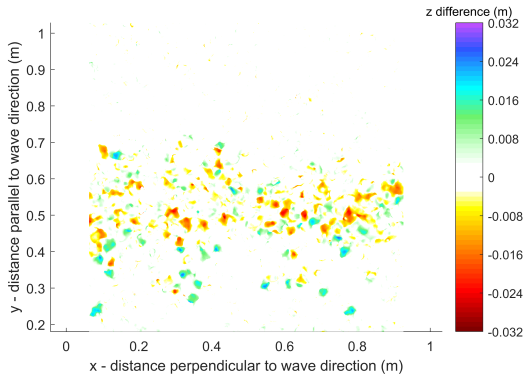

(b) z difference after run 2.

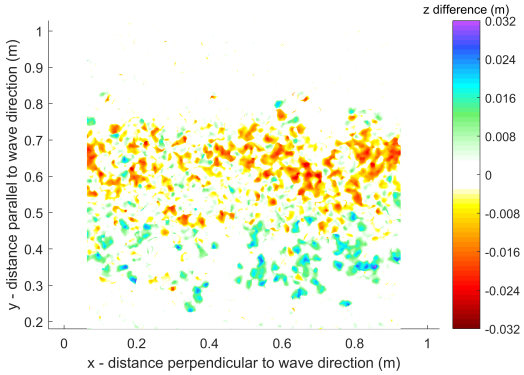

(c) z difference after run 3.

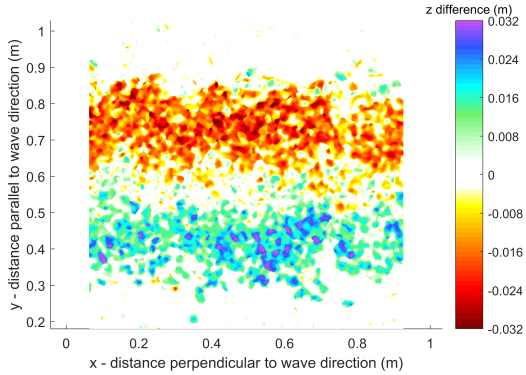

(d) z difference after run 4.

Figure B.5: Deltares tests Series 1e.

Series 2a, 2b, 2c, 2d, 2e

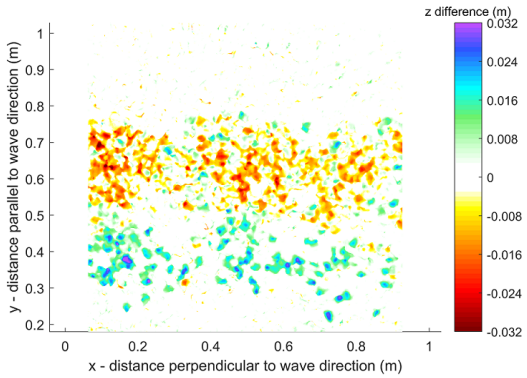

(a) Series 2a: z difference after run 1.

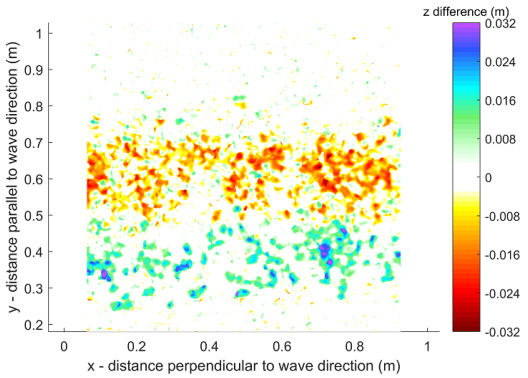

(b) Series 2b: z difference after run 1.

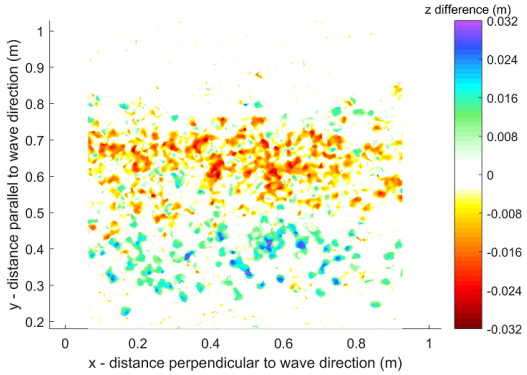

(c) Series 2c: z difference after run 1.

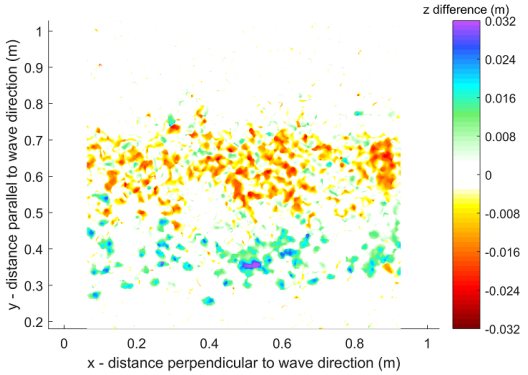

(d) Series 2d: z difference after run 1.

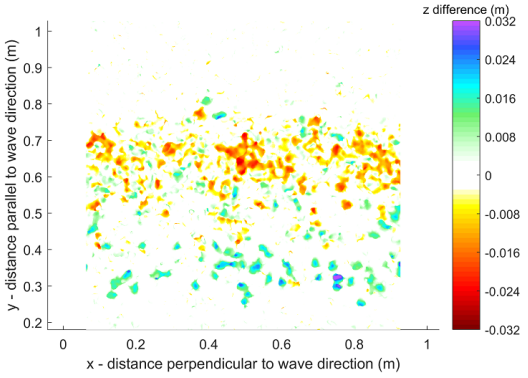

(e) Series 2e: z difference after run 1.

Figure B.6: Deltares tests Series 2a, 2b, 2c, 2d, 2e.

Series 3a

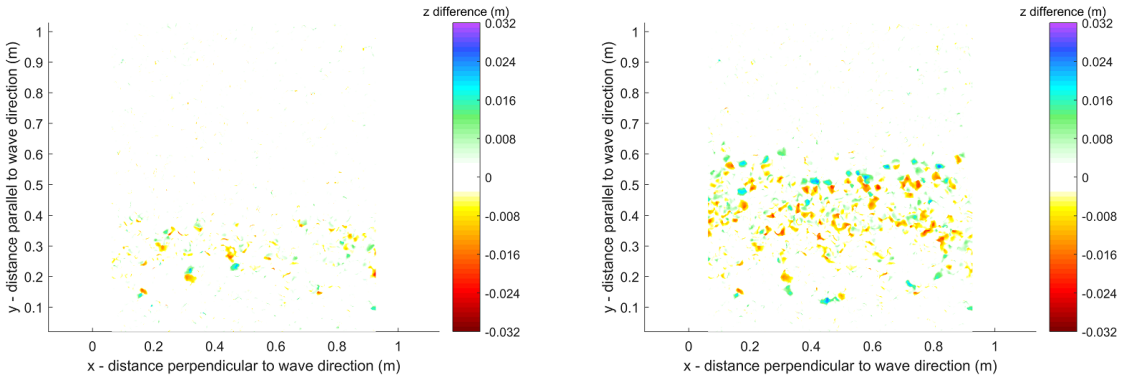

(a) z difference after run 1.

(b) z difference after run 2.

(c) z difference after run 3.

(d) z difference after run 4.

Figure B.7: Deltares tests Series 3a.

Series 4a

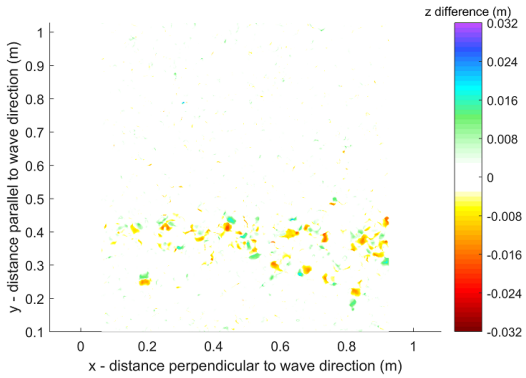

(a) z difference after run 1.

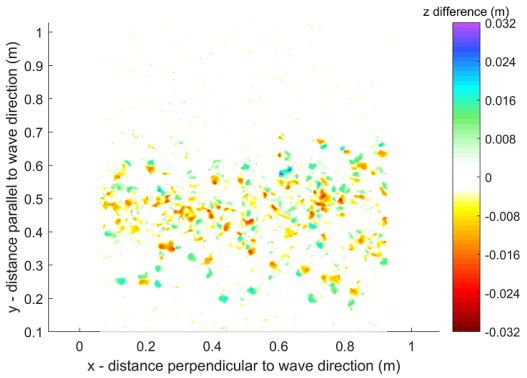

(b) z difference after run 2.

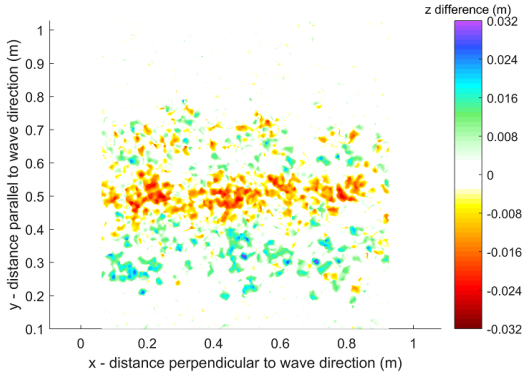

(c) z difference after run 3.

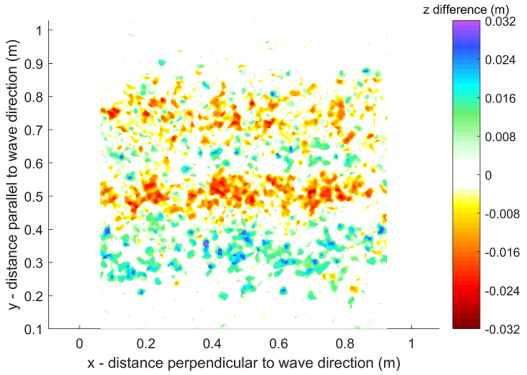

(d) z difference after run 4.

Figure B.8: Deltares tests Series 4a.

Series 5a

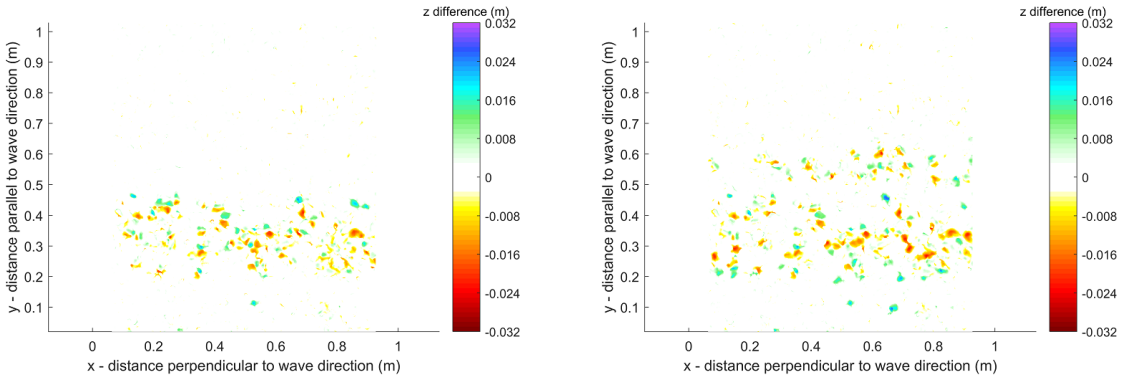

(a) z difference after run 1.

(b) z difference after run 2.

(c) z difference after run 3.

(d) z difference after run 4.

Figure B.9: Deltares tests Series 5a.

Series 6a

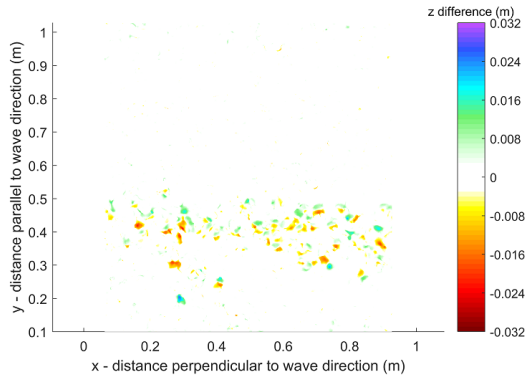

(a) z difference after run 1.

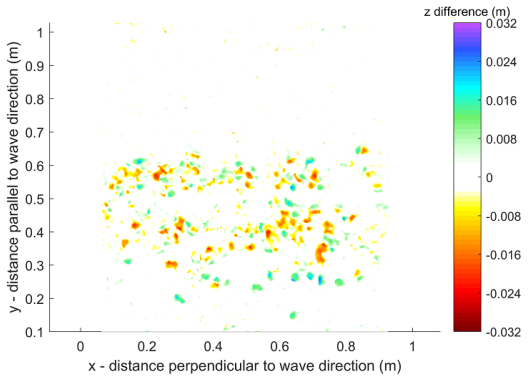

(b) z difference after run 2.

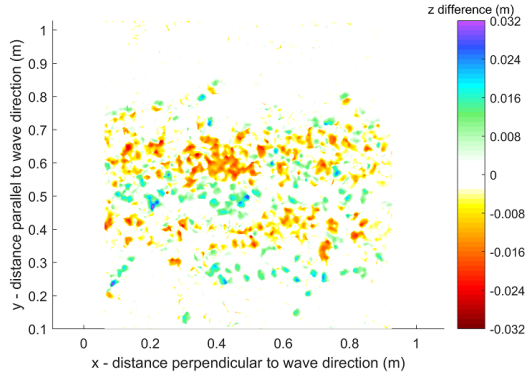

(c) z difference after run 3.

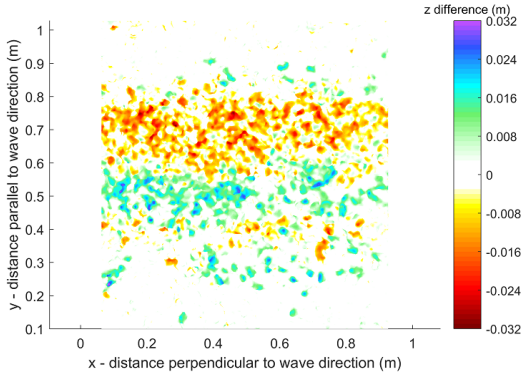

(d) z difference after run 4.

Figure B.10: Deltares tests Series 6a.

C

Characterization width analysis

Averaged data Deltares tests

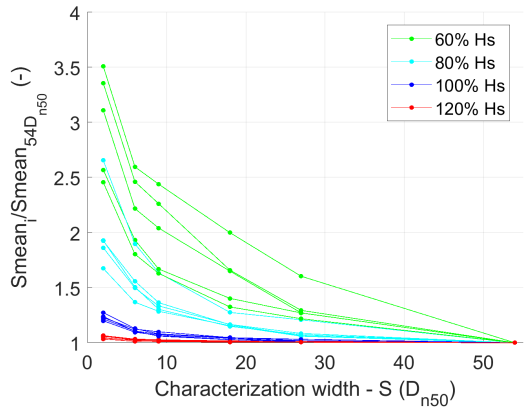

(a) All values.

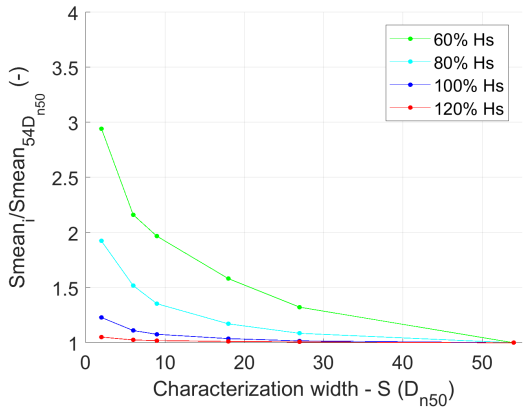

(b) Mean values.

Figure C.1: Characterization width variation - S parameter.

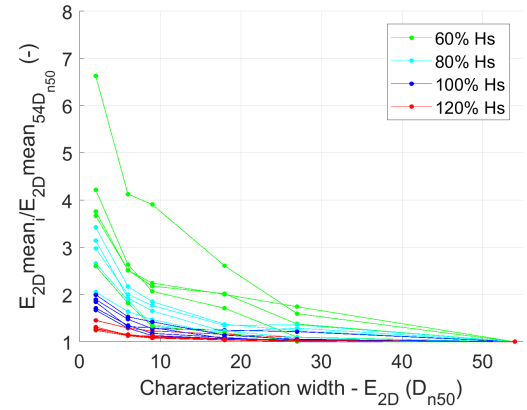

(a) All values.

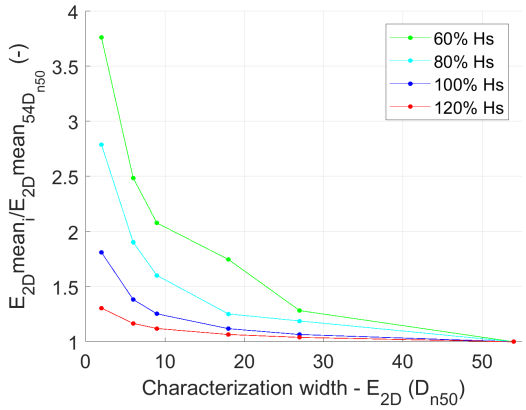

(b) Mean values.

Figure C.2: Characterization width variation - E_{2D} parameter.

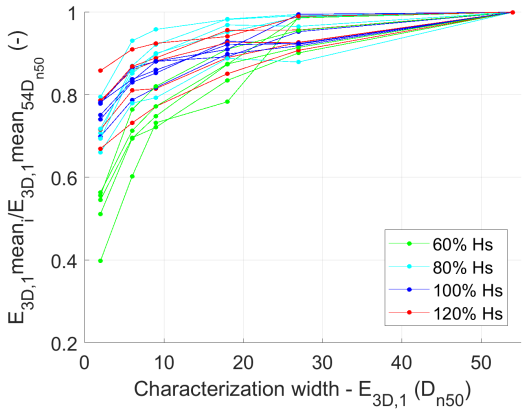

(a) All values.

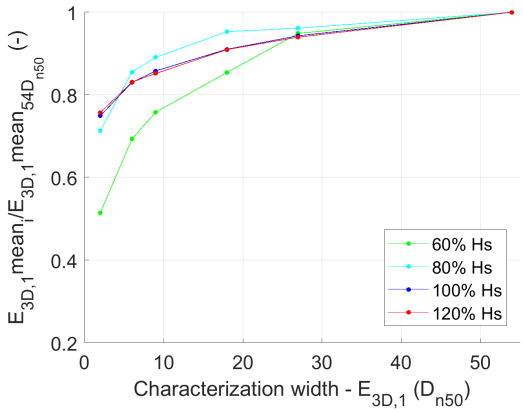

(b) Mean values.

Figure C.3: Characterization width variation - $E_{3D,1}$ parameter.

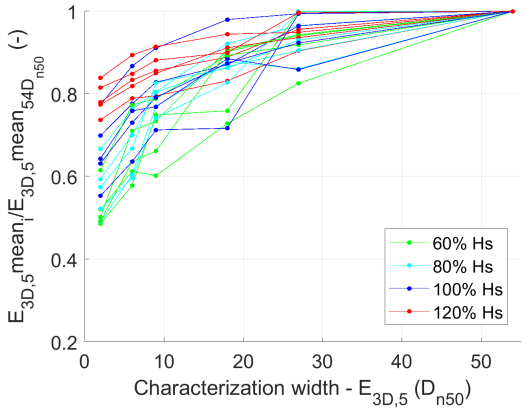

(a) All values.

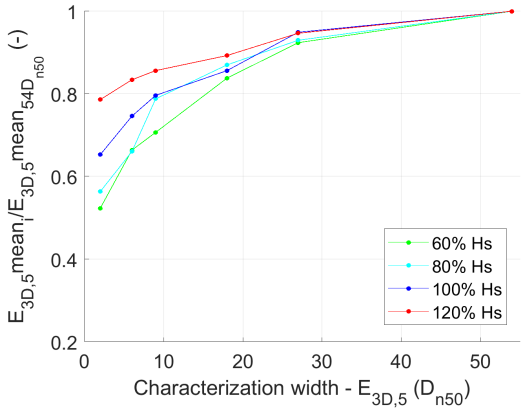

(b) Mean values.

Figure C.4: Characterization width variation - $E_{3D,5}$ parameter.

Variability Deltares tests

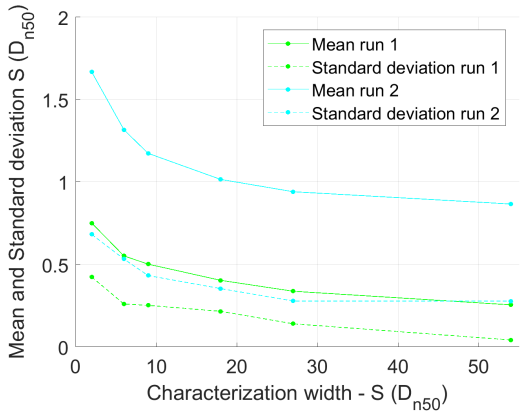

(a) Runs 1 and 2.

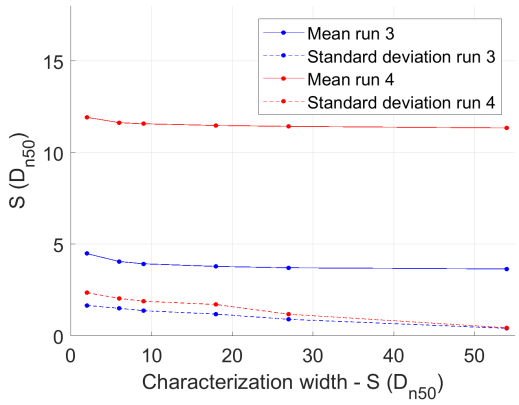

(b) Runs 3 and 4.

Figure C.5: Characterization width variation - mean and standard deviation - S parameter.

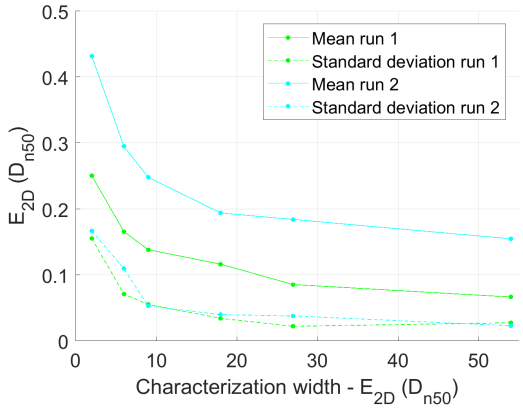

(a) Runs 1 and 2.

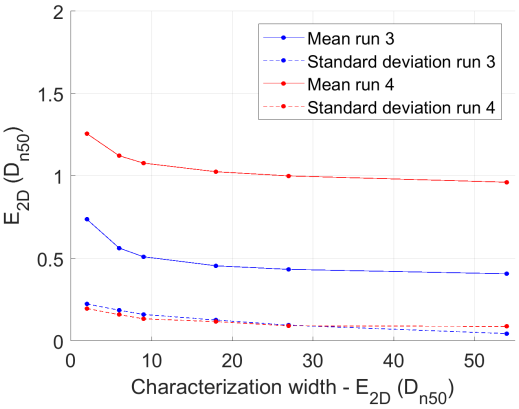

(b) Runs 3 and 4.

Figure C.6: Characterization width variation - mean and standard deviation - E_{2D} parameter.

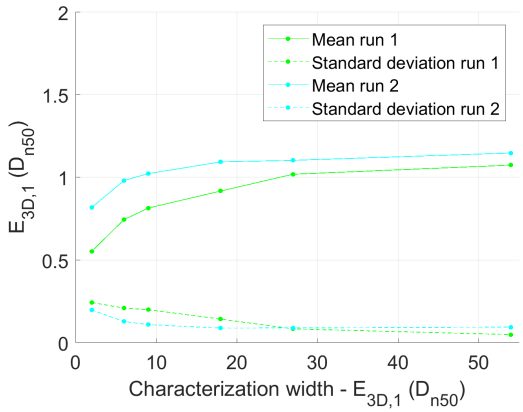

(a) Runs 1 and 2.

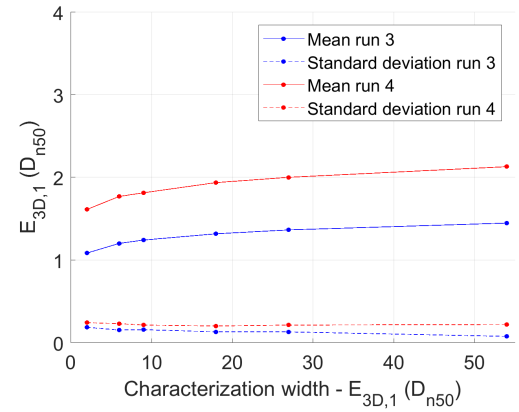

(b) Runs 3 and 4.

Figure C.7: Characterization width variation - mean and standard deviation - $E_{3D,1}$ parameter.

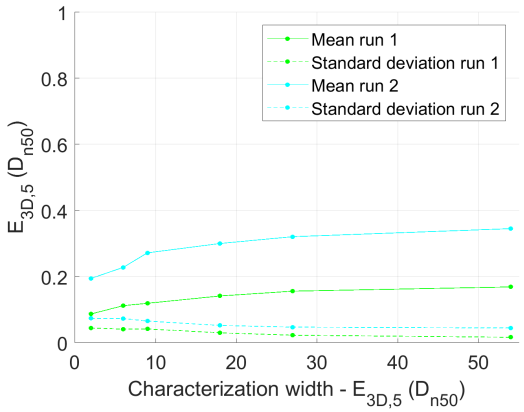

(a) Runs 1 and 2.

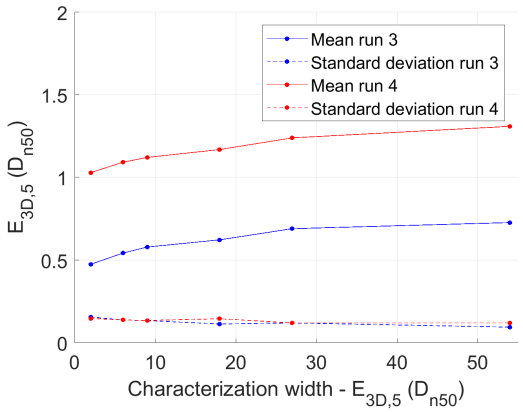

(b) Runs 3 and 4.

Figure C.8: Characterization width variation - mean and standard deviation - $E_{3D,5}$ parameter.

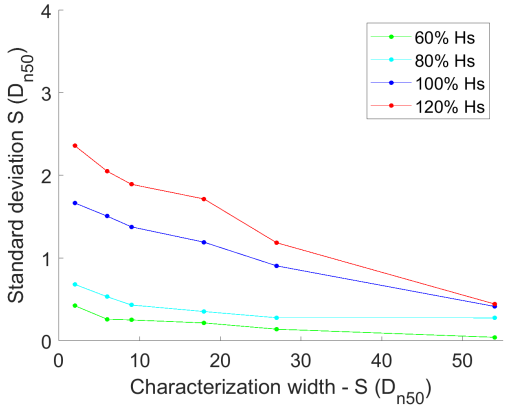

(a) S parameter.

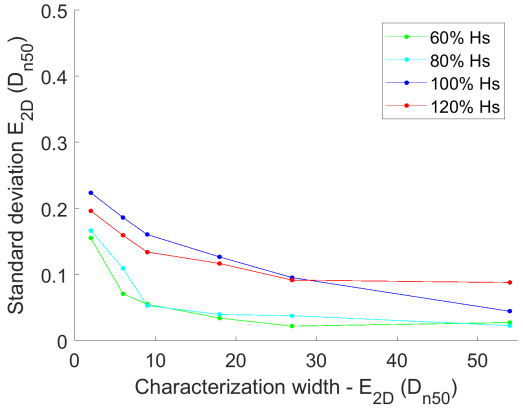

(b) E_{2D} parameter.

Figure C.9: Characterization width variation - standard deviation all runs - S and E_{2D} parameter.

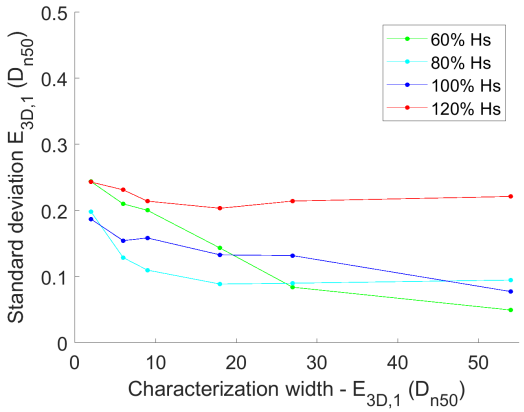

(a) S parameter.

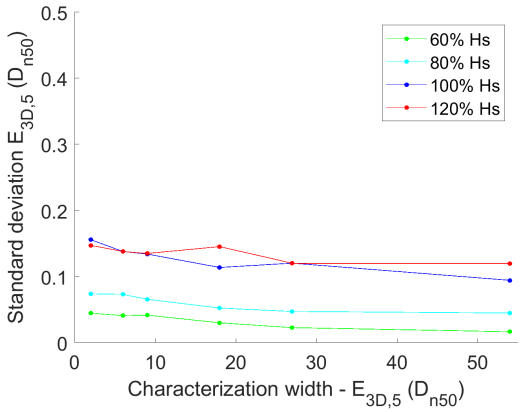

(b) E_{2D} parameter.

Figure C.10: Characterization width variation - standard deviation all runs - $E_{3D,1}$ and $E_{3D,5}$ parameter.

Averaged data UPorto tests

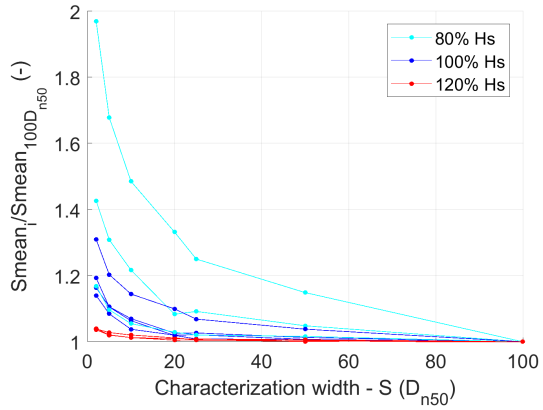

(a) S parameter.

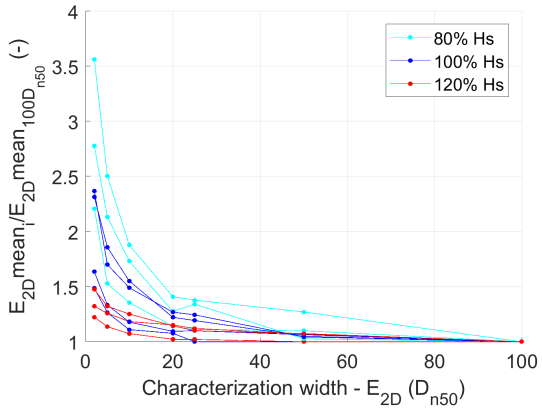

(b) E_{2D} parameter.

Figure C.11: Characterization width variation - S and E_{2D} parameter.

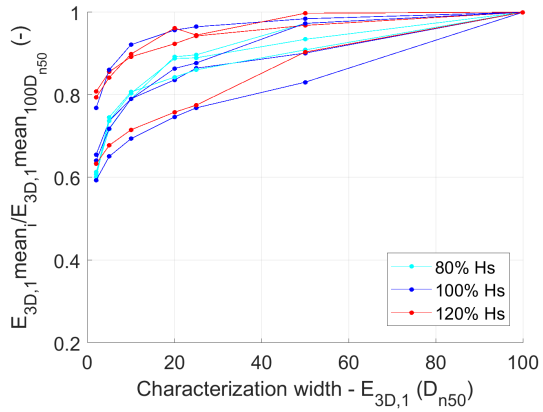

(a) $E_{3D,1}$ parameter.

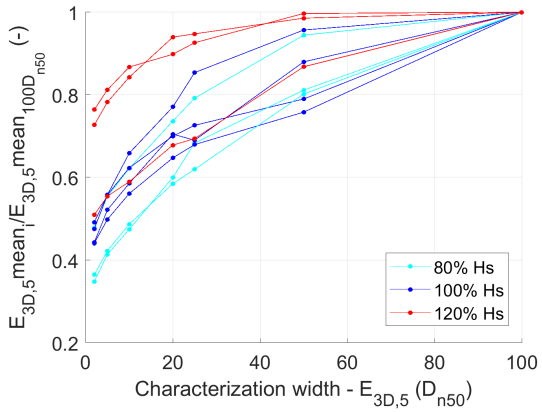

(b) $E_{3D,5}$ parameter.

Figure C.12: Characterization width variation - $E_{3D,1}$ and $E_{3D,5}$ parameter.

D

Comparison damage parameters

UPorto tests - damage parameters

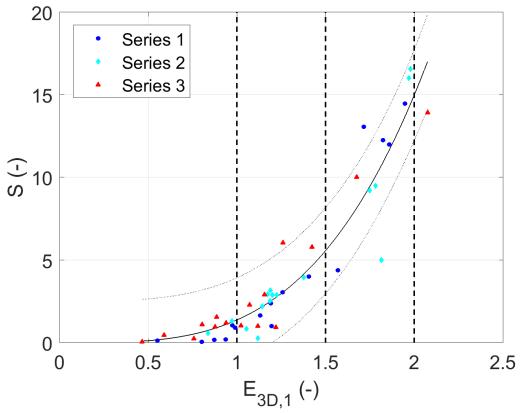

(a) $E_{3D,1}$ vs S.

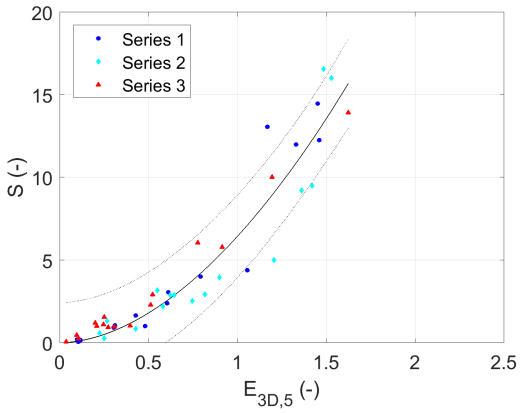

(b) $E_{3D,5}$ vs S.

Figure D.1: Damage parameters comparison.

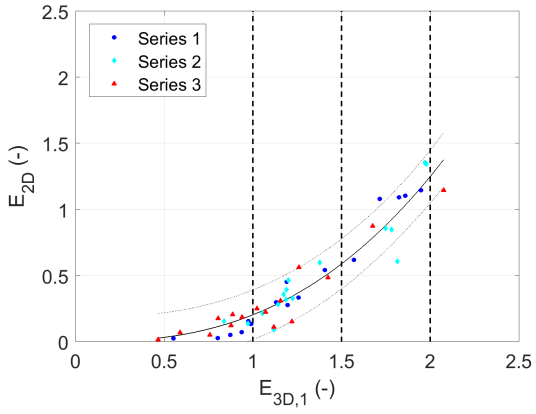

(a) $E_{3D,1}$ vs E_{2D}.

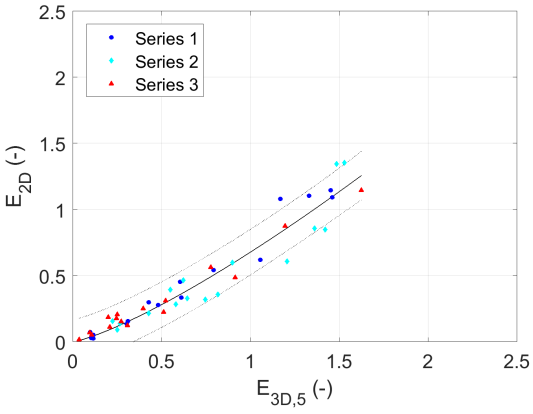

(b) $E_{3D,5}$ vs E_{2D}.

Figure D.2: Damage parameters comparison.

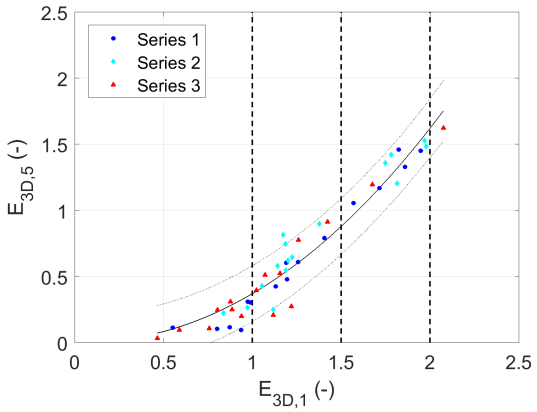

(a) $E_{3D,1}$ vs $E_{3D,5}$.

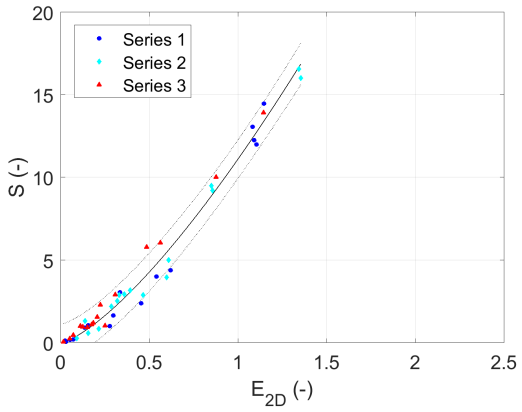

(b) E_{2D} vs S.

Figure D.3: Damage parameters comparison.

Deltares tests - damage parameters

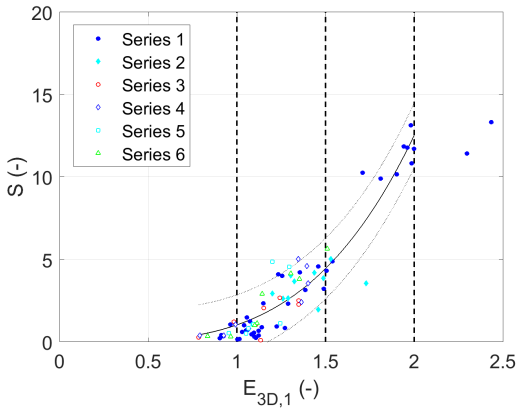

(a) $E_{3D,1}$ vs S.

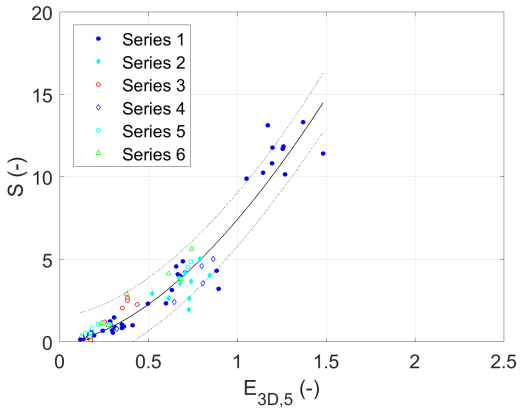

(b) $E_{3D,5}$ vs S.

Figure D.4: Damage parameters comparison.

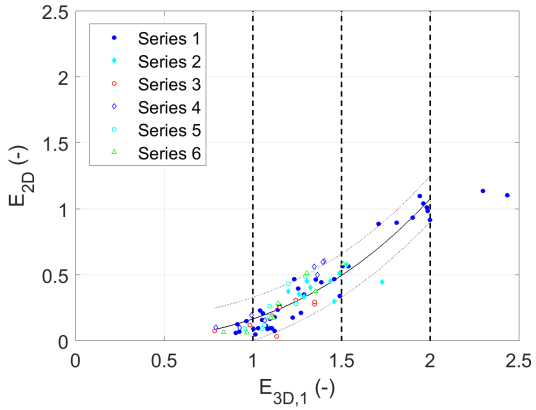

(a) $E_{3D,1}$ vs E_{2D}.

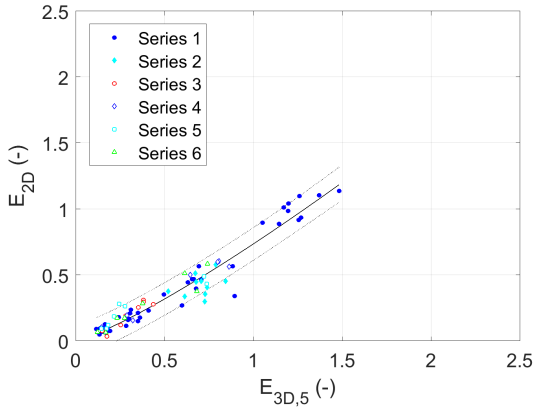

(b) $E_{3D,5}$ vs E_{2D}.

Figure D.5: Damage parameters comparison.

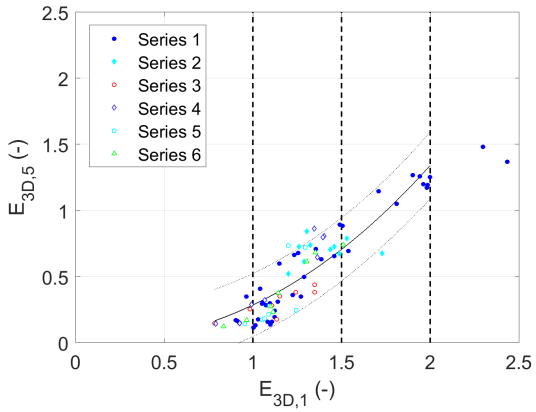

(a) $E_{3D,1}$ vs $E_{3D,5}$.

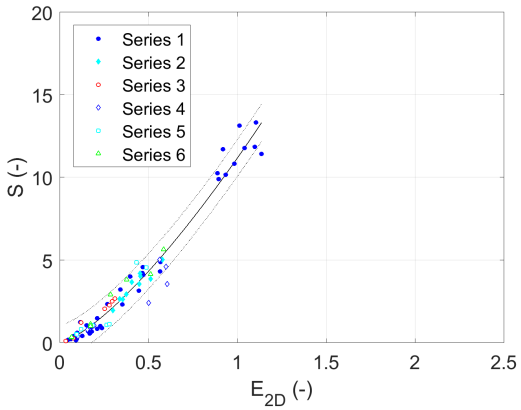

(b) E_{2D} vs S.

Figure D.6: Damage parameters comparison.

All tests (UPorto and Deltares tests) - damage parameters

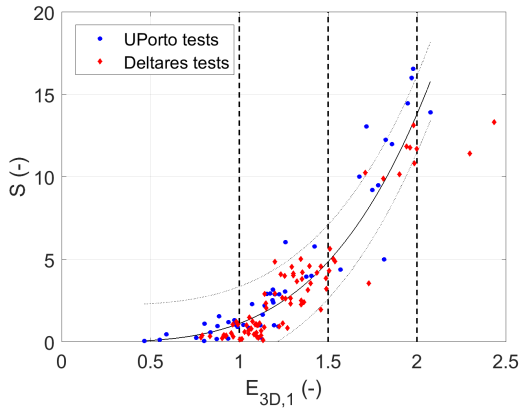

(a) $E_{3D,1}$ vs S.

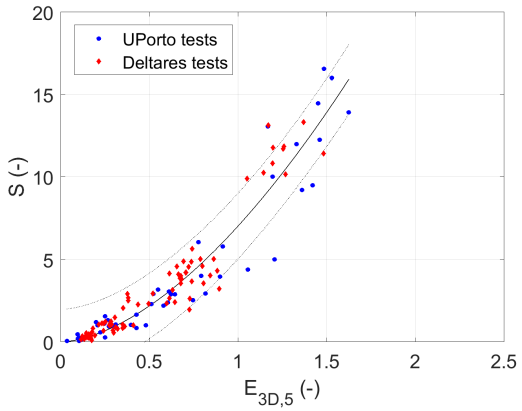

(b) $E_{3D,5}$ vs S.

Figure D.7: Damage parameters comparison.

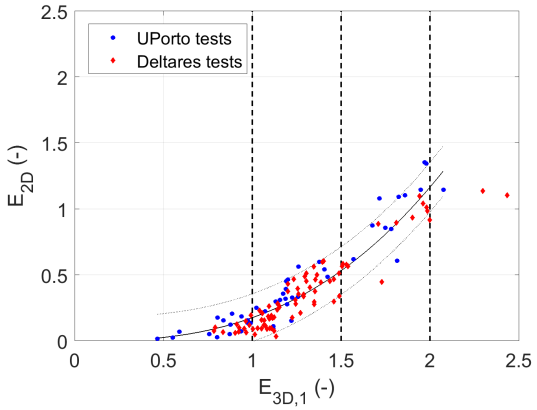

(a) $E_{3D,1}$ vs E_{2D}.

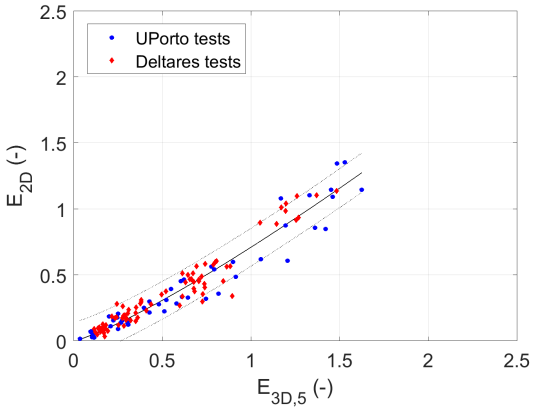

(b) $E_{3D,5}$ vs E_{2D}.

Figure D.8: Damage parameters comparison.

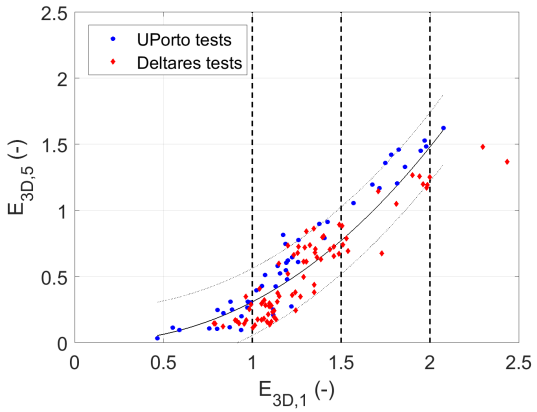

(a) $E_{3D,1}$ vs $E_{3D,5}$.

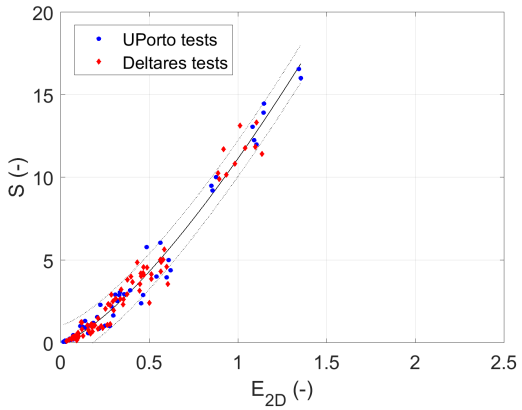

(b) E_{2D} vs S.

Figure D.9: Damage parameters comparison.

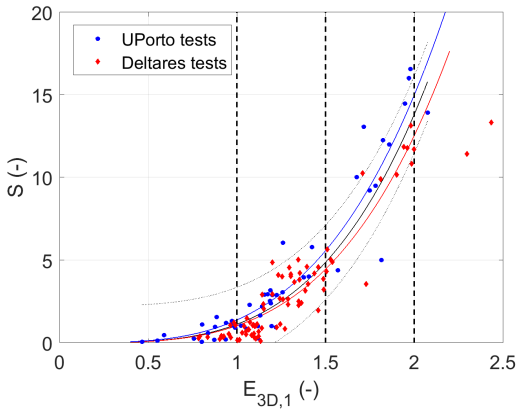

(a) $E_{3D,1}$ vs S.

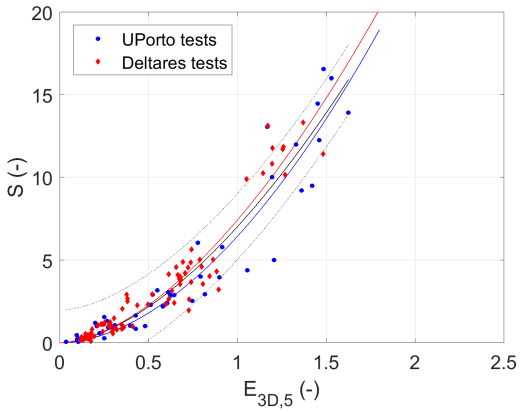

(b) $E_{3D,5}$ vs S.

Figure D.10: Damage parameters comparison.

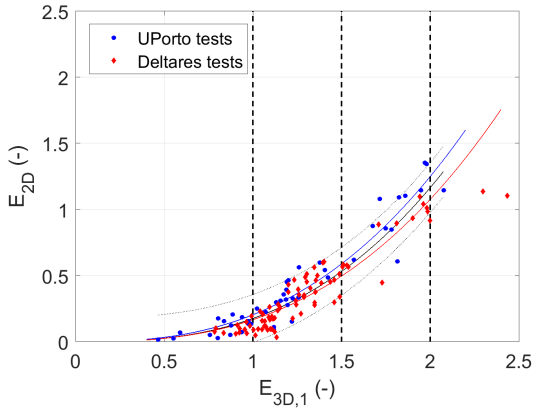

(a) $E_{3D,1}$ vs E_{2D}.

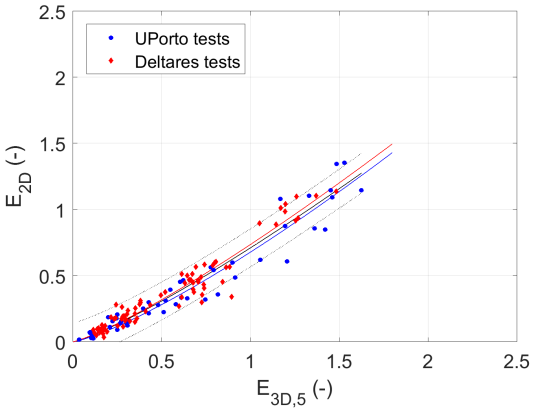

(b) $E_{3D,5}$ vs E_{2D}.

Figure D.11: Damage parameters comparison.

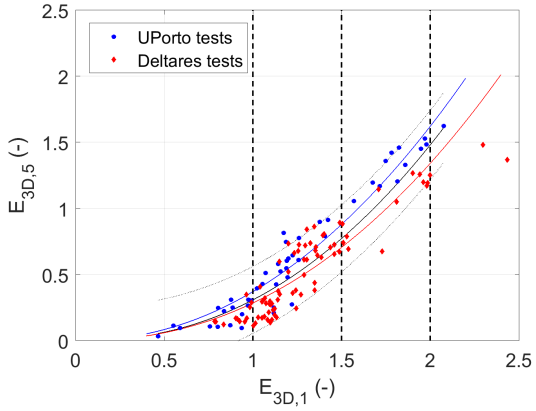

(a) $E_{3D,1}$ vs $E_{3D,5}$.

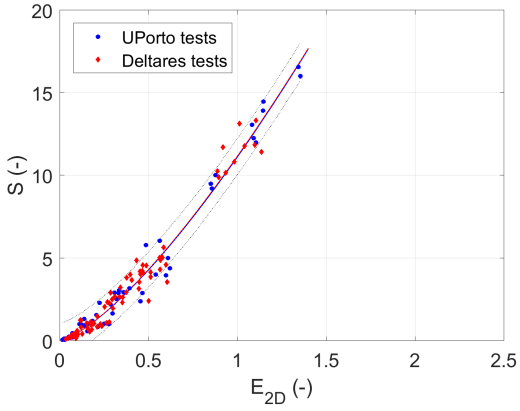

(b) E_{2D} vs S.

Figure D.12: Damage parameters comparison.

E

Validation 3D damage parameters

Variability of damage parameters

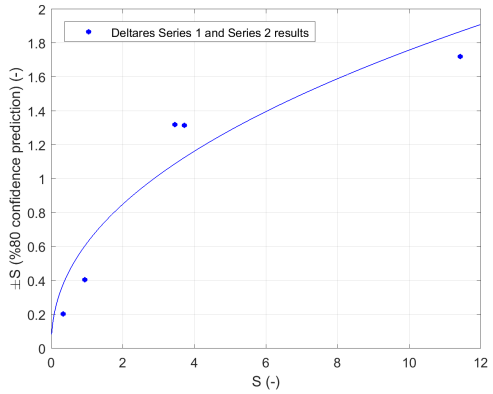

(a) S parameter.

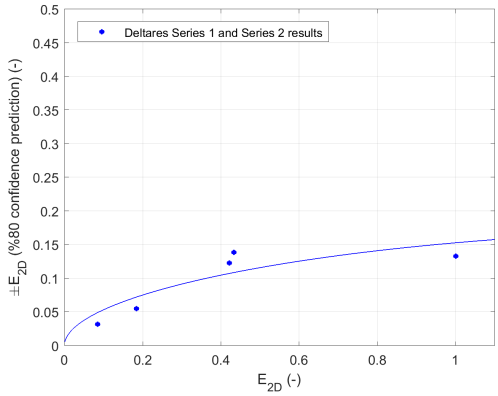

(b) E_{2D} parameter.

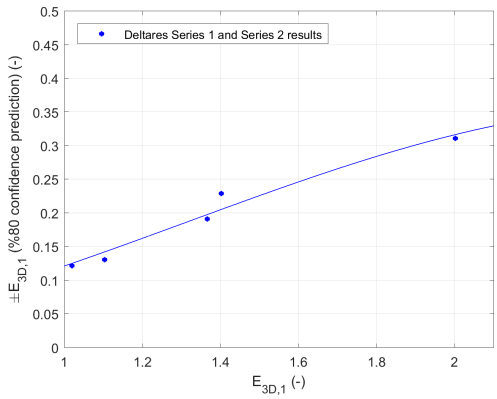

(c) $E_{3D,1}$ parameter.

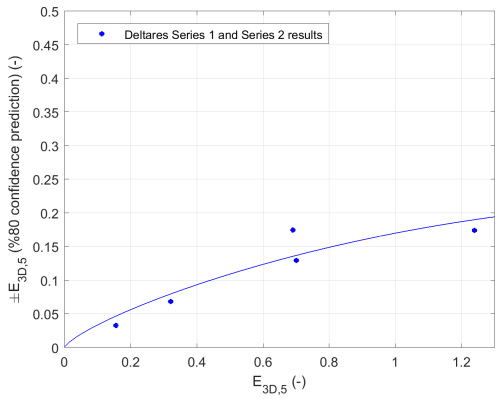

(d) $E_{3D,5}$ parameter.

Figure E.1: 80% confidence prediction interval - all parameters.

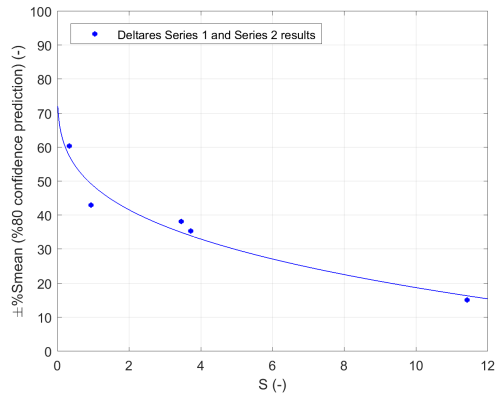

(a) S parameter.

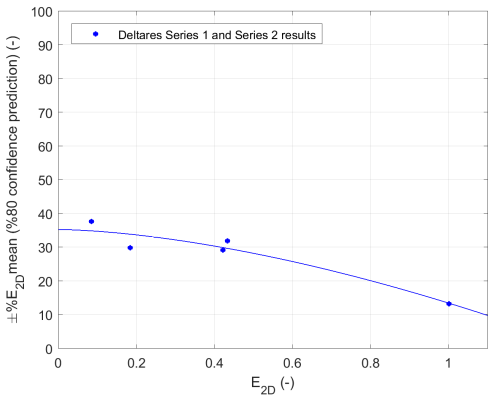

(b) E_{2D} parameter.

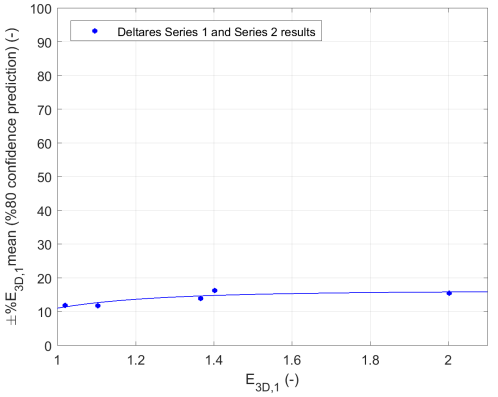

(c) $E_{3D,1}$ parameter.

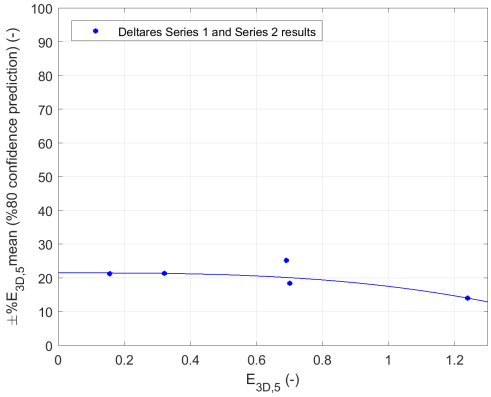

(d) $E_{3D,5}$ parameter.

Figure E.2: 80% confidence prediction interval respect to mean - all parameters.

Extreme value distribution for $E_{3D,5}$

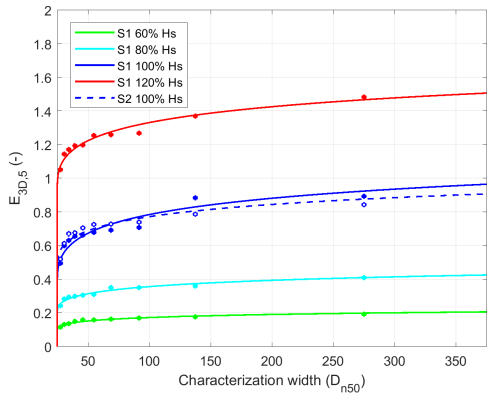

(a) Gumbel distribution.

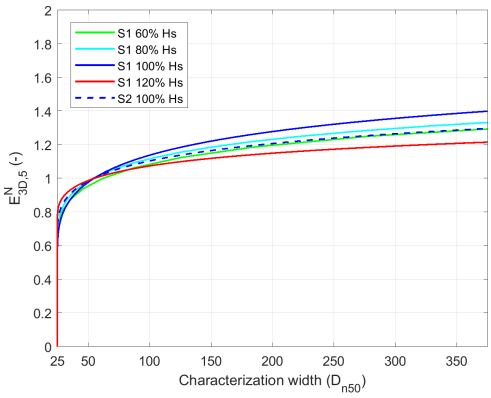

(b) Gumbel distribution normalized by the mean.

Figure E.3: Length effect $E_{3D,5}$ parameter - Gumbel distribution .

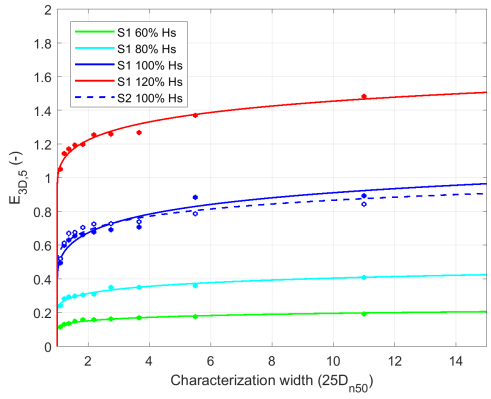

(a) Gumbel distribution.

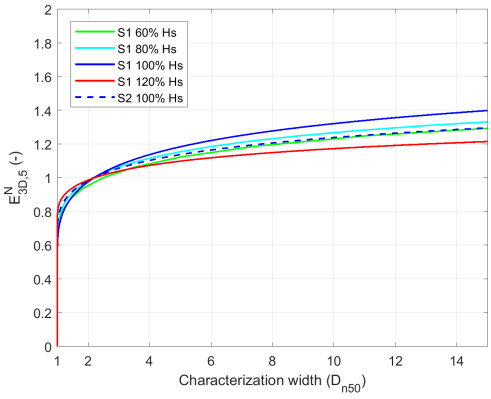

(b) Gumbel distribution normalized by the mean.

Figure E.4: Length effect $E_{3D,5}$ parameter - Gumbel distribution .

F

Evaluation of adaptation alternatives

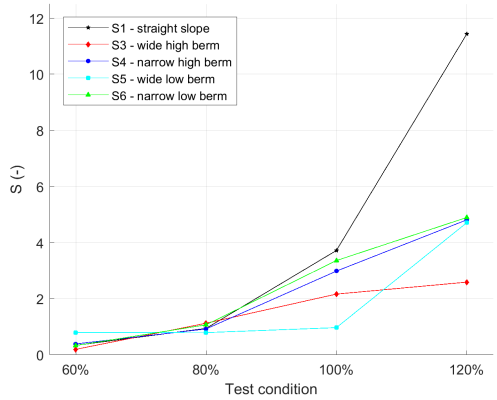

(a) S parameter.

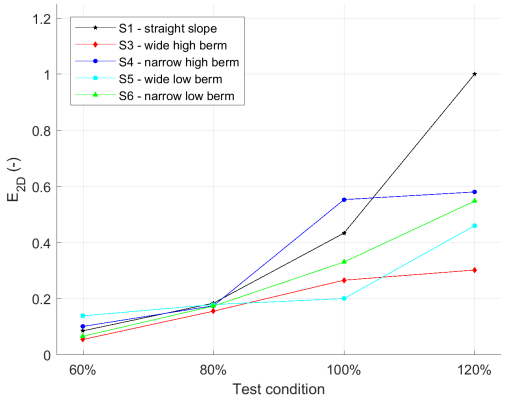

(b) E_{2D} parameter.

Figure F.1: Damage comparison - Straight slope vs Slope with a berm.

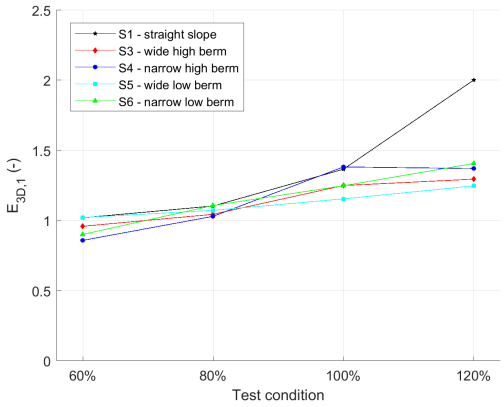

(a) $E_{3D,1}$ parameter.

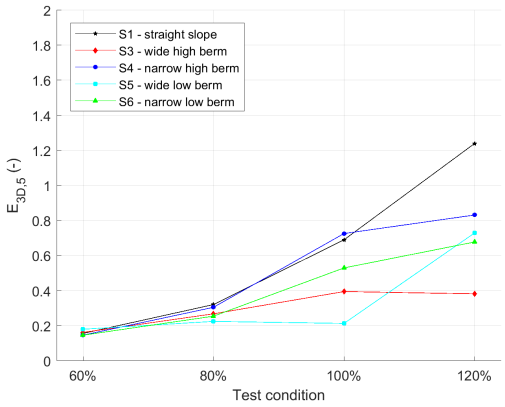

(b) $E_{3D,5}$ parameter.

Figure F.2: Damage comparison - Straight slope vs Slope with a berm.

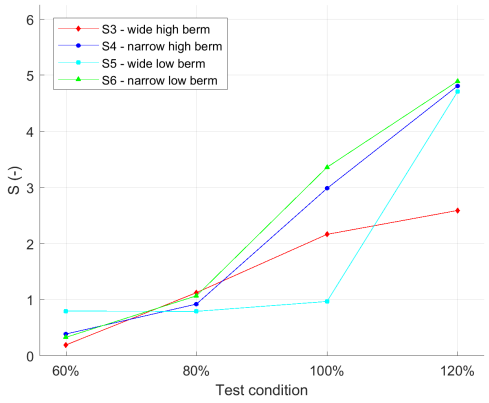

(a) S parameter.

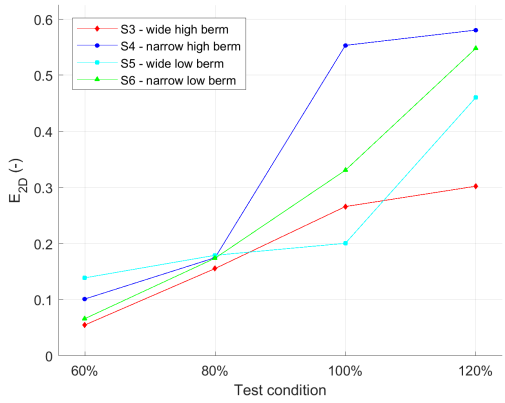

(b) E_{2D} parameter.

Figure F.3: Damage comparison - Berm configurations total damage.

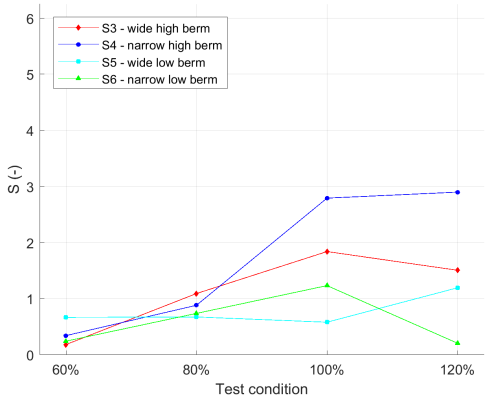

(a) S parameter.

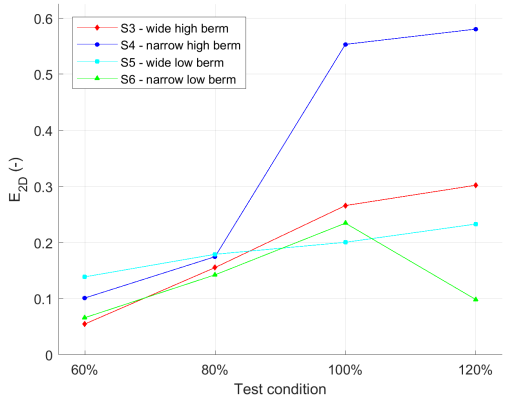

(b) E_{2D} parameter.

Figure F.4: Damage comparison - Berm configurations lower slope damage.

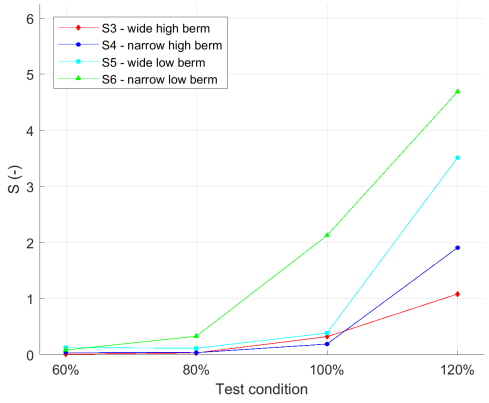

(a) S parameter.

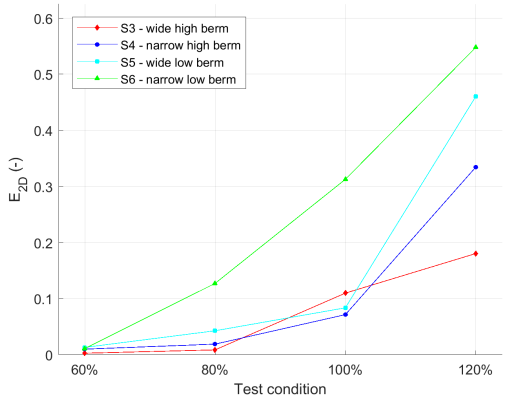

(b) E_{2D} parameter.

Figure F.5: Damage comparison - Berm configurations upper slope damage.

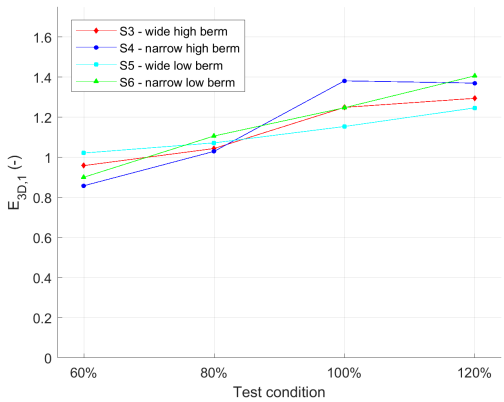

(a) $E_{3D,1}$ parameter.

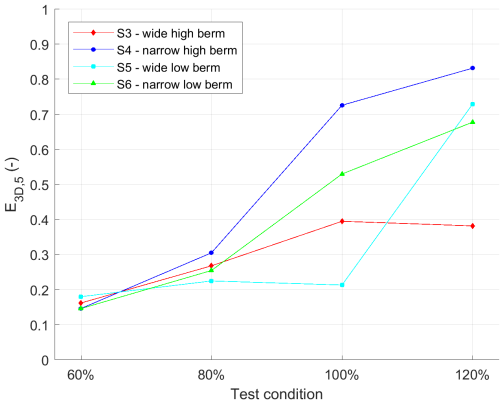

(b) $E_{3D,5}$ parameter.

Figure F.6: Damage comparison - Berm configurations total damage.

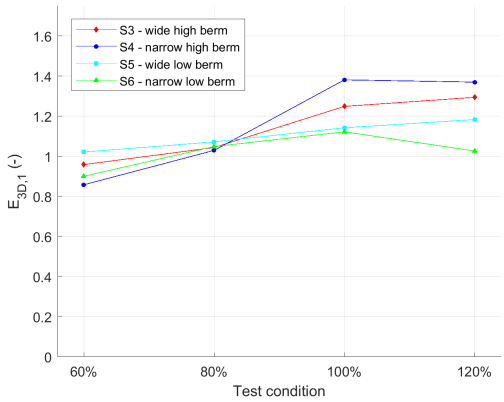

(a) $E_{3D,1}$ parameter.

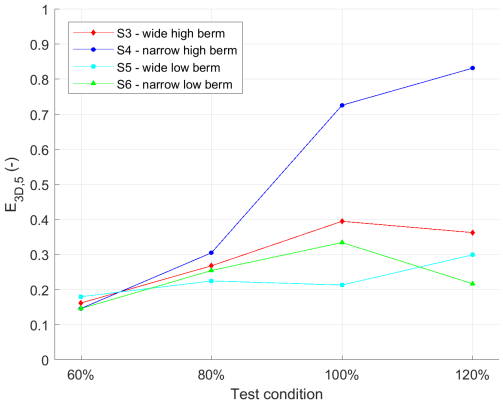

(b) $E_{3D,5}$ parameter.

Figure F.7: Damage comparison - Berm configurations lower slope damage.

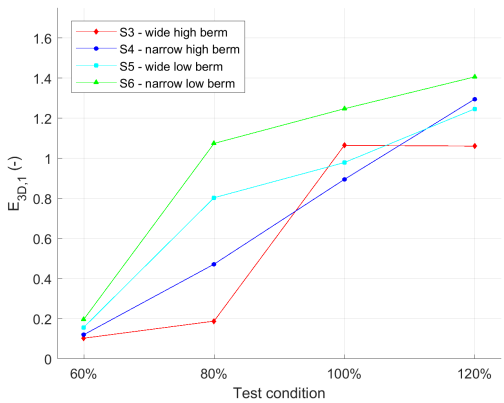

(a) $E_{3D,1}$ parameter.

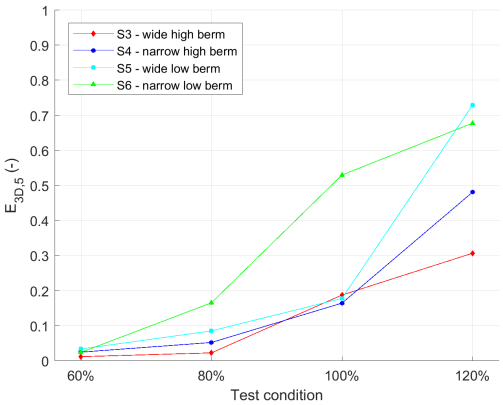

(b) $E_{3D,5}$ parameter.

Figure F.8: Damage comparison - Berm configurations upper slope damage.

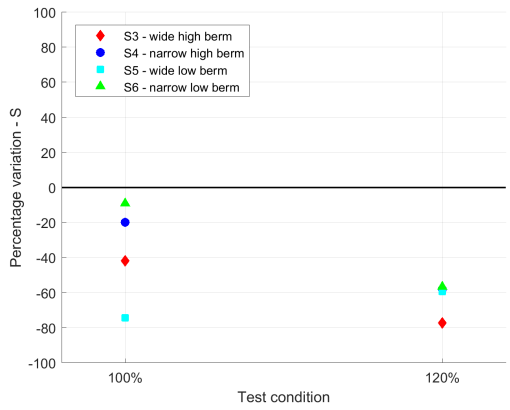

(a) S parameter.

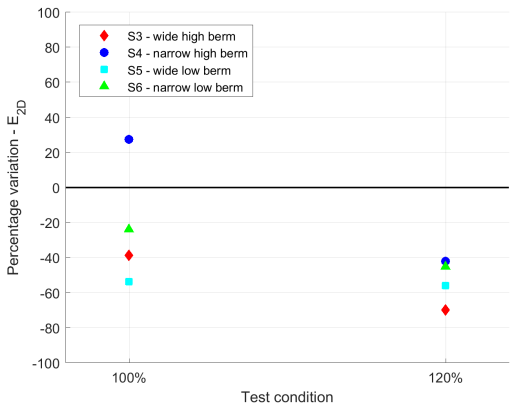

(b) E_{2D} parameter.

Figure F.9: Damage reduction for slopes with a berm.

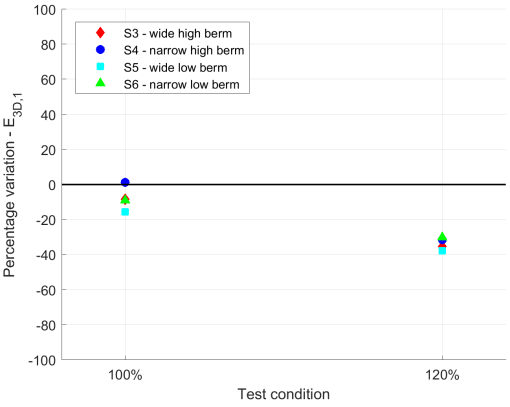

(a) $E_{3D,1}$ parameter.

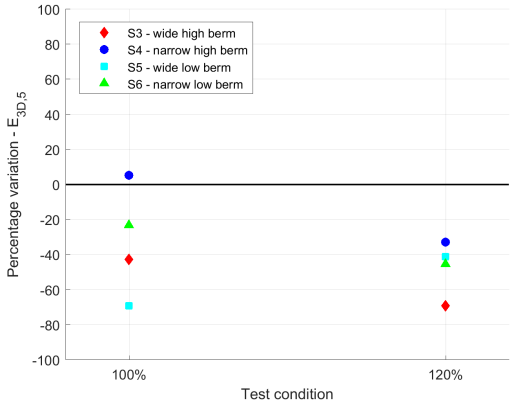

(b) $E_{3D,5}$ parameter.

Figure F.10: Damage reduction for slopes with a berm.

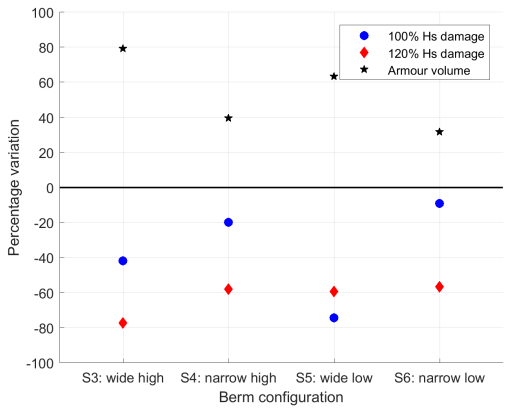

(a) S parameter.

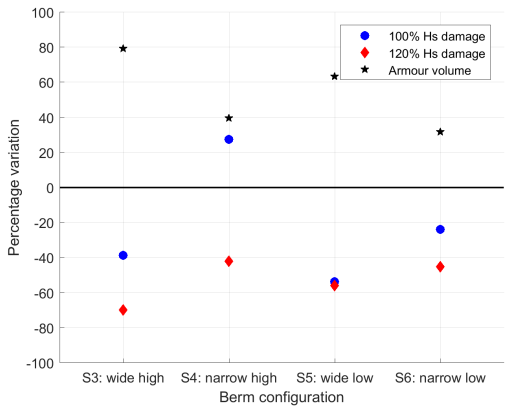

(b) E_{2D} parameter.

Figure F.11: Damage reduction for slopes with a berm.

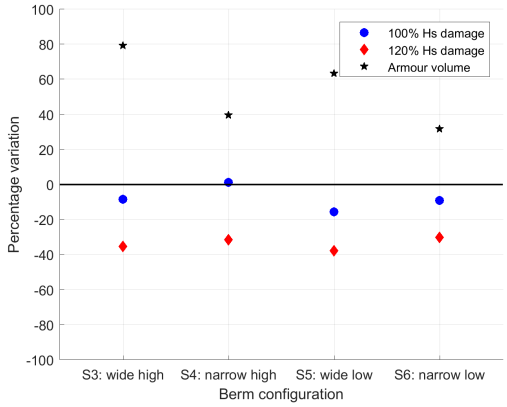

(a) $E_{3D,1}$ parameter.

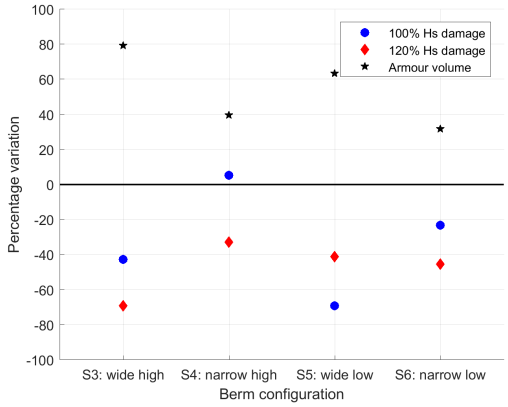

(b) $E_{3D,5}$ parameter.

Figure F.12: Damage reduction and volume increase for slopes with a berm.

G

Granular material analysis

UPorto tests

Filter

Density given by UPorto: ρ_s 2670 kg/m^3

Nominal median diameter given by UPorto (obtained from sieve diameter and Eq. 2.6): 11.6 mm

Armour

Density given by UPorto: ρ_s 2670 kg/m^3

Table G.1: UPorto size analysis (obtained from weighting of individual stones and Eq. 2.5) - armour

Sample	Nr of stones	D_{n15} (mm)	D_{n50} (mm)	D_{n85} (mm)	D_{n85}/D_{n15} (-)
Sample 1	694	28.2	31.7	35.4	1.25
Sample 2	700	28.5	32.2	35.7	1.25
Sample 3	692	28.5	32.0	35.8	1.25
All samples	**2086**	**28.5**	**32.0**	**35.7**	**1.25**

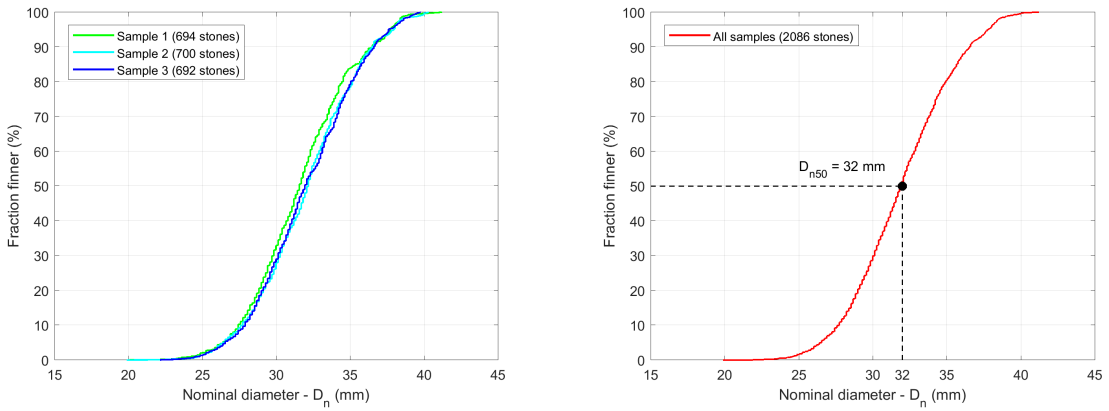

(a) Individual samples.

(b) All samples combined.

Figure G.1: UPorto sieve analysis (obtained from weighting of individual stones and Eq. 2.5) - armour.

Deltares tests

Filter

Table G.2: Deltares density analysis - filter

Sample	Dry mass (g)	Wet mass (g)	Density (kg/m^3)
Sample 1	646.4	404.2	2669
Sample 2	619.9	387.3	2665
All samples	**1266.3**	**791.5**	**2667**

Table G.3: Deltares sieve analysis (obtained from weighting of individual stones and Eq. 2.5) - filter

Sample	Nr of stones	D_{n15} (mm)	D_{n50} (mm)	D_{n85} (mm)	D_{n85}/D_{n15} (-)
All samples	**593**	**8.4**	**9.4**	**10.4**	**1.24**

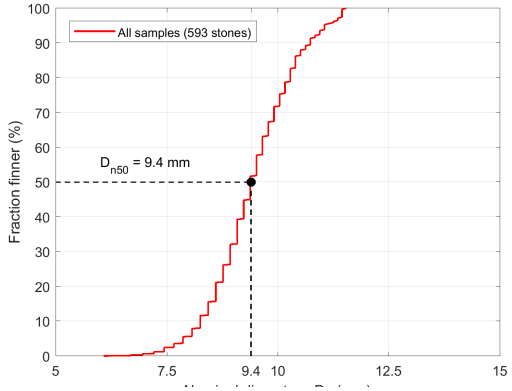

Figure G.2: Deltares sieve analysis (obtained from weighting of individual stones and Eq. 2.5) - filter.

Armour

Table G.4: Deltares density analysis - armour

Sample	Dry mass (g)	Wet mass (g)	Density (kg/m^3)
Sample 1	1488.7	939.2	2709
Sample 2	1419.2	895.5	2710
All samples	**2907.9**	**1834.7**	**2710**

Table G.5: Deltares sieve analysis (obtained from weighting of individual stones and Eq. 2.5) - armour

Sample	Nr of stones	D_{n15} (mm)	D_{n50} (mm)	D_{n85} (mm)	D_{n85}/D_{n15} (-)
All samples	**1507**	**15.0**	**16.3**	**18.0**	**1.20**

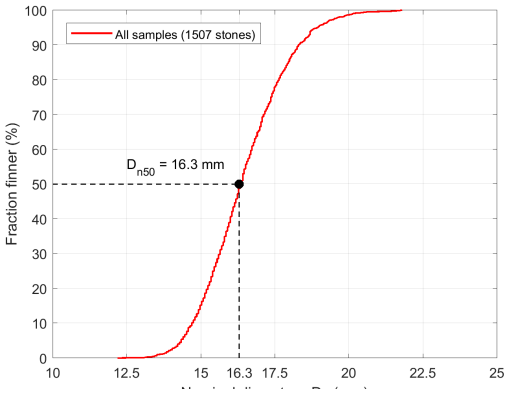

Figure G.3: Deltares sieve analysis (obtained from weighting of individual stones and Eq. 2.5) - armour.

H

All damage measurements

UPorto tests

All values calculated for a 25D$_{n50}$ characterization width (4 per test run).

Table H.1: UPorto test results - parameter S

Series	Run	Damage	Waves	h (m)	Cond.	S			
S1	R1	Cum.	Long-crested	MHW	60%	0.1	0.2	0.1	0.2
	R2	Cum.	Long-crested	MHW	80%	1.7	1.0	0.9	1.0
	R3	Cum.	Long-crested	MHW	100%	2.4	3.0	4.0	4.4
	R4	Cum.	Long-crested	MHW	120%	14.5	12.0	13.1	12.3
S2	R1	Non-cum.	Long-crested	MHW	80%	0.8	0.3	0.6	1.3
	R2	Non-cum.	Long-crested	MHW	100%	2.9	2.9	2.2	2.5
	R2r	Non-cum.	Long-crested	MHW	100%	4.0	5.0	2.9	3.2
	R3	Non-cum.	Long-crested	MHW	120%	9.5	16.6	9.2	16.0
S3	R1	Cum.	Long-crested	MHW	60%	0.1	0.3	0.5	1.0
	R2	Cum.	Long-crested	MHW	80%	1.0	1.1	1.2	2.3
	R3	Cum.	Long-crested	MHW+SLR	100%	1.0	0.9	1.6	2.9
	R4	Cum.	Long-crested	MHW+SLR	120%	10.0	6.0	5.8	13.9

Table H.2: UPorto test results - parameter E_{2D}

Series	Run	Damage	Waves	h (m)	Cond.	E_{2D}			
S1	R1	Cum.	Long-crested	MHW	60%	0.02	0.05	0.03	0.07
	R2	Cum.	Long-crested	MHW	80%	0.30	0.16	0.14	0.28
	R3	Cum.	Long-crested	MHW	100%	0.45	0.33	0.54	0.62
	R4	Cum.	Long-crested	MHW	120%	1.15	1.10	1.08	1.09
S2	R1	Non-cum.	Long-crested	MHW	80%	0.22	0.09	0.16	0.14
	R2	Non-cum.	Long-crested	MHW	100%	0.36	0.33	0.29	0.32
	R2r	Non-cum.	Long-crested	MHW	100%	0.60	0.61	0.47	0.39
	R3	Non-cum.	Long-crested	MHW	120%	0.85	1.35	0.86	1.35
S3	R1	Cum.	Long-crested	MHW	60%	0.02	0.05	0.07	0.11
	R2	Cum.	Long-crested	MHW	80%	0.12	0.18	0.18	0.22
	R3	Cum.	Long-crested	MHW+SLR	100%	0.25	0.15	0.21	0.31
	R4	Cum.	Long-crested	MHW+SLR	120%	0.88	0.56	0.49	1.15

Table H.3: UPorto test results - parameter $E_{3D,1}$

Series	Run	Damage	Waves	h (m)	Cond.	$E_{3D,1}$			
S1	R1	Cum.	Long-crested	MHW	60%	0.55	0.87	0.80	0.94
	R2	Cum.	Long-crested	MHW	80%	1.13	0.97	0.99	1.20
	R3	Cum.	Long-crested	MHW	100%	1.19	1.26	1.41	1.57
	R4	Cum.	Long-crested	MHW	120%	1.95	1.86	1.72	1.83
S2	R1	Non-cum.	Long-crested	MHW	80%	1.05	1.12	0.84	0.97
	R2	Non-cum.	Long-crested	MHW	100%	1.17	1.23	1.14	1.19
	R2r	Non-cum.	Long-crested	MHW	100%	1.38	1.82	1.20	1.19
	R3	Non-cum.	Long-crested	MHW	120%	1.78	1.98	1.75	1.97
S3	R1	Cum.	Long-crested	MHW	60%	0.46	0.76	0.59	1.12
	R2	Cum.	Long-crested	MHW	80%	0.88	0.80	0.94	1.07
	R3	Cum.	Long-crested	MHW+SLR	100%	1.02	1.22	0.89	1.16
	R4	Cum.	Long-crested	MHW+SLR	120%	1.68	1.26	1.42	2.08

Table H.4: UPorto test results - parameter $E_{3D,5}$

Series	Run	Damage	Waves	h (m)	Cond.	$E_{3D,5}$			
S1	R1	Cum.	Long-crested	MHW	60%	0.12	0.12	0.10	0.10
	R2	Cum.	Long-crested	MHW	80%	0.43	0.31	0.30	0.48
	R3	Cum.	Long-crested	MHW	100%	0.61	0.61	0.79	1.06
	R4	Cum.	Long-crested	MHW	120%	1.45	1.33	1.17	1.46
S2	R1	Non-cum.	Long-crested	MHW	80%	0.43	0.25	0.23	0.27
	R2	Non-cum.	Long-crested	MHW	100%	0.82	0.65	0.58	0.75
	R2r	Non-cum.	Long-crested	MHW	100%	0.90	1.21	0.62	0.55
	R3	Non-cum.	Long-crested	MHW	120%	1.42	1.49	1.36	1.53
S3	R1	Cum.	Long-crested	MHW	60%	0.04	0.11	0.10	0.21
	R2	Cum.	Long-crested	MHW	80%	0.31	0.25	0.20	0.51
	R3	Cum.	Long-crested	MHW+SLR	100%	0.40	0.27	0.25	0.52
	R4	Cum.	Long-crested	MHW+SLR	120%	1.20	0.78	0.91	1.63

Table H.5: UPorto test results - measured incident wave conditions

Series	Run	Damage	Waves	h (m)	Cond.	T_m (s)	T_p (s)	H_{m0} (m)
S1	R1	Cum.	Long-crested	MHW	60%	1.04	1.30	0.072
	R2	Cum.	Long-crested	MHW	80%	1.29	1.67	0.092
	R3	Cum.	Long-crested	MHW	100%	1.55	1.81	0.118
	R4	Cum.	Long-crested	MHW	120%	1.80	2.19	0.139
S2	R1	Non-cum.	Long-crested	MHW	80%	1.26	1.67	0.096
	R2	Non-cum.	Long-crested	MHW	100%	1.56	1.81	0.117
	R2r	Non-cum.	Long-crested	MHW	100%	1.55	1.74	0.120
	R3	Non-cum.	Long-crested	MHW	120%	1.81	2.19	0.141
S3	R1	Cum.	Long-crested	MHW	60%	1.04	1.30	0.072
	R2	Cum.	Long-crested	MHW	80%	1.28	1.67	0.096
	R3	Cum.	Long-crested	MHW+SLR	100%	1.52	1.74	0.118
	R4	Cum.	Long-crested	MHW+SLR	120%	1.78	2.19	0.142

Deltares tests

All values calculated for a 27D_{n50} characterization width (2 per test run).

Table H.6: Deltares test results - parameters S and E_{2D}

Series	Run	Damage	B (m)	d_b (m)	Cond.	S		E_{2D}	
S1a	R1	Cum.	-	-	60%	0.1	0.6	0.09	0.10
	R2	Cum.	-	-	80%	1.2	1.5	0.12	0.21
	R3	Cum.	-	-	100%	4.6	4.1	0.47	0.47
	R4	Cum.	-	-	120%	11.7	10.3	0.92	0.89
S1b	R1	Cum.	-	-	60%	0.5	0.3	0.09	0.10
	R2	Cum.	-	-	80%	0.7	1.0	0.16	0.23
	R3	Cum.	-	-	100%	3.2	4.0	0.44	0.40
	R4	Cum.	-	-	120%	11.4	11.8	1.14	1.04
S1c	R1	Cum.	-	-	60%	0.4	0.2	0.08	0.06
	R2	Cum.	-	-	80%	0.7	0.6	0.18	0.17
	R3	Cum.	-	-	100%	2.3	4.9	0.35	0.57
	R4	Cum.	-	-	120%	9.9	13.1	0.90	1.01
S1d	R1	Cum.	-	-	60%	0.3	0.2	0.07	0.05
	R2	Cum.	-	-	80%	1.1	0.8	0.15	0.21
	R3	Cum.	-	-	100%	4.3	3.2	0.57	0.34
	R4	Cum.	-	-	120%	13.3	10.8	1.10	0.98
S1e	R1	Cum.	-	-	60%	0.3	0.4	0.10	0.13
	R2	Cum.	-	-	80%	0.9	0.9	0.24	0.18
	R3	Cum.	-	-	100%	2.3	4.2	0.27	0.47
	R4	Cum.	-	-	120%	11.8	10.2	1.10	0.93
S2a	R1	Non-cum.	-	-	100%	3.6	2.7	0.45	0.34
S2b	R1	Non-cum.	-	-	100%	4.0	5.0	0.45	0.58
S2c	R1	Non-cum.	-	-	100%	3.9	4.2	0.51	0.45
S2d	R1	Non-cum.	-	-	100%	2.9	3.7	0.38	0.41
S2e	R1	Non-cum.	-	-	100%	2.0	2.6	0.30	0.35
S3	R1	Cum.	$10D_{n50}$	100%	60%	0.3	0.1	0.08	0.03
	R2	Cum.	$10D_{n50}$	100%	80%	1.2	1.0	0.12	0.19
	R3	Cum.	$10D_{n50}$	100%	100%	2.1	2.3	0.25	0.28
	R4	Cum.	$10D_{n50}$	100%	120%	2.7	2.5	0.31	0.29
S4	R1	Cum.	$5D_{n50}$	100%	60%	0.4	0.4	0.10	0.10
	R2	Cum.	$5D_{n50}$	100%	80%	1.1	0.8	0.19	0.16
	R3	Cum.	$5D_{n50}$	100%	100%	3.6	2.4	0.61	0.50
	R4	Cum.	$5D_{n50}$	100%	120%	5.0	4.6	0.56	0.60
S5	R1	Cum.	$10D_{n50}$	80%	60%	0.5	1.1	0.09	0.18
	R2	Cum.	$10D_{n50}$	80%	80%	0.5	1.1	0.10	0.26
	R3	Cum.	$10D_{n50}$	80%	100%	0.8	1.1	0.12	0.28
	R4	Cum.	$10D_{n50}$	80%	120%	4.9	4.6	0.43	0.49
S6	R1	Cum.	$5D_{n50}$	80%	60%	0.3	0.3	0.06	0.07
	R2	Cum.	$5D_{n50}$	80%	80%	1.1	1.0	0.17	0.17
	R3	Cum.	$5D_{n50}$	80%	100%	3.8	2.9	0.38	0.29
	R4	Cum.	$5D_{n50}$	80%	120%	5.6	4.2	0.58	0.51

Table H.7: Deltares test results - parameters $E_{3D,1}$ and $E_{3D,5}$

Series	Run	Damage	B (m)	d_b (m)	Cond.	$E_{3D,1}$		$E_{3D,5}$	
S1a	R1	Cum.	-	-	60%	1.00	0.03	0.12	0.18
	R2	Cum.	-	-	80%	1.07	1.06	0.28	0.31
	R3	Cum.	-	-	100%	1.46	1.23	0.66	0.66
	R4	Cum.	-	-	120%	2.00	1.71	1.25	1.14
S1b	R1	Cum.	-	-	60%	1.08	1.11	0.16	0.16
	R2	Cum.	-	-	80%	1.05	1.04	0.30	0.41
	R3	Cum.	-	-	100%	1.39	1.26	0.63	0.68
	R4	Cum.	-	-	120%	2.30	1.96	1.48	1.20
S1c	R1	Cum.	-	-	60%	1.12	0.90	0.19	0.17
	R2	Cum.	-	-	80%	1.12	1.10	0.24	0.30
	R3	Cum.	-	-	100%	1.29	1.54	0.50	0.69
	R4	Cum.	-	-	120%	1.81	1.98	1.05	1.17
S1d	R1	Cum.	-	-	60%	0.92	1.01	0.15	0.13
	R2	Cum.	-	-	80%	0.96	1.27	0.35	0.35
	R3	Cum.	-	-	100%	1.51	1.49	0.88	0.89
	R4	Cum.	-	-	120%	2.43	1.99	1.37	1.19
S1e	R1	Cum.	-	-	60%	1.10	0.91	0.14	0.16
	R2	Cum.	-	-	80%	1.14	1.22	0.31	0.36
	R3	Cum.	-	-	100%	1.15	1.36	0.60	0.71
	R4	Cum.	-	-	120%	1.94	1.90	1.26	1.27
S2a	R1	Non-cum.	-	-	100%	1.73	1.29	0.68	0.61
S2b	R1	Non-cum.	-	-	100%	1.31	1.53	0.84	0.79
S2c	R1	Non-cum.	-	-	100%	1.49	1.44	0.67	0.71
S2d	R1	Non-cum.	-	-	100%	1.20	1.32	0.52	0.74
S2e	R1	Non-cum.	-	-	100%	1.46	1.26	0.73	0.73
S3	R1	Cum.	$10D_{n50}$	100%	60%	0.79	1.13	0.15	0.18
	R2	Cum.	$10D_{n50}$	100%	80%	0.98	1.11	0.25	0.28
	R3	Cum.	$10D_{n50}$	100%	100%	1.15	1.35	0.35	0.44
	R4	Cum.	$10D_{n50}$	100%	120%	1.24	1.35	0.38	0.38
S4	R1	Cum.	$5D_{n50}$	100%	60%	0.93	0.79	0.15	0.14
	R2	Cum.	$5D_{n50}$	100%	80%	0.99	1.07	0.29	0.32
	R3	Cum.	$5D_{n50}$	100%	100%	1.40	1.36	0.81	0.65
	R4	Cum.	$5D_{n50}$	100%	120%	1.35	1.40	0.86	0.80
S5	R1	Cum.	$10D_{n50}$	80%	60%	0.95	1.09	0.14	0.22
	R2	Cum.	$10D_{n50}$	80%	80%	1.05	1.09	0.17	0.28
	R3	Cum.	$10D_{n50}$	80%	100%	1.07	1.24	0.18	0.24
	R4	Cum.	$10D_{n50}$	80%	120%	1.20	1.30	0.74	0.72
S6	R1	Cum.	$5D_{n50}$	80%	60%	0.97	0.84	0.17	0.12
	R2	Cum.	$5D_{n50}$	80%	80%	1.11	1.10	0.23	0.28
	R3	Cum.	$5D_{n50}$	80%	100%	1.35	1.14	0.68	0.38
	R4	Cum.	$5D_{n50}$	80%	120%	1.51	1.31	0.74	0.61

Table H.8: Deltares test results - measured incident wave conditions

Series	Run	Damage	B (m)	d_b (m)	Cond.	$T_{m-1,0}$ (s)	$H_{1/3}$ (m)	$H_{2\%}$ (m)
S1a	R1	Cum.	-	-	60%	1.59	0.029	0.034
	R2	Cum.	-	-	80%	1.53	0.041	0.048
	R3	Cum.	-	-	100%	1.42	0.052	0.063
	R4	Cum.	-	-	120%	1.39	0.061	0.074
S1b	R1	Cum.	-	-	60%	1.60	0.030	0.036
	R2	Cum.	-	-	80%	1.54	0.041	0.049
	R3	Cum.	-	-	100%	1.40	0.052	0.061
	R4	Cum.	-	-	120%	1.38	0.061	0.075
S1c	R1	Cum.	-	-	60%	1.55	0.030	0.036
	R2	Cum.	-	-	80%	1.51	0.041	0.048
	R3	Cum.	-	-	100%	1.39	0.052	0.062
	R4	Cum.	-	-	120%	1.37	0.061	0.073
S1d	R1	Cum.	-	-	60%	1.55	0.030	0.036
	R2	Cum.	-	-	80%	1.49	0.041	0.048
	R3	Cum.	-	-	100%	1.41	0.052	0.060
	R4	Cum.	-	-	120%	1.38	0.061	0.076
S1e	R1	Cum.	-	-	60%	1.63	0.029	0.036
	R2	Cum.	-	-	80%	1.50	0.041	0.049
	R3	Cum.	-	-	100%	1.39	0.052	0.060
	R4	Cum.	-	-	120%	1.38	0.060	0.074
S2a	R1	Non-cum.	-	-	100%	1.42	0.052	0.062
S2b	R1	Non-cum.	-	-	100%	1.41	0.052	0.062
S2c	R1	Non-cum.	-	-	100%	1.41	0.052	0.062
S2d	R1	Non-cum.	-	-	100%	1.43	0.052	0.062
S2e	R1	Non-cum.	-	-	100%	1.42	0.051	0.062
S3	R1	Cum.	$10D_{n50}$	100%	60%	1.62	0.029	0.035
	R2	Cum.	$10D_{n50}$	100%	80%	1.49	0.040	0.047
	R3	Cum.	$10D_{n50}$	100%	100%	1.43	0.052	0.062
	R4	Cum.	$10D_{n50}$	100%	120%	1.38	0.061	0.075
S4	R1	Cum.	$5D_{n50}$	100%	60%	1.59	0.030	0.036
	R2	Cum.	$5D_{n50}$	100%	80%	1.48	0.041	0.049
	R3	Cum.	$5D_{n50}$	100%	100%	1.42	0.052	0.061
	R4	Cum.	$5D_{n50}$	100%	120%	1.38	0.060	0.073
S5	R1	Cum.	$10D_{n50}$	80%	60%	1.64	0.029	0.035
	R2	Cum.	$10D_{n50}$	80%	80%	1.53	0.041	0.048
	R3	Cum.	$10D_{n50}$	80%	100%	1.41	0.052	0.061
	R4	Cum.	$10D_{n50}$	80%	120%	1.39	0.061	0.074
S6	R1	Cum.	$5D_{n50}$	80%	60%	1.59	0.030	0.036
	R2	Cum.	$5D_{n50}$	80%	80%	1.49	0.041	0.048
	R3	Cum.	$5D_{n50}$	80%	100%	1.41	0.052	0.061
	R4	Cum.	$5D_{n50}$	80%	120%	1.39	0.061	0.074

I

Tests results comparison

Deltares tests

Plunging conditions

For berm configurations with plunging conditions (100% and 120% wave conditions), the formula from van Gent (2013) is used in its original form as described in Section 2.1.3 (Equations 2.17 and 2.18):

For the upper slope stability:

$$\frac{H_s}{\Delta D_{n50}} = \left(\frac{1}{\gamma_{berm,up}\gamma_{pos}}\right)^{0.2} c_{pl} P^{0.18} \left(\frac{S}{\sqrt{N}}\right)^{0.2} \left(\frac{H_s}{H_{2\%}}\right) \left(\xi_{m-1,0}\right)^{-0.5} \tag{I.1}$$

For the lower slope stability:

$$\frac{H_s}{\Delta D_{n50}} = \frac{1}{\gamma_{berm,low}} c_{pl} P^{0.18} \left(\frac{S}{\sqrt{N}}\right)^{0.2} \left(\frac{H_s}{H_{2\%}}\right) \left(\xi_{m-1,0}\right)^{-0.5} \tag{I.2}$$

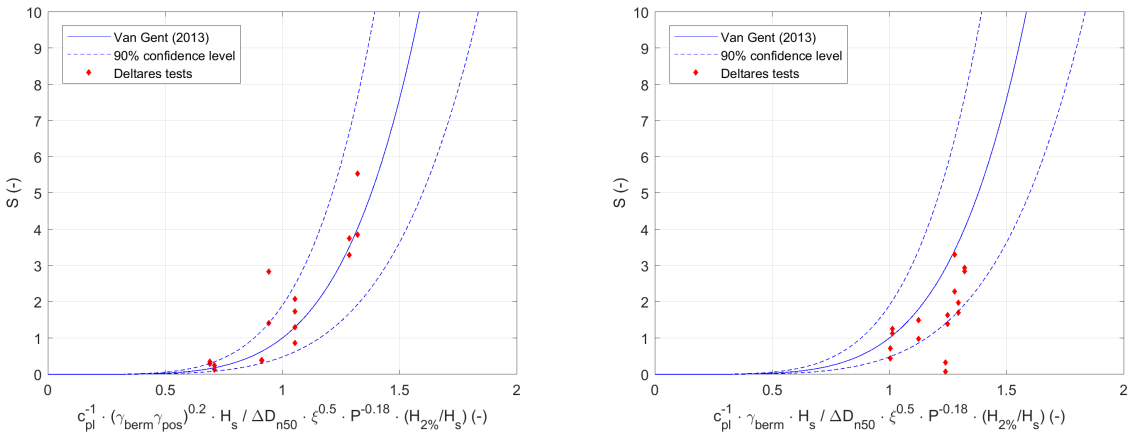

(a) Upper slope.

(b) Lower slope.

Figure I.1: Deltares damage for slopes with a berm compared with van Gent (2013) - plunging conditions.

Surging conditions

For berm configurations with surging conditions (60% and 80% wave conditions), the formula from van Gent (2013) shown in Section 2.1.3 (Equations 2.17 and 2.18) is adapted according to Equation 2.14 (from van der Meer (1988) formulae modified by van Gent et al. (2003)). This results in the following adapted formulae for berm configurations with surging breaking conditions:

For the upper slope stability:

$$\frac{H_s}{\Delta D_{n50}} = \left(\frac{1}{\gamma_{berm,up}\gamma_{pos}}\right)^{0.2} c_s P^{-0.13} \left(\frac{S}{\sqrt{N}}\right)^{0.2} \left(\frac{H_s}{H_{2\%}}\right) \sqrt{\cot\alpha}\,(\xi_{m-1,0})^P \tag{I.3}$$

For the lower slope stability:

$$\frac{H_s}{\Delta D_{n50}} = \frac{1}{\gamma_{berm,low}} c_s P^{-0.13} \left(\frac{S}{\sqrt{N}}\right)^{0.2} \left(\frac{H_s}{H_{2\%}}\right) \sqrt{\cot\alpha}\,(\xi_{m-1,0})^P \tag{I.4}$$

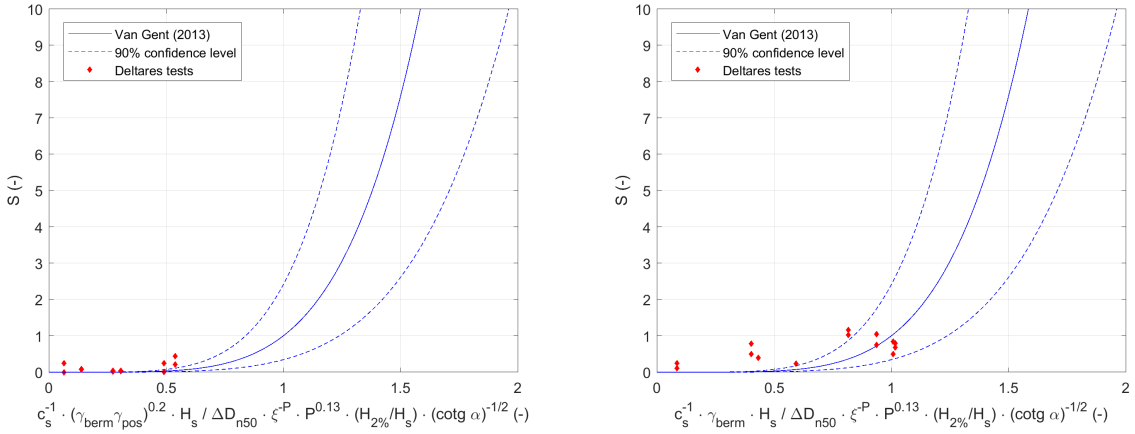

(a) Upper slope. (b) Lower slope.

Figure I.2: Deltares damage for slopes with a berm compared with van Gent (2013) - surging conditions.

J

Damage limits prediction

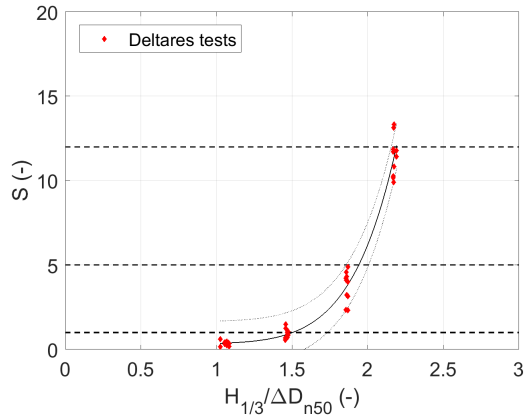

(a) S parameter.

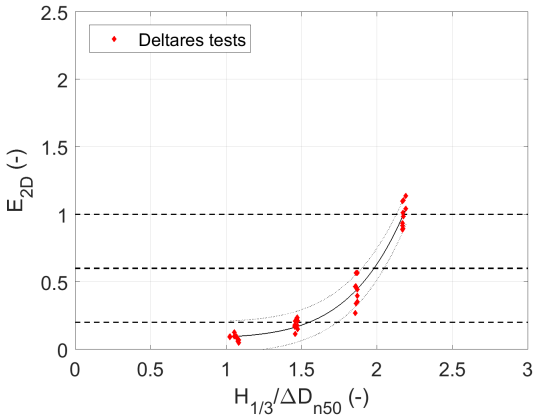

(b) E_{2D} parameter.

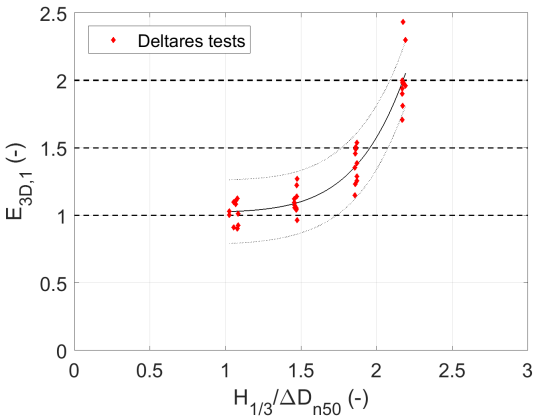

(c) $E_{3D,1}$ parameter.

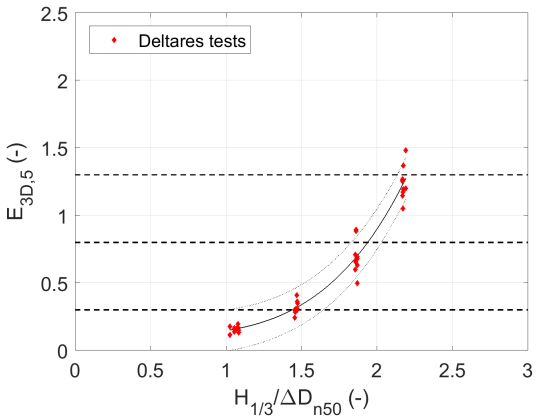

(d) $E_{3D,5}$ parameter.

Figure J.1: Deltares tests - Measured damage.

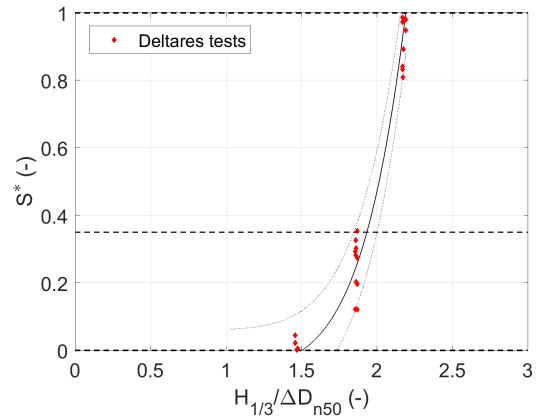

(a) S parameter.

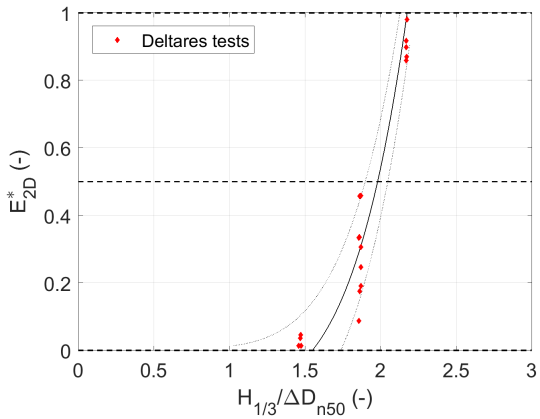

(b) E_{2D} parameter.

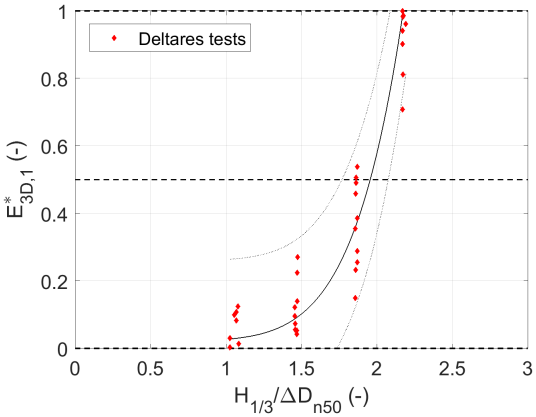

(c) $E_{3D,1}$ parameter.

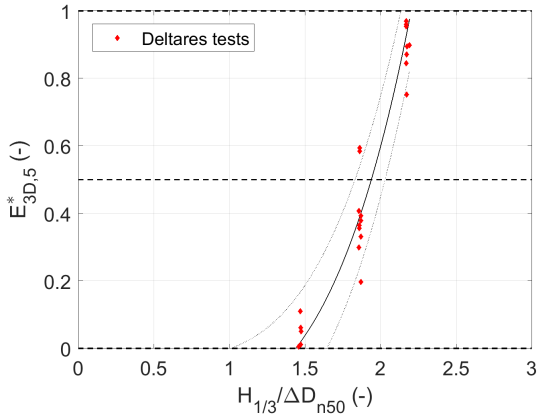

(d) $E_{3D,5}$ parameter.

Figure J.2: Deltares tests - Normalized damage.